Charles University in Prague
Faculty of Mathematics and Physics

MASTER THESIS

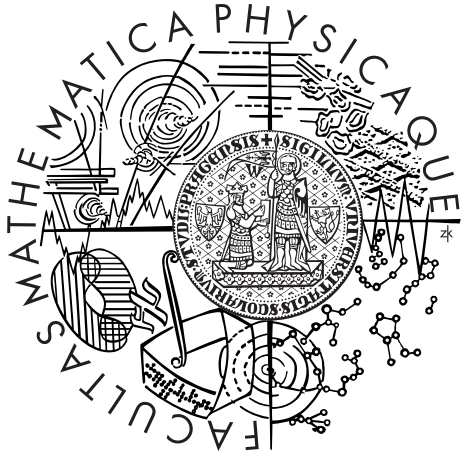

Bc. Radim Slovák

Top Quark Physics with the ATLAS Detector

Institute of Particle and Nuclear Physics

Supervisor of the master thesis: Mgr. Jiří Kvita, Ph.D.
Study programme: Physics
Specialization: Nuclear and subnuclear physics

Prague 2013

I would like to thank to my supervisor Mgr. Jiří Kvita, Ph.D. for his leadership and useful comments. He always immediately replied to all my questions. I appreciate his attitude. I'm glad that I could learn so much under his guidance. I want to thank him that he looked after me during my stay in CERN.

I thank to University of Geneva Tier-3 and Ian Watson for samples used in the thesis. Than I thank to J. Chudoba and to Pragues Tier-2 to grant me the access to their resources.

Finally I thank to the Institute of Particle and Nuclear Physics in Prague that supported my visit to CERN.

I declare that I carried out this master thesis independently, and only with the cited sources, literature and other professional sources.

I understand that my work relates to the rights and obligations under the Act No. 121/2000 Coll., the Copyright Act, as amended, in particular the fact that the Charles University in Prague has the right to conclude a license agreement on the use of this work as a school work pursuant to Section 60 paragraph 1 of the Copyright Act.

In Prague, on 30.7.2013

Název práce: Fyzika top kvarku v experimentu Atlas

Autor: Bc. Radim Slovák

Katedra: Ústav částicové a jaderné fyziky

Vedoucí diplomové práce: Mgr. Jiří Kvita, Ph.D., Ústav částicové a jaderné fyziky

Abstrakt: V diplomové práci studuji rekonstrukci top antitop systému v proton-protonových srážkách s celkovou energií 7 TeV produkovaných na urychlovači LHC v CERNu detekovaných experimentem ATLAS. Jsou zde popsány ALPGEN a MC@NLO generátory jako dvě hlavní metody simulací top antitopových párů. Srovnávám události simulované generátory s daty z LHC. Je zde popsáno pozadí a cuty pro jeho potlačení. Dále popisuji různé metody rekonstrukce top antitop párů a pro nejlepší řešení jsou zde uvedeny i další pozorovatelné veličiny. Nakonec je studována i hypotetická částice Z'.

Klíčová slova: top kvark, kinematika, experiment, fyzika vysokých energií

Title: Top Quark Physics with the ATLAS Detector

Author: Bc. Radim Slovák

Department: Institute of particle and nuclear physics

Supervisor: Mgr. Jiří Kvita, Ph.D., Institute of Particle and Nuclear Physics

Abstract:

In the presented diploma thesis we study the reconstruction the of top antitop system in proton-proton colisions with central mass energy 7 TeV delivered by LHC accelerator at CERN to the ATLAS experiment. ALPGEN and MC@NLO generators are described as two main method of the top antitop pairs simulations. We compare events simulated by generators to data from LHC. The background and selection criteria are summarized. Next we described various methods of the top antitop reconstruction. Finally the Z' particle was also studied.

Keywords: top quark, kinematics, experiment, high energy physics

Contents

Introduction

For all today's complex experiments in physics of high energies the simulation of events is one of the most important aspect of its successful design.

The main goal of the thesis is to reconstruct $t\bar{t}$ pairs from simulated samples by ALPGEN and MC@NLO generators and from data delivered by LHC to the ATLAS experiment at center of mass energy of 7 TeV.

First, we summarize basics fact about Standard Model theory and about the top quark which is a useful electroweak laboratory challenging the understanding of the experimental apparatus as well as all the processes which are a background of the top quark final state.

In the second section the ATLAS detector and LHC collider are described. Further, the ALPGEN and MC@NLO generators are described.

After introduction with basics principles and with selection cuts top antitop pair are reconstructed. We developed several method which are summarized in the last chapter. In the end the samples from the hypothetical particle Z' were included and their shapes were compared.

1 Theory

The Standard Model (SM) is a very successful theory describing modern physics at a sub-nuclear scale by relativistic quantum field theory. SM contains two different types of particle interactions. The electroweak theory (EWT) unifies weak and electromagnetic interactions while quantum chromodynamics (QCD) describes strong interactions of quarks through gluons.

In quantum field theory [1], elementary particles are described by fields. Fermions are described by half integer spin spinors and can represent leptons $l = e, \nu_e, \mu,\ \nu_\mu, \tau, \nu_\tau$ and quarks $q = d, u, s,\ c, b, t$. Integer spin fields describes gauge bosons $W^{\pm}$, gluon g, γ and Z which are mediators of the interactions.

SM is based on local gauge symmetry group $\mathrm{SU}(3)_{QCD} \otimes \mathrm{SU}(2)_L \otimes \mathrm{U}(1)_Y$ leading, as said above, to the description of the strong and electroweak interactions. QCD is based on the gauge group $\mathrm{SU}(3)_{QCD}$, with strong coupling constant α_S, is mediated by eight gauge bosons called gluons g. The gauge group $\mathrm{SU}(2)_L \otimes \mathrm{U}(1)_Y$, with the fine structure constant α, describes electroweak interactions, mediated by gauge bosons W and Z for the weak force and the photon γ for the electromagnetic force [2]. The quarks are involved in all tree interactions. The charged leptons only participate in electroweak force. Gravitational force can be neglected.

Every particle has its own antiparticle. Antiparticles have the same symbol as particle plus they have over line above them. So thus antiparticle to top quark t is $\bar{t}$. They have the same mass, the same live time but opposite quantum numbers.

The leptons and quarks are grouped into generations, first are (e, ν_e) and (u, d), second are (μ, ν_μ) and (c, s) and finally third are (τ, ν_τ) and (t, b), respectively. For lepton from one family the quantum lepton number is conserved. That is why for instance the muon can decay only with creation of additional electron and muon neutrinos $\mu \to e\bar{\nu_e}\nu_\mu$. This rule can't be applied for quarks that can interact with other quarks with different generations by weak interaction. Quarks can decay weakly into other quarks of a different flavour, controlled by Cabbiho-Kobayasi-Maskawa (CKM) 3×3 matrix [3].

In analogy to of electric charge, new quantum number of strong interaction color is presented in QCD. Color has three various possible states donated as blue, red and green. Mediators are gluons, there are eight of them because of possible interactions among them. All free particles in nature are observed to be color neutral so one cannot find quarks and gluons as free particles. Two or three free quarks can form a composite objects. A quark-antiquark pair is called a meson and they are bosons. A bound state of three quarks are called baryons and they are fermions.

2 CERN

CERN is the largest research center with the most important impact to modern physics. Since founded in 1954 on northwest from Geneva on French-Swiss border it is the biggest laboratory for elementary particle physics. Many interesting technologies were invented there as the World Wide Web and many responses to fundamental questions of particle physics were founded. Yet some still are waiting for their discovery. Nowadays there are associated more then twenty

Type	Particle	Charge	Mass
Fermions	u	$+\frac{2}{3}$	5 MeV
	d	$-\frac{1}{3}$	7 MeV
	c	$+\frac{2}{3}$	1.4 GeV
	s	$-\frac{1}{3}$	150 MeV
	t	$+\frac{2}{3}$	172.5 GeV
	b	$-\frac{1}{3}$	4.3 GeV
	e	-1	511 keV
	ν_e	0	0 MeV
	μ	-1	105.7 MeV
	ν_μ	0	0 MeV
	τ	-1	1777 MeV
	ν_τ	0	0 MeV
Bosons	$W^\pm$	± 1	80.4 GeV
	Z^0	0	91.2 GeV
	g	0	0 MeV
	γ	0	0 MeV
	H^0	0	$\sim$ 125 GeV

Table 1.1: Elementary particles and their charges and masses [4].

member countries with more then 9 500 scientists from 500 universities all over the world. A range of experiments at CERN investigate physics from cosmic rays to super symmetry.

2.1 Large Hadron Collider

The Large Hadron Collider (LHC) shown in Figure (2.1) is the biggest proton-proton collider in the world with a circumference of 27 km and is located around 100 m underground at CERN. The total integrated luminosity accumulated by the ATLAS and CMS experiments in 2010 at $\sqrt{s} = 7$ TeV, with up to 368 bunches per beam, corresponds to 47 pb^{-1}. And only in the first month of operation in 2011, the LHC had already accumulated an integrated luminosity of 28 pb^{-1}, which corresponds to over 50% of the total delivered to the experiments in 2010 [5]. In the first seven months of 2012, the LHC had delivered more than twice as many collisions to the ATLAS and CMS experiments this year as it did in all of 2011. On 4 August 2012, the integrated luminosity recorded by each of the experiments passed the 10 fb^{-1} mark. Last year, they each recorded data corresponding to around 5.6 fb^{-1}. On 22 August 2012, the more specialized LHCb experiment passed 1.11 fb^{-1}, the same as its entire data sample for 2011. At the beginning of September last year, CMS and ATLAS had already recorded more than 13 fb^{-1}. The maximum of specific luminosity was increased from the 2010 value of $2 \cdot 10^{32}$ cm^{-2}s^{-1} to $3.6 \cdot 10^{33}$ cm^{-2}s^{-1} raising the number of bunches per beam to 1 380. The design luminosity of LHC is supposed to be of the order of 10^{34} cm^{-2}s.

Several systems of detectors and others apparatuses are prepared for LHC experiment. The biggest ones ATLAS (A Toroidal LHC ApparatuS) and CMS (The

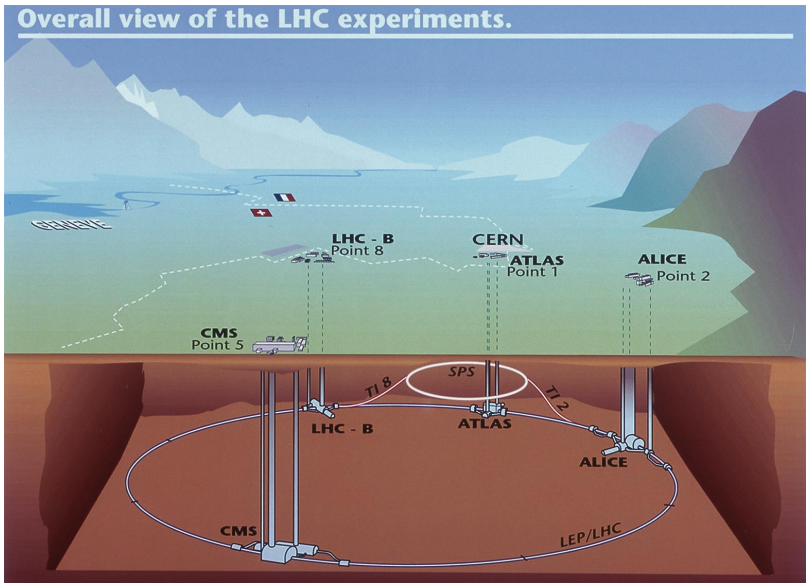

Figure 2.1: LHC accelerator and its experiments.

Compact Muon Solenoid) are general purpose detectors investigating proton-proton interaction and in this frame especially finding the Higgs boson and particles that constitute the dark matter. The main difference between these detectors is their independent design which is important in cross-confirm of any new discovery. ALICE (A Large Ion Collider Experiment) investigates lead ion collisions and quark-gluon plasma which with high probability existed in the Big Bang. LHCb (Large Hadron Collider beauty) concentrate on the CP symmetry violation in b quark interactions. It explores differences between matter and antimatter and should respond to question of composition of the universe. TOTEM (TOTal Elastic and diffractive cross-section Measurement) studies forward particles to focus on physics that is not accessible to the general-purpose experiments. It measures, in effect, the size of the proton and monitors the LHC luminosity. LHCf (Large Hadron Collider forward) uses protons or heavy ions created by LHC as a source of cosmic like radiation in the laboratory conditions.

2.2 The ATLAS experiment

The ATLAS experiment (2.2), as said above, is one of the main experiments at the LHC. It detects proton-proton collisions delivered by the LHC collider. Detector itself weights about 7 000 tons and is 44 m long and 22 m high. ATLAS is compiled from various types of subdetectors. From the center of the detector there are located layouts arranged symmetrically around the interaction point and the beam pipe: the inner detector, the electromagnetic and the hadronic calorimeters and the last one is the muon spectrometer. In each of these layouts different particles interact differently so one can recognize which particles were created in the collision.

2.2.1 The Inner Detector

The Inner detector (2.3) is placed closest to the interaction point because most particles are created here. It can estimate the position of interaction point and momenta and impact parameters of charged particles with acceptance in pseudorapidity $|\eta| < 2.5$. It is a barrel with radius 115 cm and length 690 cm.

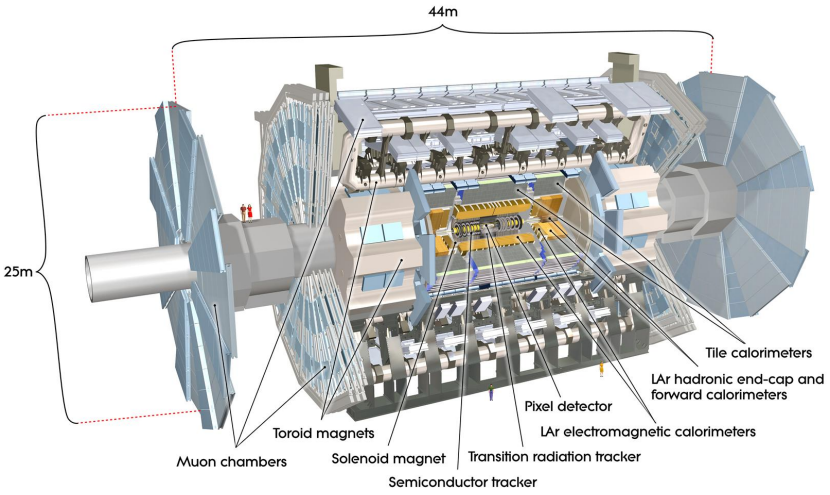

Figure 2.2: The ATLAS experiment.

The system is cooled to temperature of -7° C. Above the subdetector there is a solenoid with homogeneous magnetic field of 2 T [6].

The inner detector consists of three parts, the Pixel detector, the Semiconductor Tracker and from the Transition Radiation Tracker. Each individual part consists of several barrels closed by forward or end-cap. The pixel detector is formed from small micrometer rectangles that determine spatilally its resolution because particles which go through the detector leave an electric signal. So we are able to find out where the particle went through. The semiconductor tracker is made of strips approximately ten centimeters long. The transition radiation tracker is made of thousands of gas filled thin straws. The transition radiation is emitted when a particle goes through different environment with a periodical change of refractive index. When the particle goes through the straw, the gas is ionized and creates electric pulses on electrodes. From the pulse reconstruction one can precisely determine the location of the particle.

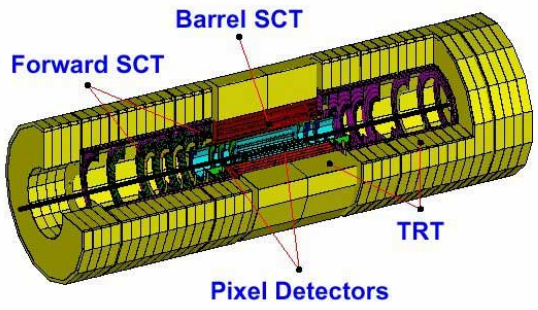

Figure 2.3: Inner detector.

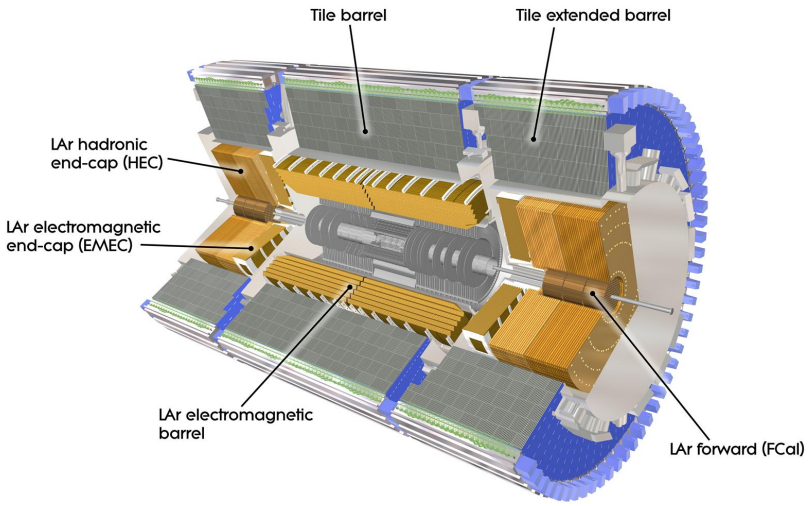

Figure 2.4: The calorimeters.

2.2.2 The Calorimeters

The sampling calorimeters are detectors measuring energy and direction of neutral or charged particles. Their resolution is better when the energy of the particle is bigger so they are suitable for measurement of high energy particles. The calorimeter composes of two parts. The first is an absorber, where the electromagnetic or hadronic shower take place, and the second part is an active material where we can measure the energy of particles. In the electromagnetic shower there are high energetic electrons or photons and in the hadronic shower there can be protons, neutrons, pions or kaons. In ATLAS there are more types of calorimeters. We divide then into two categories, namely into electromagnetic Liquid Argon (LAr) calorimeters which are closer to the beam pipe of ATLAS experiment and the hadronic Tile calorimetr (TileCal), as shown in Figure (2.4). The energy resolution of a calorimeter is generally described by a formula.

$$\frac{\sigma\left(E\right)}{E} = \frac{a}{\sqrt{E}}\left[\text{GeV}\right] \oplus \frac{b}{E}\left[\text{GeV}\right] \oplus c, \tag{2.1}$$

where a is the stochastic term, b is the noise term and c is the constant term.

In the electromagnetic calorimeter only photons and electrons stops. The absorber is lead and the active material is liquid argon which is also used in the other parts of the hadronic calorimeter. These two layouts take turns in the detector and liquid argon is divided in two parts by reading electrodes. Particles create ions in liquid argon which generate electric signals on electrodes. Is consists of four parts, the electromagnetic barrel calorimeter (EMB), electromagnetic endcap calorimeter (EMEC), hadronic endcap calorimeter (HEC) and forward calorimeter (FCal). The first two of them, EMB and EMEC, are the sampling electromagnetic calorimeters. They register particles in ranges as $|\eta| < 1.475$ for EMB and $1.375 < |\eta| < 3.2$ for EMEC. Their designed resolution terms are $a = 10\%$, $b = 30\%$ and $c = 0.7\%$. The rest of the region from EMEC i.e. $1.5 < |\eta| < 3.2$ is covered by HEC which detects hadronic showers. The designed resolution of HEC terms are $a = 50\%$ and $c = 3\%$. The FCal detect particles in the region $3.2 < |\eta| < 4.8$. The designed resolution terms are $a = 100\%$ and $c = 10\%$.

Due to the hadronic Tile Calorimeter and appropriate algorithms we can reconstruct jets and their energy. The absorber is lead and as the active material are scintillation tiles used plastic. The volume ratio between absorber and active material is $4.67 : 1$ [7]. It is divided into three parts. The main part is 5.8 m long and it covers the region with pseudorapidity $|\eta| < 1.0$ and two end-cap parts each 2.6 m long covering region with pseudorapidity $0.8 < |\eta| < 1.7$. Its designed energy resolution terms are $a = 50\%$ and $c = 3\%$. Inner radius of all three parts is 2.28 m and outer radius is 4.25 m. Each part of the calorimeter consists of 64 modules compound to the barrel. When an ionizing particle goes though the scintillator, about 3% of its energy is radiated in the light form which wave length corresponds to the blue color. Wavelength shifting fibers (WLS) collect the light from each part of the scintillator. In these fibers the blue light is absorbed and it is again radiated as a green light. The wavelength shifting is caused by absorption and emission of the light in a particular dye which is added into fibers. The material should have the most conceivable refractive index to receive as much as possible of the light. In the photomultipliers the light signal is transformed into an electric signal. From PhotoMultiplier blocks (PTM) we can obtain shaped a electric signal which is digitized every 25 ns by 10 bits ADC changer. Collected data are stored in pipeline memory unless the first level trigger release the signal. Digitized data are transform though optic fibers and loaded to the hard drives.

2.2.3 The muon spectrometer

Muons are charged particles which leave tracks in the inner detector. They are the only particles (together with neutrinos) which can go though the Tile Calorimeter but neutrinos cannot be detected because they have low cross-section. Because of this the muon spectrometer is the most distant subdetector of all at ATLAS. Muons are approximately 200 times heavier then electrons, they don't scatter on atom nuclei and don't generate showers in the electromagnetic calorimeter. The muon spectrometer primary measures muons transverse momenta, for second it measures the muon track in the magnetic field. They are located Monitored Drift Tubes (MDT). The chambers consist of multiple tubes layouts. The basic elements are aluminum gas filled tubes. In the middle of the each tube is high energy wire. When the muon comes though the tube, it causes ionization and the ions drift towards to the wire where they create an electric pulse. If we measure the time of the pulses, we can determine the location of the muon with precision better the 0.1 mm [8]. In the end-cap there are installed Cathode Strip Chambers (CSC) because for the small angles of outgoing particles the MDT chambers cannot be used because of the radiation background.

2.2.4 The trigger

The trigger filters a huge amount of data in order to register only important events that can be very rare. The filtration is used also at ATLAS because it is not possible to record all the incoming information from the collisions. The trigger at ATLAS has three levels, where each level filters these events that came though the previous level.

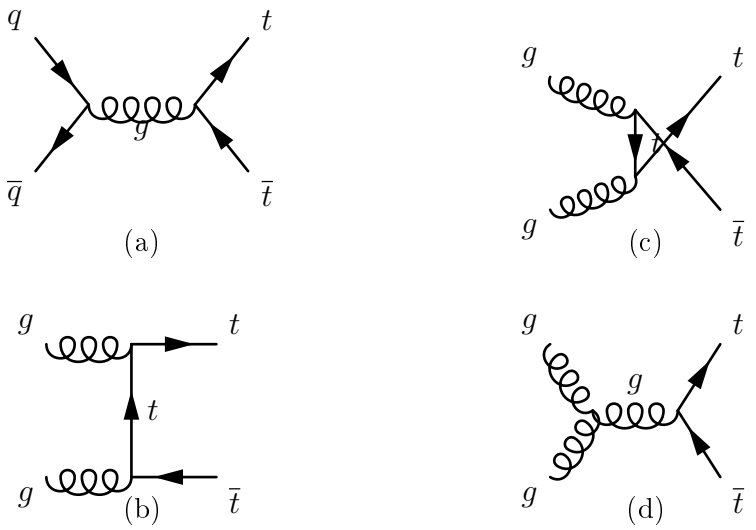

Figure 3.1: Leading order Feynman diagrams for $t\bar{t}$ production

3 The top anti-top pairs production in p-p collisions on LHC

The cross section $\sigma_{t\bar{t}}$ for $p\overline{p} \to t\bar{t}$ can be expressed using the factorization theorem as

$$\sigma_{t\bar{t}} = \sum_{a,b} \int \mathrm{d}x_a \mathrm{d}x_b f_a^p\left(x_a, \mu_R^2\right) f_b^{\overline{p}}\left(x_b, \mu_R^2\right) \widehat{\sigma}\left(ab \to t\bar{t}; \widehat{s}, \mu_R^2, m_t\right), \tag{3.1}$$

where the summation over a and b goes over eight gluons or light quarks. Parton distribution functions f_a^p and $f_b^{\overline{p}}$ describe parton momenta inside the proton. The dependence of the cross section at parton level $\widehat{\sigma}$ on the energy of the parton-parton interaction is $\sqrt{\widehat{s}} = \sqrt{x_a x_b s}$, where $\sqrt{s}$ is central mass energy, a and b are partons that carry respectively a fraction x_a and x_b of the proton and anti-proton momentum. Mass of the top quark is m_t and μ_R^2 is a renormalization scale.

Top and anti-top pairs $\left(t\bar{t}\right)$ can be produced in proton-proton collisions on Large Hadron Collider via QCD process [9]. The main leading orders (LO) diagrams contributing to $t\bar{t}$ are shown in Figure (3.1). Each Feynman diagram represents a term in the expression for the matrix element that is later used to calculate the probability for the interaction to occur. At the leading order there are only two processes which contribute. It is the quark anti-quark annihilation $q\overline{q} \to t\bar{t}$ (3.1a) and gluon-gluon fusion $gg \to t\bar{t}$ (3.1b), (3.1d). The Feynman diagram (3.1c) is a cross diagram to diagram (3.1b). There could be also γ, Z or H boson in the propagator instead of gluon g in Figure (3.1a) but these contributions are suppressed because of the contribution of strong force. Theoretical predictions for the relative contributions from the quark anti-quark annihilation is 10% and from gluon-gluon fusion is 90%.

There exists also the single top production. It is though electroweak processes $q_1\overline{q_2} \to t\overline{b}$ or $q_1 b \to q_2 t$ and though QCD electroweak process $gb \to tW^-$.

Top quark can decay only through the weak interaction $t \to W^+ b$ or $\overline{t} \to W^- \overline{b}$ with branching ratio almost 100%. The other decay channels to Ws and Wd are

suppressed by the square matrix elements V_{ts} and V_{td} of CKM matrix. Because of SM prediction of $V_{td} : V_{ts} : V_{tb} = 0.01 : 0.04 : 0.99$ the decay to b quark is dominant.

The top quark decay width Γ_t is according to the SM [10]:

$$\Gamma_t = \frac{G_F m_t^3}{8\pi\sqrt{2}} \left(1 - \frac{M_W^2}{m_t^2}\right)^2 \left(1 + 2\frac{M_W^2}{m_t^2}\right)^2 \left[1 - \frac{2\alpha_s}{3\pi}\left(\frac{2\pi^2}{3} - \frac{5}{2}\right)\right] \tag{3.2}$$

where G_F is Fermi constant, m_t and M_W is top quark mass and W boson mass respectively and α_s is strong coupling constant. Terms of order m_b^2/m_t^2, α_s^2 and $\alpha_s M_W^2/\pi m_t^2$ or higher are neglected. However when higher electroweak orders and α_s QCD corrections are included, the total theoretical uncertainty is less then 1%. Using numerical expressions in Equation (3.2) and setting $m_t =$ 172.5 GeV the top quark decays width is 1.5 GeV. The top quark decay before it can hadronize to top-flavored hadrons or $t\bar{t}$ mesons (toponium). That is because its enormous mass and thus the large decay width and short life time (in the order of $5 - 10 \times 10^{-24}$ s). So as a result this provides the unique opportunity to study the behavior of a "bare" quark.

Top and anti-top quark $t\bar{t}$ can decay into W boson and b quarks as $t\bar{t} \rightarrow W^- b$ $W^+\bar{b}$. Charged intermediate bosons W can decay to lepton ℓ and relevant neutrino ν_ℓ as $W \rightarrow \ell\nu_\ell$ or into quark and anti-quark as $W \rightarrow q\bar{q}$. It means there are three possible final states: two leptons and two neutrinos $\ell\nu_\ell\ell\nu_\ell$, known as leptonic or dilepton channel where both W bosons decay leptonically to $\ell = e, \nu, \tau$. Lepton, neutrino, quark and anti-quark $\ell\nu_\ell q\bar{q}$, known as semileptonic or lepton+jets channel where one W boson decays hadronically to light quarks $q = u, d, s, c$ and the other W boson decays leptonically. And finally two quarks and two anti-quarks $q\bar{q}q\bar{q}$, known as hadronic or all-jets channel where both W bosons decay hadronically. In Table (3.1) are listed different branching fractions for the three different final states.

Decay channel	W boson decays	Branching fraction [%]
dilepton	$\ell\nu_\ell + \ell\nu_\ell$	10.27 ± 0.17
lepton + jets	$\ell\nu_\ell + q\bar{q}$	43.49 ± 0.27
all-jet	$q\bar{q} + q\bar{q}$	46.19 ± 0.48

Table 3.1: Predicted branching fractions for $t\bar{t}$ [11].

4 Background and $t\bar{t}$ process

In reconstruction of $t\bar{t}$ pairs there are apart from signal a lot of processes contributing to overall background. The production of $t\bar{t}$ pairs has a smaller cross section than the background events. That is why we need to develop various analysis techniques to diminish background and than be able to study properties of the top quark.

Most of the background events originate from W or Z + jets processes that contains a real lepton which can pass lepton identification criteria. QCD background refers to events where the lepton does not come from the decay of a W or

Z boson. These include lepton and missing energy fakes as well as semileptonic B decay.

But there still are background processes of higher or comparable cross section:

- signal: $pp \to t\bar{t}$, $t\bar{t}$ decaying in single lepton channel;
- W + jets: $pp \to WX$, $W \to l\nu_l$;
- Z + jets: $pp \to ZX$, $Z \to l^+l^-$;
- dilepton background: $pp \to t\bar{t}X$, $t\bar{t}$ decaying in dilepton channel;
- single top background:
  - $pp \to tX$, W from t decaying leptonically;
  - $pp \to tWX$, one W decaying leptonically;
- QCD background: $pp \to$ jets, one jet is identified as lepton, this background is called instrumental; however QCD background is not considered in out analysis because the total contribution compared to the signal is about 2%,

where X is other particles.

One can find out that signal and background events are dissimilar due to production of at least two b-jets in $t\bar{t}$ events than in background events. The single top, the W + jets, Z + jets and dilepton background have very comparable signature as the $t\bar{t}$. The single top background has the most similar one: the top quark produces a b-jet, lepton and missing transverse energy and other jets can be produced along. Fortunately, the single top background has a small cross section. The W + jets background is the most significant background, it is similar to $t\bar{t}$ events because of large and real missing transverse energy, one high p_T lepton and high p_T jets. But in general, the number of high p_T jets are smaller.

5 ALPGEN and MC@NLO

The ALPGEN generator [12] is a collection of codes for the generation of multi-parton processes in hadronic collisions. The code performs, at the leading order in QCD and EW interactions, the calculations of the exact matrix elements for a large set of parton-level processes. Parton-level events are generated, providing full information on their color and flavor structure, enabling the evolution of the partons into fully hadronised final states.

Matrix element generators compute real emissions diagrams before starting the shower. Process is calculated at LO, some of the diagrams contribute to the NLO cross section. But there are two problems: First are divergent diagrams and the second problem is double counting that is why we need proper matching to shower. To solve this problem we need a cut-off parameter. Solutions can be found in matching of ME and parton shower. There exist various matching schemes, most common are CKKW and MLLM. They generate parton matrix elements according to the LO cross section and generate parton-level events. Then they add parton showering which can double count the ME events and then they remove double counting through various schemes involving jet-like reconstruction.

Parton shower Monte Carlos (MC) provide more general and flexible tools compared to next-to-leading-order (NLO) computations. The reason why the MC are so popular among experimentalists is that they provide a faithful description of the real events detected by real experiments. However, NLO computations have theirs advantages; they can handle hard emissions and they can estimate total rates with better accuracy than MC. The role of observables, the presence of negative contributions and the necessity of considering inclusive quantities in order to get rid of infinities are emphasized. MC@NLO [13] is a Parton Shower Monte Carlo (PSMC) which works just like any other PSMC. It outputs events similar to those seen in detectors. The defining feature of MC@NLO is that partonic hard sub processes are computed by including the full next-leading-order (NLO) QCD corrections. Including NLO corrections it provides the only way to sensibly compute the K factors event by event and use this information in detector simulation.

As far as the NLO calculations are concerned, the others QCD approximations are not performed, neither at the level of matrix elements, nor at the level of phase space. The subtraction method is adopt in order to cancel the infrared divergences that occur in the intermediate steps of the computation. MC@NLO has a couple of characteristics. The output is a set of events, which are fully exclusive. Total rates are accurate to NLO. The results of NLO for all observables are recover upon expansion of MC@NLO results in α_s. Hard emissions are treated as in NLO computations. Soft or collinear emissions are considered as in MC. The matching between hard and soft emission region is smooth and MC hadronization models are adopted. The JIMMY Generator generates multiple parton scattering events in proton-proton collisions. An event can have ± 1 weight originating from the MC@NLO approach. This weight has to be correctly taken into account when histogram are filled.

6 Selection rules for data analysis

The main goal of this section is to choose a suitable selection criteria to distinguish signal from the backgrounds processes. But first of all we will summarize basics facts about coordinate system used on ATLAS and about variables that we will use later.

The standard ATLAS coordinate system is defines as follows:

- x axis points to the center of the LHC ring;
- y axis points to the ground;
- z axis is parallel with the beam pipe.

An angle $\theta \in (0, \pi)$ is defined as the polar angle, the azimuthal angle $\phi \in (-\pi, \pi)$ and the radial coordinate r which is the radial distance from the origin of coordinate system, describe a cylindrical coordinate system. The interaction point of the pp collision is set to be the origin of ATLAS coordinate system.

At hadron colliders, it is useful to work with variables which are not very sensitive to the boost of the particle interaction. As the initial momentum transfer of the pp interaction is not known, most coordinates are parametrized as Lorentz-vectors as a function

Pseudorapidity η is a commonly used spatial coordinate describing the angle of a particle relative to the beam axis defined as:

$$\eta = -\ln\left(\tan\frac{\theta}{2}\right), \tag{6.1}$$

where θ is the angle between the particle momentum $\mathbf{p}$ and the beam axis.

In general it is useful to parametrize the distance between two object in η and ϕ space through a variable called the cone distance defined as:

$$\Delta R = \sqrt{(\Delta\eta)^2 + (\Delta\phi)^2}. \tag{6.2}$$

The variable ΔR expresses the angular difference of two objects, where $\Delta\eta$ and $\Delta\phi$ are the differences of the pseudorapidities and the azimuthal angles. It is also invariant to the boost along the z axis because as $\Delta\eta$ and as $\Delta\phi$ are invariant to the boost along the z axis.

Transverse momentum p_T of given particle with the momentum is the magnitude of the particle's momentum $\mathbf{p}$ projected to the xy plane. It can be also expressed as $p_T = \sqrt{p_x^2 + p_y^2} = |\vec{p}| \sin\theta$.

The W boson transverse mass m_T^W is defined as

$$m_T^W = \sqrt{2p_T^\ell p_T^\nu \left(1 - \cos\left(\phi^\ell - \phi^\nu\right)\right)}, \tag{6.3}$$

where p_T^l or p_T^ν are traverse momentum and ϕ^l or ϕ^ν are azimutal angles of the ℓ - lepton or ν - neutrino respectively.

In this section we will focus only on signal, Z + jets and W + jets backgrounds.

We consider following cuts in order to diminish relevant backgrounds:

1. Cut on the missing transverse energy greater then 30 GeV. This cut enhances the backgrounds with hard, high p_T neutrinos, reducing mainly Z + jets and QCD.

2. Exactly one muon or electron passing the lepton selection criteria that means transverse momentum $p_T > 20$ GeV for lepton. For muon channel the pseudorapidity is $|\eta| < 2.5$ and for electron channel the pseudorapidity is $|\eta| < 1.37 \cup 1.52 < |\eta| < 2.5$.

   This diminishes backgrounds with no or more then one lepton, Z + jets, dilepton, QCD.

3. At least four jets passing the jet selection criteria on transverse momentum $p_T > 25$ GeV and pseudorapidity $|\eta| < 2.5$.

   Diminishes mainly W + jets background but also the other ones because events from this background have usually lower number of high p_T jets compared to $t\bar{t}$ events

4. Cut on W boson transverse mass $m_T^W > 30$ GeV reduces Z + jets background and QCD, that is backgrounds without neutrinos from hard processes.

5. Cut on the number of b-jets, this should diminish W + jets and Z + jets backgrounds, actually it reduces all of them. In the analysis we require at least two b jets in the event.

Cuts that were applied in the analysis, in this order are:

1. Cut on the missing transverse energy;
2. Cut on the W boson transverse mass;
3. Cut on the lepton transverse momentum;
4. Cut on the lepton pseudorapidity;
5. Cut on the jet transverse momentum;
6. Cut on the jet pseudorapidity;
7. Cut on the number of jets;
8. Cut on the number of b tagged jets.

The numbers of events that passed our cuts are shown in Figure (6.1). In the first column is the number of event before any cuts were performed. Values are higher before cut because we didn't consider the QCD background. In the next columns are numbers of events that passed particular cut plus that passed the previous cuts. For example the number of events that passed cut on the W boson transverse mass is a number of events that passed this cut plus cut on the missing transverse energy etc. The number of events is reduced after first cut on the missing energy to the third and after last cut on the number of b jets where

we require at least two b jets is reduced to the tenth of the initial number of events of MC $t\bar{t}$ pairs.

Cumulative cut efficiency is a ratio of number of events after some particular cut and number of events before any cut were performed. So we always compare the numbers of events that pass various cuts to the numbers of events before any cut was executed. Relative cut efficiency is that a ratio of number of events after some particular cut and number of events after the previous cut.

The relative cut efficiency is shown in Figure (6.2) and the cumulative cut efficiency is in Figure (6.3).

The cut on the missing transverse energy has a better efficiency about 15% than a cut on the W boson transverse mass. The cut on the number of jets and jets transverse momentum or pseudorapidity have almost the same efficiency. Only a third of events passes these cuts. However the cut on the numbers of b jets reduces a fifth of incoming events so it has the biggest efficiency of all used cuts. For example the background from $We\nu$ is diminished only by the cut on the number of the b jets. This is happening because this background doesn't have a b jet. On the other hand the background from Wbb has a b jet so it means that is can't be reduced by the cut on the number of the b jets. These combination of particular cuts ensures that the background is diminished enough. However, we aren't able to eliminate all backgrounds so some parts of it will always remain.

Data and generators are already after cut on the transverse momentum and after cut on the pseudorapidity. That is why the efficiency of the cut on the transverse momentum and pseudorapidity is so low.

From now we do a limitation on the number of b tagged jets to exactly two of them in the event. We choose these b tagged jets where the first b tagged jet has the highest value of transverse momentum and the second b tagged jet has the second highest value of transverse momentum from all considered b tagged jets that passed the selection criteria. In each figure the values of integral of given variable is written in the legend with prefix i.

In the next figures we present basics variables for jet, lepton and missing transverse energy as a default point for further analysis. In Figures (6.4) and (6.5) are shown transverse momentum and pseudorapidity for jet with the highest value of transverse momentum of all jets respectively. In Figures (6.6) and (6.7) are shown transverse momentum and pseudorapidity for lepton. And in figures (6.8), (6.9) and (6.10) are shown missing transverse energy and the x and y component missing transverse energy.

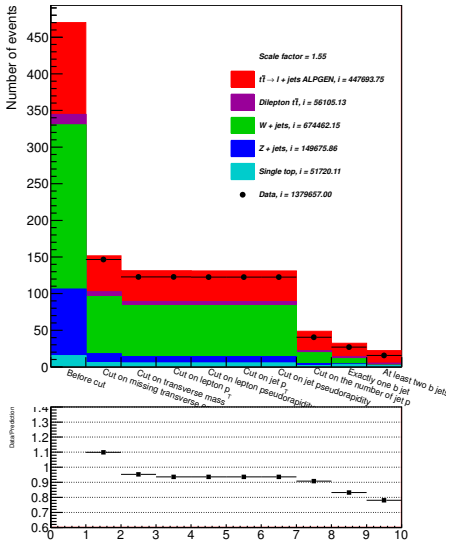

(a) ALPGEN in electron channel.

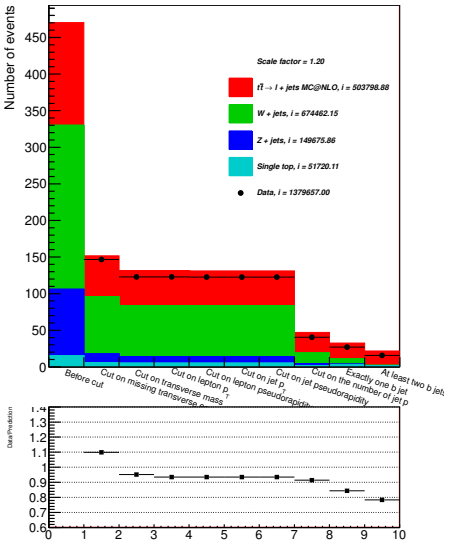

(c) MC@NLO in electron channel.

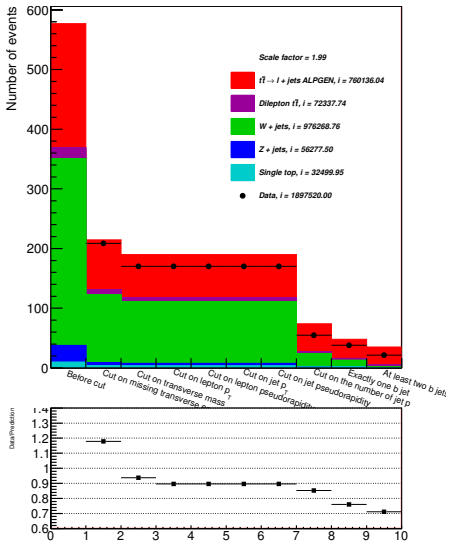

(b) ALPGEN in muon channel.

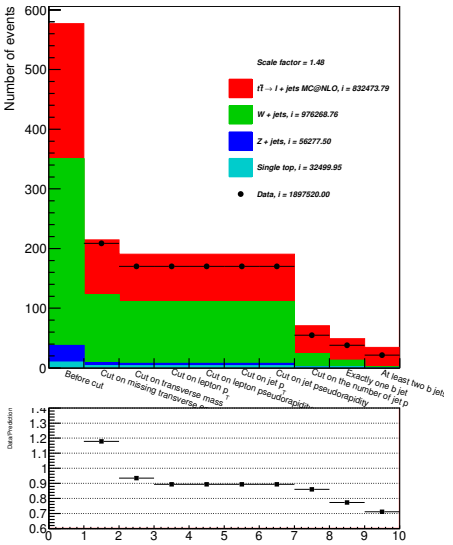

(d) MC@NLO in muon channel.

Figure 6.1: The numbers of events that pass the selection criteria (6). In the first column is number of events before any cut was performed. In the next columns are names of cuts and its respective number of event that passed relevant cut. Cuts are in order how they were performed in the analysis. Only cut on the number of b jets is splitted into two cuts. In the first cut on the number of b jets we require exactly one b jet and in the second cut on the number of b jets we require at least two b jets in the event. In the legend are shown all samples used in the analysis. Each sample was given a particular color. Black markers were assigned to data.

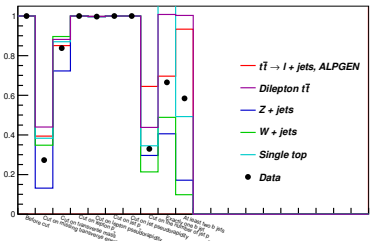

(a) ALPGEN in electron channel.

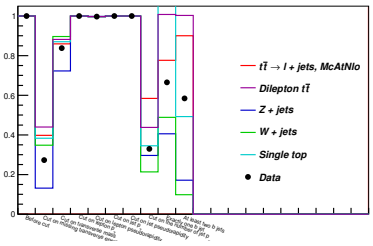

(c) MC@NLO in electron channel.

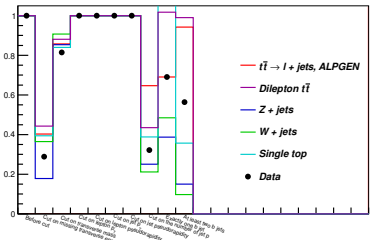

(b) ALPGEN in muon channel.

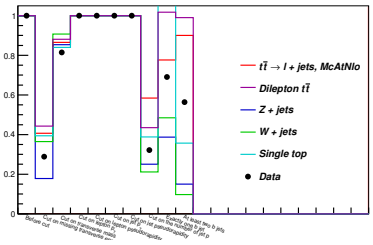

(d) MC@NLO in muon channel.

Figure 6.2: Relative cut efficiency. Is it a ratio of number of events after some particular cut and number of events after the previous cut.

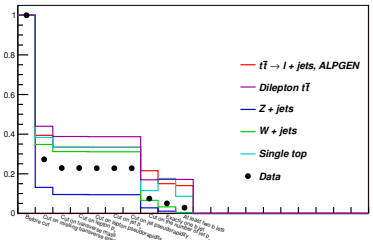

(a) ALPGEN in electron channel.

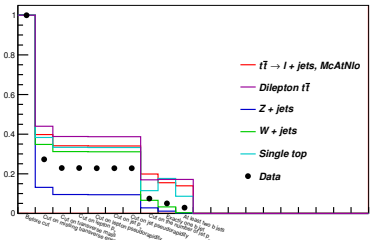

(c) MC@NLO in electron channel.

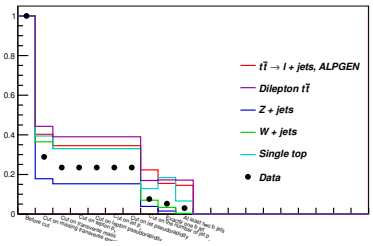

(b) ALPGEN in muon channel.

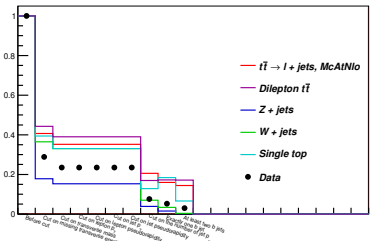

(d) MC@NLO in muon channel.

Figure 6.3: Cumulative cut efficiency. Is it a ratio of number of events after some particular cut and number of events before any cut were performed.

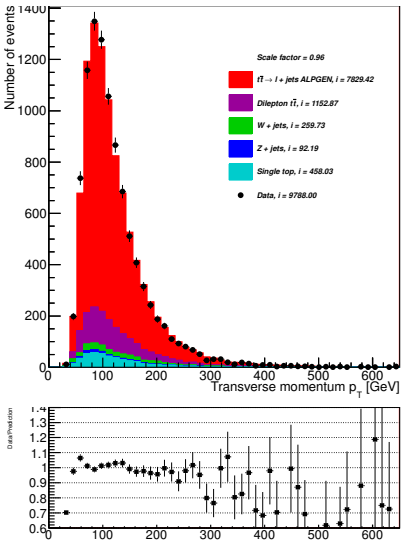

(a) ALPGEN generator and electron channel.

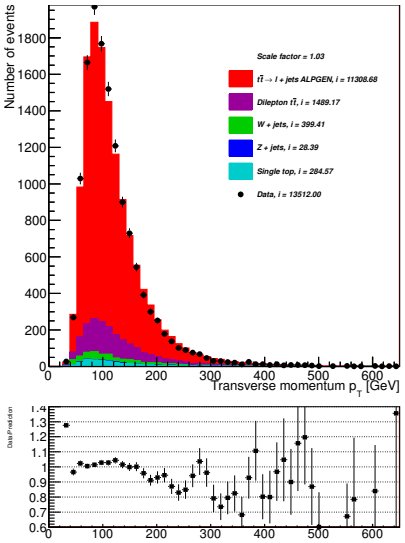

(b) ALPGEN generator and muon channel.

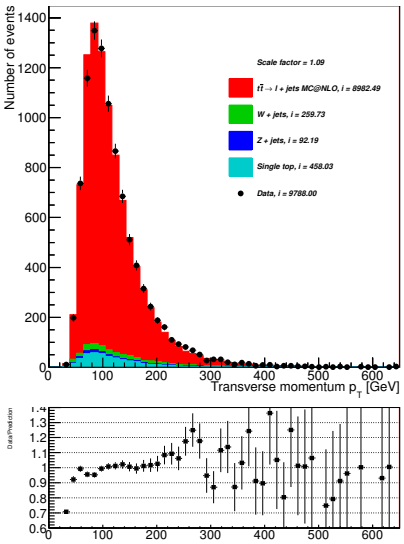

(c) MC@NLO generator and electron channel.

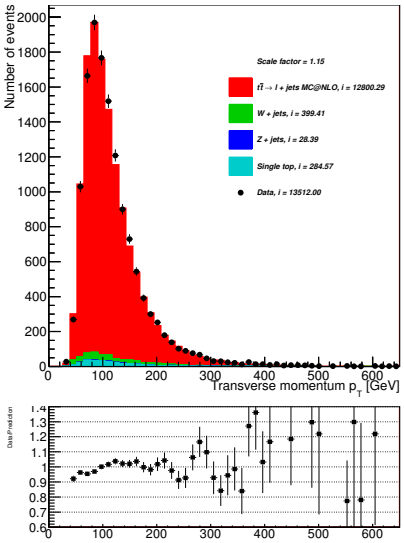

(d) MC@NLO generator and muon channel.

Figure 6.4: Transverse momentum of leading jet. That means jet with the highest value of the transverse momentum. In selection criteria jets were required to have transverse momentum $p_T > 25$ GeV.

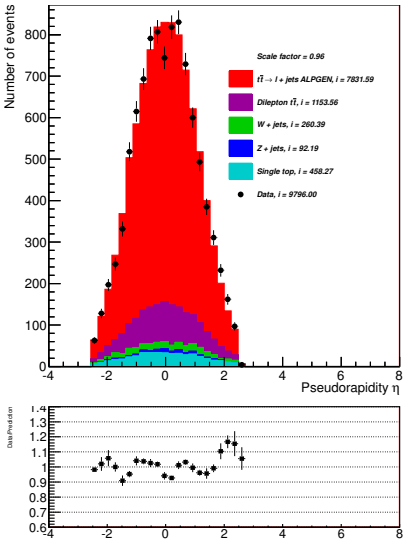

(a) ALPGEN generator and electron channel.

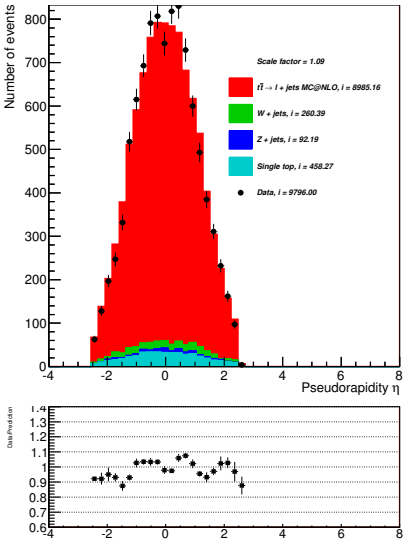

(c) MC@NLO generator and electron channel.

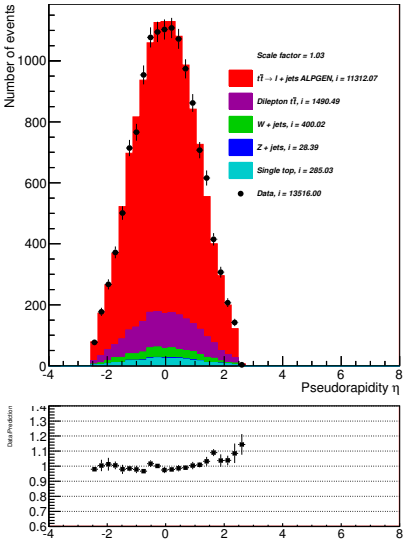

(b) ALPGEN generator and muon channel.

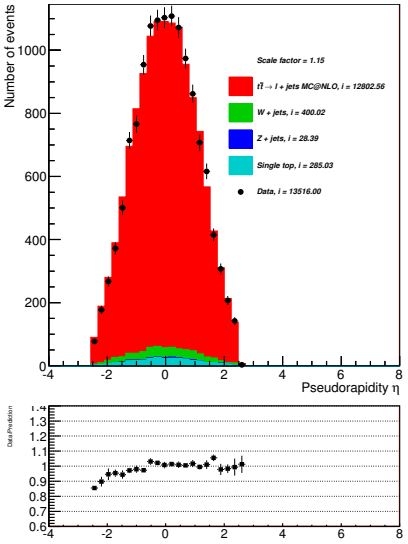

(d) MC@NLO generator and muon channel.

Figure 6.5: Distribution of pseudorapidity for jet with the highest value of the transverse momentum. Cut on the jet pseudorapidity is $|\eta| < 2.5$.

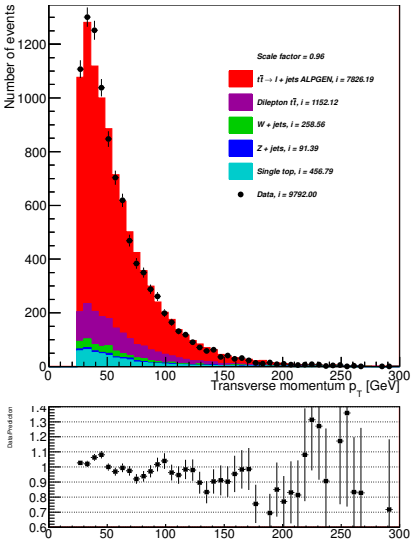

(a) ALPGEN generator and electron channel.

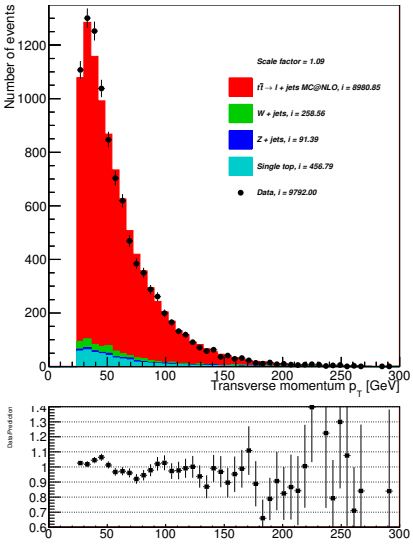

(c) MC@NLO generator and electron channel.

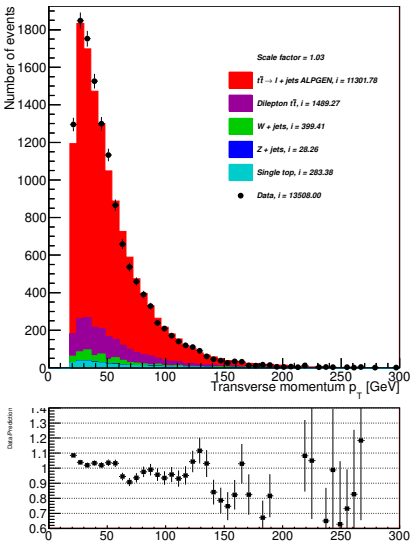

(b) ALPGEN generator and muon channel.

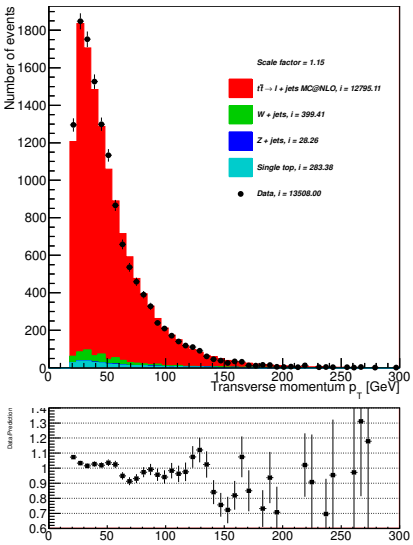

(d) MC@NLO generator and muon channel.

Figure 6.6: Lepton transverse momentum. Exactly one lepton is required in the selection criteria. Cut on the lepton transverse momentum $p_T > 20$ GeV.

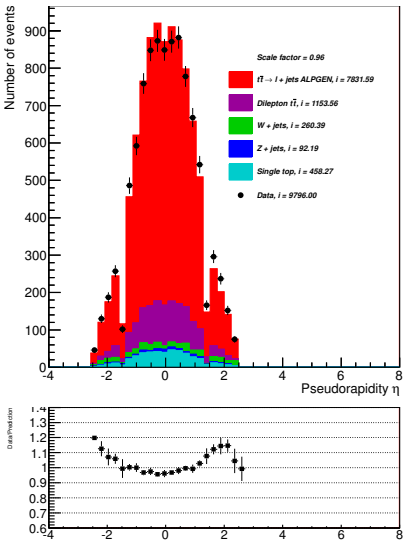

(a) ALPGEN generator and electron channel.

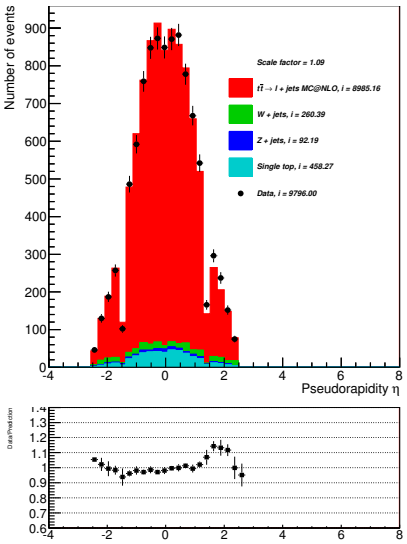

(c) MC@NLO generator and electron channel.

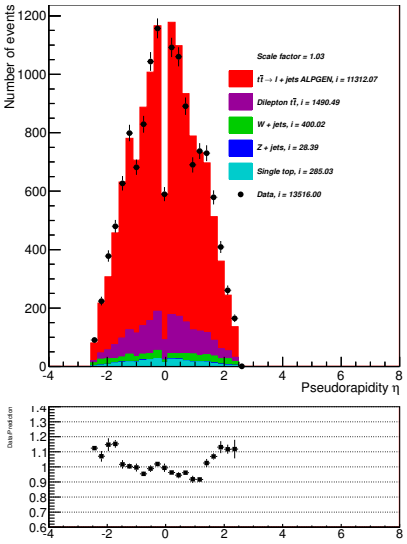

(b) ALPGEN generator and muon channel.

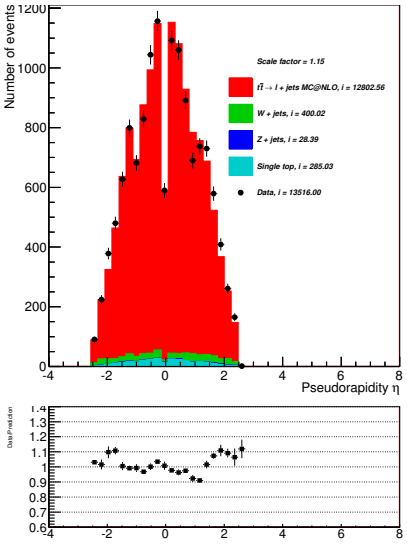

(d) MC@NLO generator and muon channel.

Figure 6.7: Distribution of lepton pseudorapidity. For muon channel the cut on the pseudorapidity is $|\eta| < 2.5$ and for electron channel the cut on the pseudorapidity is $|\eta| < 1.37$ or $1.52 < |\eta| < 2.5$.

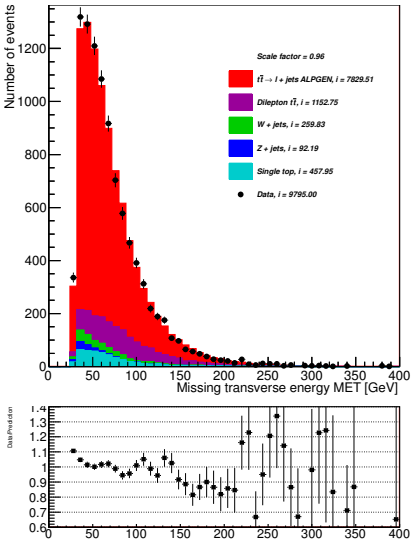

(a) ALPGEN generator and electron channel.

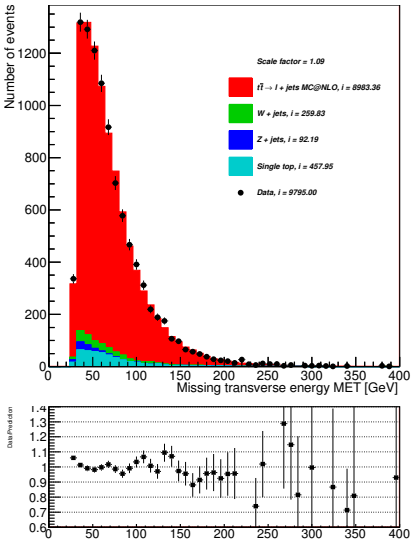

(c) MC@NLO generator and electron channel.

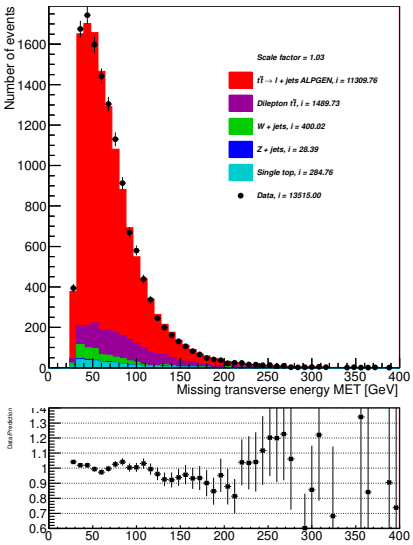

(b) ALPGEN generator and muon channel.

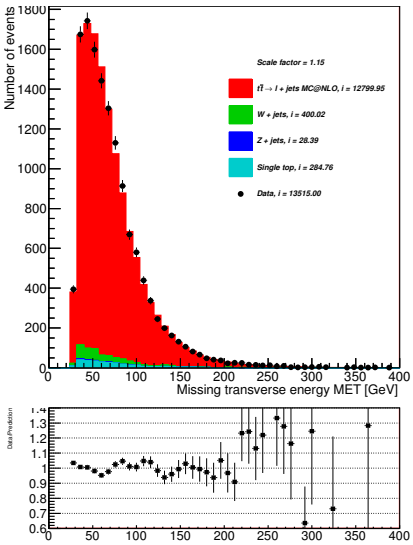

(d) MC@NLO generator and muon channel.

Figure 6.8: Distribution of missing transverse energy. It is used for x and y component of the neutrino fourvector as a first approximation.

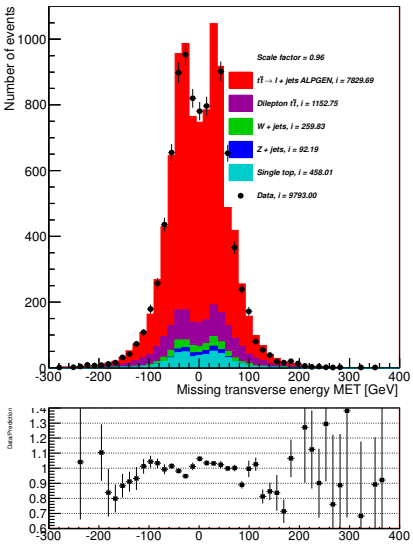

(a) ALPGEN generator and electron channel.

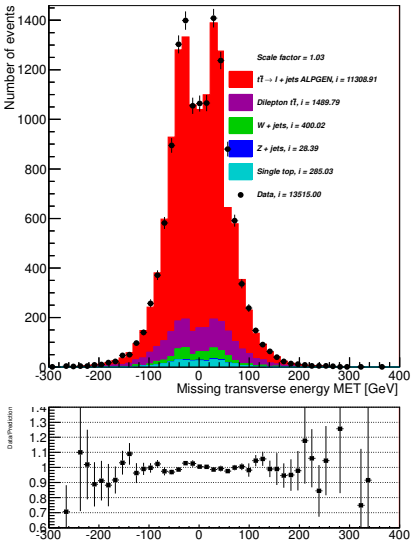

(b) ALPGEN generator and muon channel.

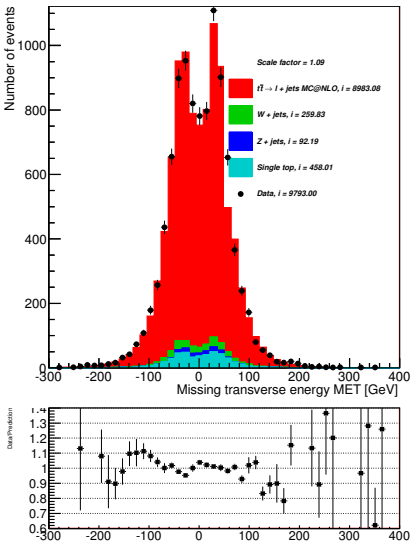

(c) MC@NLO generator and electron channel.

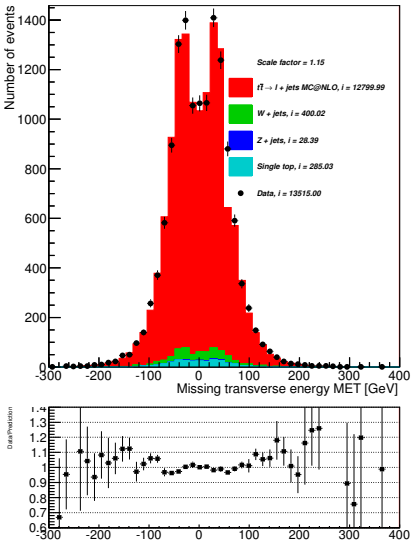

(d) MC@NLO generator and muon channel.

Figure 6.9: Distribution of the x component of missing transverse energy.

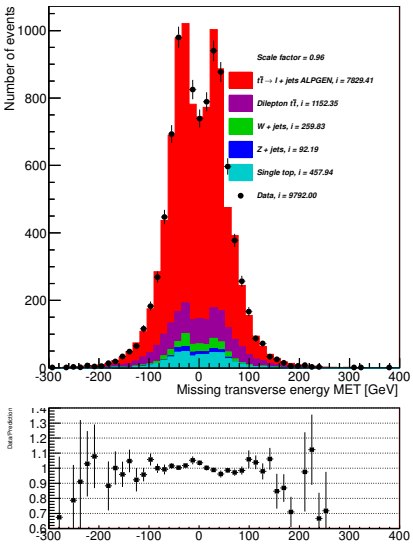

(a) ALPGEN generator and electron channel.

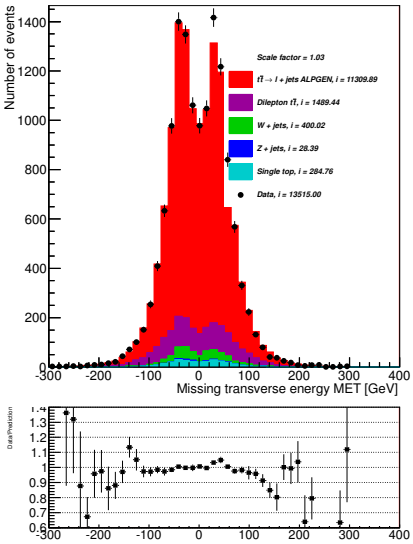

(b) ALPGEN generator and muon channel.

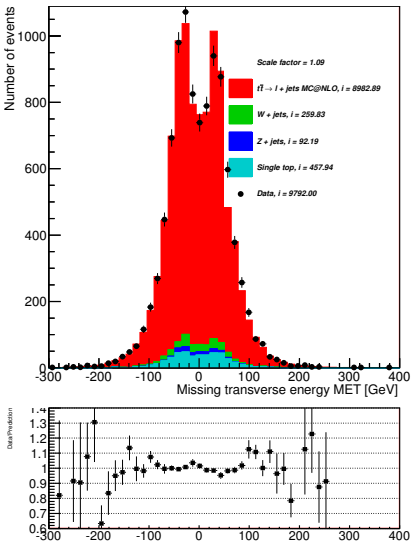

(c) MC@NLO generator and electron channel.

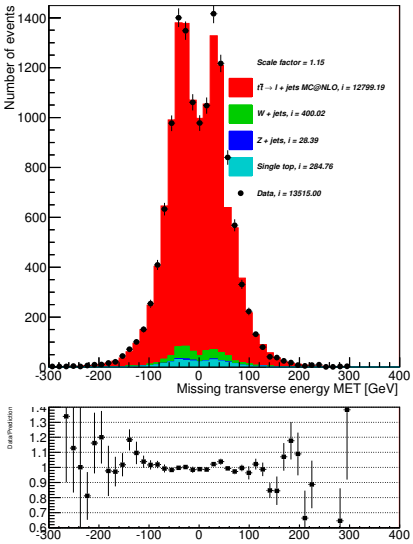

(d) MC@NLO generator and muon channel.

Figure 6.10: Distribution of the y component of missing transverse energy.

7 Data reconstruction

In this section we are going to study ALPGEN and MC@NLO samples as models of the $t\bar{t}$ events. Using Monte Carlo generator, one can generate an arbitrary number of events N. Our goal is to scale histograms to a unit luminosity so that these histograms can be compared. Eventually one scales it to data luminosity L_{DATA} (7.1) and compares with them. Normalization is based on cross sections of considered samples. Each sample is normalized by a weight corresponding to its own cross sections.

$$w = L_{\mathrm{DATA}} \frac{1}{L_{\mathrm{MC}}}, \tag{7.1}$$

where w is a weight which every sample is normalized and L_{MC} is luminosity counted as number of generated events divided by the cross section of each sample.

Events of $t\bar{t}$ pairs were simulated with the MC@NLO generator ($t\bar{t} \to \ell +$jets MC@NLO) and APLGEN generator interfaced with HERWIG [14] and JIMMY ($t\bar{t} \to \ell +$jets ALPGEN). The dilepton background was simulated with the same generators as signal sample. Background events W + jets and Z + jets were simulated APLGEN generator interfaced with JIMMY [15]. Due to the recommendation of ATLAS Top Group the single top background was simulated in t channel with AcerMC, in s channel with MC@NLO interfaced with JIMMY.

The data samples that were used in the analysis correspond to integrated luminosity of $L_{\mathrm{DATA}} = 4\,655.74$ pb^{-1} collected by the ATLAS detector at $s = 7$ TeV in 2011. All $t\bar{t}$ generator are normalized on approximate NNLO cross-section of 166.78 pb [16]. Data and samples from generators were analyzed in a data analysis framework ROOT [17].

At the reco level, the missing transverse energy is used for the component of transverse momentum and for azimuthal angle of neutrino.

The overall integral of data should be the overall integral of signal and background samples together. Because the signal from ALPGEN and MC@NLO generator doesn't correspond with data, we scaled the signal samples to data. The scales factor are listed in Table (7.1).

Yields from W transverse mass are in table (7.2) which is divided into two parts for electron and muon channel. For ALPGEN generator the signal is $t\bar{t} \to \ell$+jets plus dilepton $t\bar{t}$. MC@NLO generator isn't split because it contains dilepton $t\bar{t}$.

Number of jets which passed out selection criteria is shown in Figure (7.1). The smallest number of jets is four because we require at least four jets in it the event with given transverse momentum and pseudorapidity. MC@NLO generator is in agreement with data for smaller number of jets that 6. For bigger numbers of jets ALPGEN is better in description because it contains diagrams where $t\bar{t}$ pairs are produced by harder partons.

Figure (7.2) is a spectrum of W boson transverse mass for signal, W + jets, Z + jets background and for data. Histograms are normalized to unity. The cut on the missing transverse energy and the cut on the W boson transverse mass were not used. The different shape for backgrounds Z + jets and W + jets with signal $t\bar{t}X$, where X is other particle, is then clearly visible. Signal, data and W + jets background contain high energy neutrino which takes away some real missing energy. This does not happen with Z + jets plus one have to consider

the measurement uncertainty and the fluctuations. Therefore the peak for signal, data and W + jets background is around 80 GeV. For small transverse mass data differs from signal and W + jets background because data contains some contributions from Z + jets background and multijet. That is why cut on the W boson transverse mass diminishes Z + jets background and for this property cut was included into our selection criteria.

B jets take a important role in $t\bar{t}$ events with relatively low cross sections. There are always at least two of them. So that is why we want them to separate from the others jets. Identification of b jets, so called b tagging, is based on specific properties of B hadrons. They have a long lifetime, large mass and large branching ratio into leptons. The discrimination of b from light quark jets originates mainly in the relatively long lifetime of b flavoured hadrons, resulting in a significant flight path length. This leads to measurable secondary vertexes in tracking detectors and an impact parameters of the decay products.

In Figure (7.3) is shown the W boson transverse mass stacked histograms from more sub samples before cut on the number of b jets. However the other cuts were also performed. In Figure (7.4) is then shown the W boson transverse mass after b tagging and also after the other cuts. It is nicely demonstrated that cut on the number of at least two b jets reduces all types of backgrounds and that its use is essential for further analysis. Data/prediction fits closer to number one then before b tagging.

Generator	ALPGEN		MC@NLO	
Channel	Electron	Muon	Electron	Muon
k-factor	0.96	1.03	1.09	1.15

Table 7.1: Scale factors used to scale signal so that the total prediction matches the data for both generators and each channel.

Samples	Values
$t\bar{t} \to e$ + jets, ALPGEN	7829.46
Dilepton $t\bar{t}$, ALPGEN	1128.98
$t\bar{t} \to e$ + jets, MC@NLO	8961.90
W + jets	259.83
Z + jets	91.41
Single top	456.78
Data	9774
Expected S/BG for ALPGEN	11.08
Expected S/BG for MC@NLO	11.09

Samples	Values
$t\bar{t} \to \mu$ + jets, ALPGEN	11308.60
Dilepton $t\bar{t}$, ALPGEN	1463.60
$t\bar{t} \to \mu$ + jets, MC@NLO	12774.30
W + jets	399.46
Z + jets	28.25
Single top	283.19
Data	13488
Expected S/BG for ALPGEN	17.96
Expected S/BG for MC@NLO	17.97

Table 7.2: Yields for W transverse mass. Upper table is for ℓ + jets channel and lower table for μ + jets channel. S refers to the samples signal and BG to the background. Signal is divided into ALPGEN and MC@NLO generator respectively. $t\bar{t} \to \ell$ + jets, ALPGEN and dilepton $t\bar{t}$, ALPGEN are considered as signal for ALPGEN generator, $t\bar{t} \to \ell$ + jets, MC@NLO is considered as signal for MC@NLO generator. Samples from W + jets, Z + jets and from single top refers to the background. There is also shown expected ratio between signal and background for both generator and each channel.

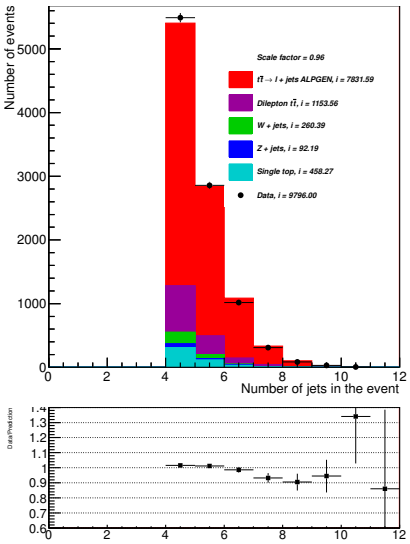

(a) ALPGEN generator and electron channel.

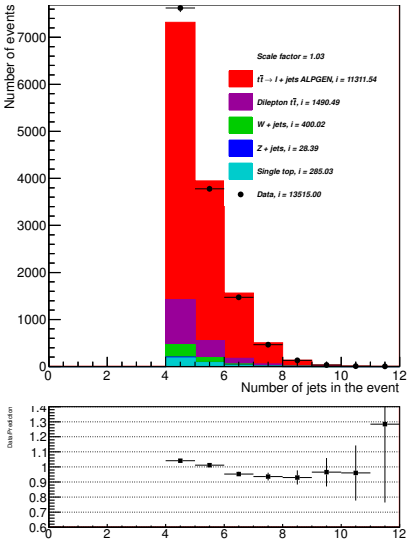

(b) ALPGEN generator and muon channel.

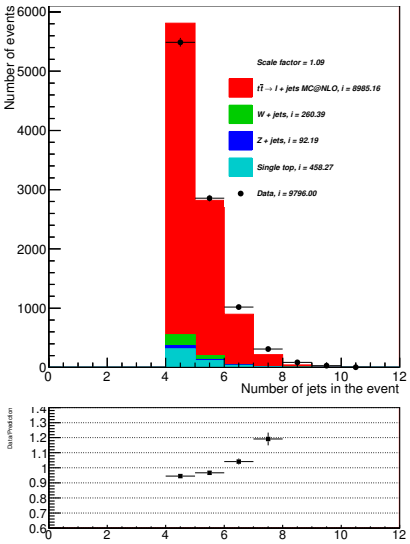

(c) MC@NLO and electron channel.

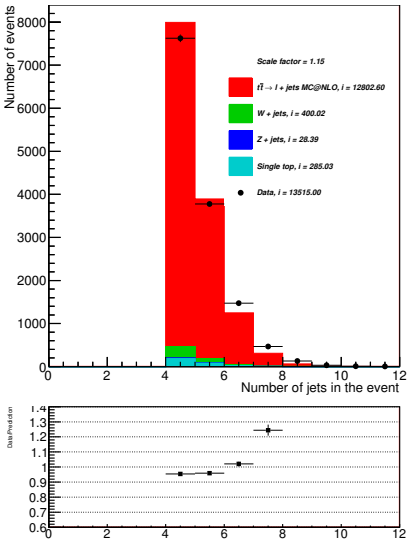

(d) MC@NLO and muon channel.

Figure 7.1: Number of jets distribution after all cuts were performed. There are always at least four jets in the event because of the cut on the number of jets.

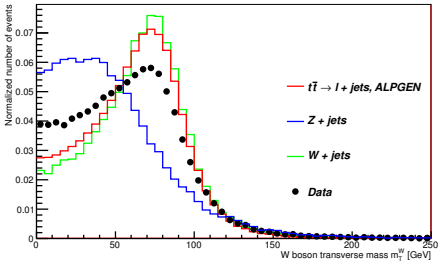

(a) ALPGEN generator and electron channel.

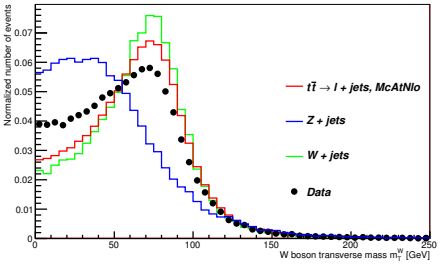

(c) MC@NLO generator and electron channel.

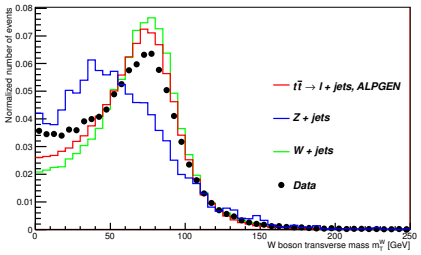

(b) ALPGEN generator and muon channel.

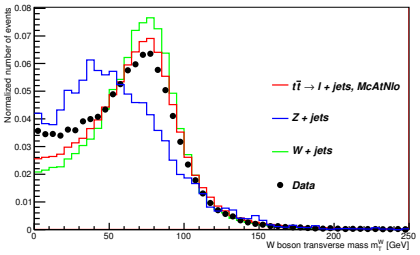

(d) MC@NLO generator and muon channel.

Figure 7.2: Spectrum of W boson transverse mass. Samples are normalized to unitary integral. Cut on W boson transverse mass and cut on the missing energy were not performed. Then the different shape of samples spectra is visible.

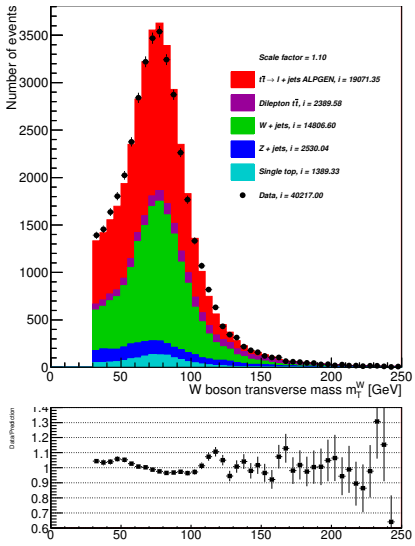

(a) ALPGEN generator and electron channel.

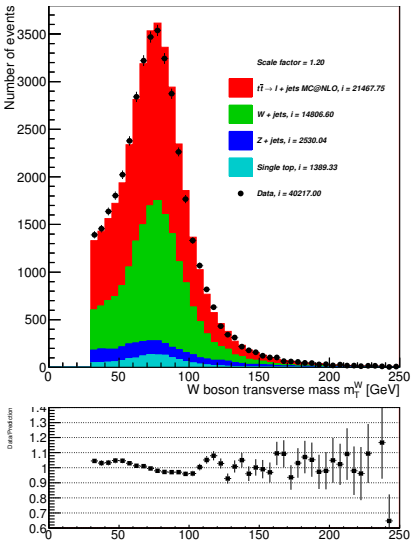

(c) MC@NLO generator and electron channel.

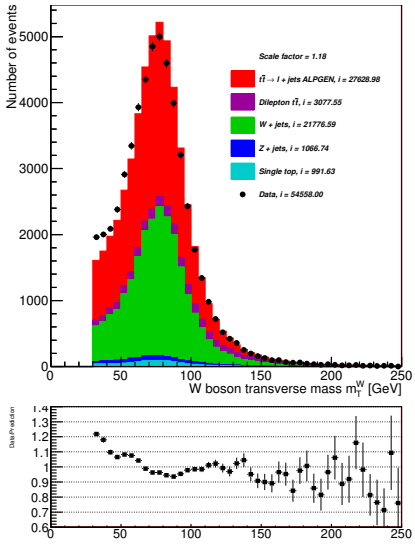

(b) ALPGEN generator and muon channel.

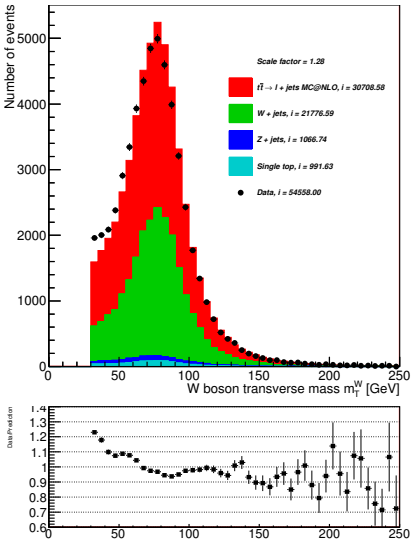

(d) MC@NLO generator and muon channel.

Figure 7.3: W boson transverse mass m_T^W computed from Equation (6.3) before the cut on the numbers of b jets.

In the Section (4) the signal and the background processes are described. As a signal we consider $t\bar{t} \to \ell + \text{jets}$ single lepton process. Everything else is for us consider as a background. It's useful to introduce a new variable called data/prediction. Data is integral of data sample, prediction is sum of integral over signal sample plus all backgrounds samples. The radio between them is data/prediction. The importance is in its ability to tell us if we have diminished all types of backgrounds. We assume that after integration the result of signal and background contributions are same as data contributions. So the data/prediction should be around number one. Then there are variables as the signal purity which is ratio of signal to signal plus backgrounds contributions. Signal significance is ratio of signal to the square root of background contributions.

To count the data/prediction we chose the W boson transverse mass distribution after b tagging (7.4) but spectrum of any variable could have been chosen.

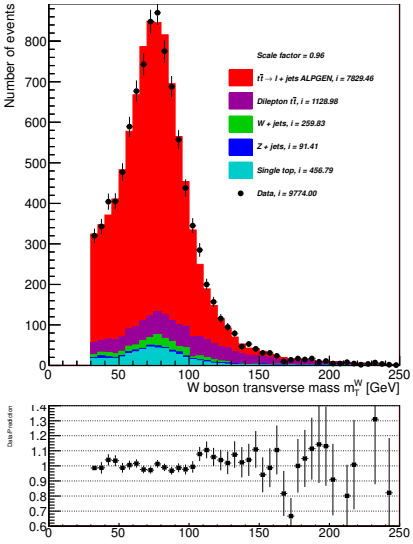

(a) ALPGEN generator and electron channel.

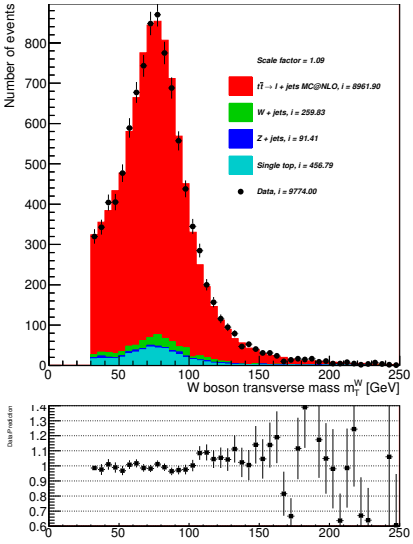

(c) MC@NLO generator and electron channel.

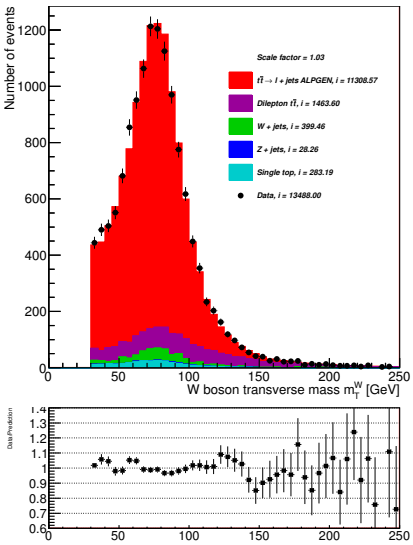

(b) ALPGEN generator and muon channel.

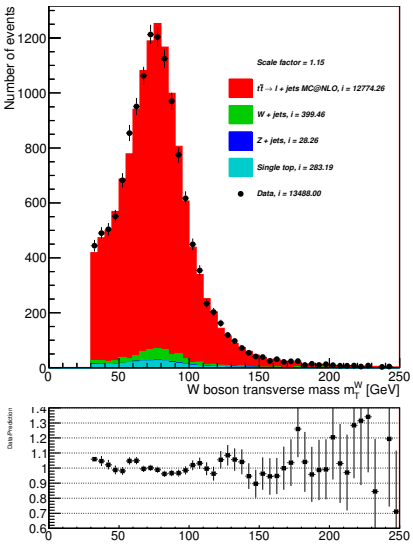

(d) MC@NLO generator and muon channel.

Figure 7.4: W boson transverse mass m_T^W computed from Equation (6.3) after cut on the numbers of b jets. At least two b jets were required in the event. Also the other cuts were performed. It is shown how b tagging diminishes all types of backgrounds. The difference before and after b tagging can be compared with Figure (7.3). Data/prediction fits better then before the cut on W boson transverse mass.

8 Top - antitop pairs reconstruction

For unstable, quickly decaying particles we cannot measure mass directly, but we can determine it from kinematics parameters of decay products. Therefore we specify an equivalent variable to energy E called invariant mass m_{inv} which is defined as:

$$m_{\text{inv}}^2 = \left(\sum_{l=1}^{n} P_l\right)^2 = \left(\sum_{l=1}^{n} E_l\right)^2 - \left(\sum_{l=1}^{n} \vec{p}_l\right)^2 \tag{8.1}$$

where P_l are four-impulses of n particles from reaction where a decays to n secondary particles c in the final state f:

$$a \to c_1 + c_2 + \ldots c_n. \tag{8.2}$$

If in the final state of interaction (8.2) these particles come from the decay of a bound state with mass m_{R}, the maximum in distribution m_{R}^2 is displayed at corresponding value with width that is usually dominated by the experimental resolution.

By requiring exactly one lepton passing our chosen cut described in Section (6), $t\bar{t}$ pairs have to decay through semileptonic channel $t\bar{t} \to W^- b W^+ \bar{b} \to \ell\nu_l b + q\bar{q}\bar{b}$ where the first W boson decays leptonically and the other hadronically. In this section we want to reconstruct invariant mass of $t\bar{t}$ therefore we need to reconstruct two W bosons and then the invariant mass of t and $\bar{t}$ quarks separately and finally reconstruct the $t\bar{t}$ pair. Just reminding that we have at least four jets in the event where two of them are b tagged. In the worst case scenario we have just two non b tagged jets that are used to restore the W boson invariant mass, than we have lepton and neutrino, missing transverse energy that is used to restore the other W boson invariant mass and two b tagged jets that are used with W boson to restore t or $\bar{t}$ quark.

1. Reconstruct W boson from hadronic decay $W \to q\bar{q}$.
   (a) Using two non b tagged light jets. The first jet has the highest value of transverse momentum and the second jet has the second highest value of transverse momentum
   (b) Using two non b tagged jets label as jet_i and jet_k with minimal value of $\Delta R\,(\text{jet}_\text{i}, \text{jet}_\text{k})$
2. Using Equation (8.3) to compute the z component of the neutrino four momentum. For the other components x, y we use missing transverse energy in the first approximation. Reconstruct W boson from neutrino and lepton.
3. Reconstruct individually t and $\bar{t}$ quark. Because we don't know how to assign b jets to W bosons we will do this four approaches:
   (a) To the hadronic and leptonic W boson assign b jet where both b jets will be tried. Then we have two entries per event.
   (b) Assign such a b jet to the lepton where $\Delta R\,(b\text{jet}, \text{lepton}) = \text{min}$. This b jet will be assign to the leptonic W boson and the other b jet to the hadronic W boson.

(c) Assign first b jet to the leptonic and second b jet to the hadronic W boson on the result of $\chi^2_{b1,b2,\text{fixed}}$ test described in Equations (8.4), (8.5).

(d) Assign first b jet to the leptonic and second b jet to the hadronic W boson on the result of $\chi^2_{b1,b2,\text{free}}$ test described in Equations (8.6), (8.7).

4. Do a cut on the W boson invariant mass.

5. Reconstruct invariant mass of $t\bar{t}$ pair and other kinematic variables.

In Figure (8.1) is displayed the invariant mass of hadronically decaying W boson reconstructed from two light non b tagged jets. These jets were chosen to have the highest value of transverse momentum where one light jet is jet with the highest value of transverse momentum of all non b tagged jets and the other light jet has the second highest value. The peak is about 80 GeV as expected so we consider this approach as suitable for use in the further analysis.

The invariant mass of hadronically decaying W boson reconstructed from two light non b tagged jets labeled as jet_i and jet_k with minimal value of $\Delta R\,(\text{jet}_\text{i}, \text{jet}_\text{k})$ is in Figure (8.2). We pick in each event all possible combination of light jets and we calculate their ΔR. In the end the W boson is reconstructed from jets with the minimal value of ΔR. The peak is around 80 GeV as well but there is for lower energies a sub peak from reconstructions where jets weren't assigned correctly. That is why we don't consider this approach as suitable and we will use the previous approach with two non b tagged jets where first jet has the highers value of the transverse momentum and the second jet has the second highers value of the transverse momentum of all non b tagged jets further in our analysis.

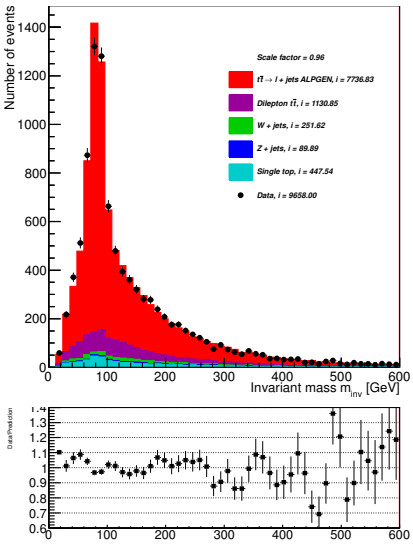

(a) ALPGEN generator and electron channel.

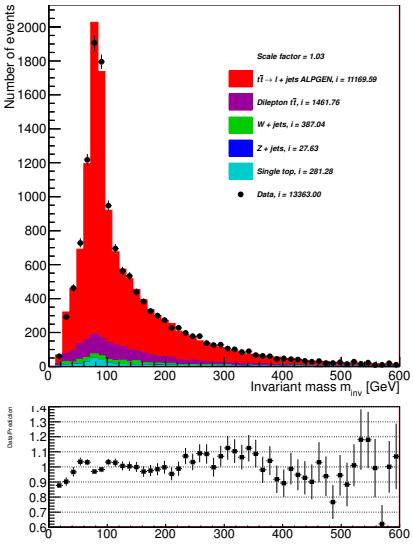

(b) ALPGEN generator and muon channel.

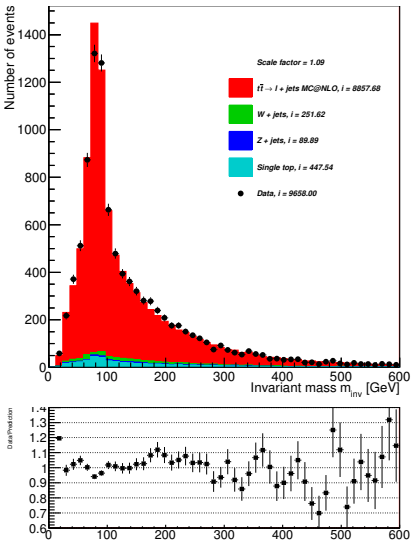

(c) MC@NLO generator and electron channel.

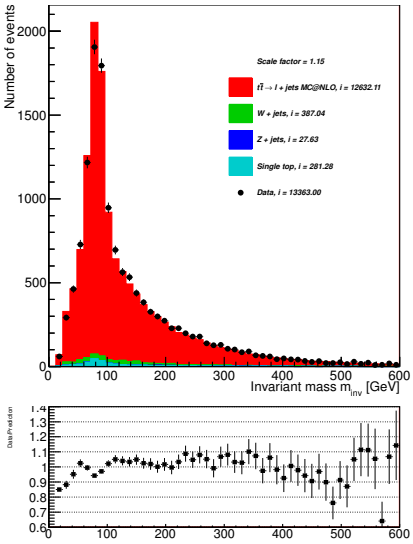

(d) MC@NLO generator and muon channel.

Figure 8.1: Invariant mass of hadronically decaying W boson reconstructed from two highest p_T non b tagged jets that passed the jet selection criteria.

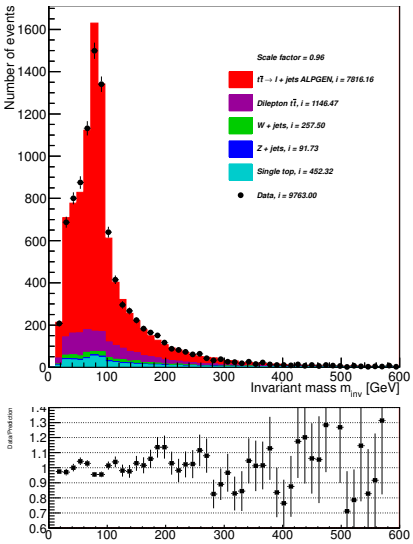

(a) ALPGEN generator and electron channel.

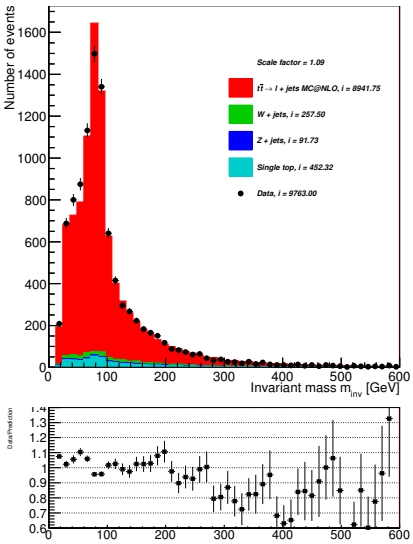

(c) MC@NLO generator and electron channel.

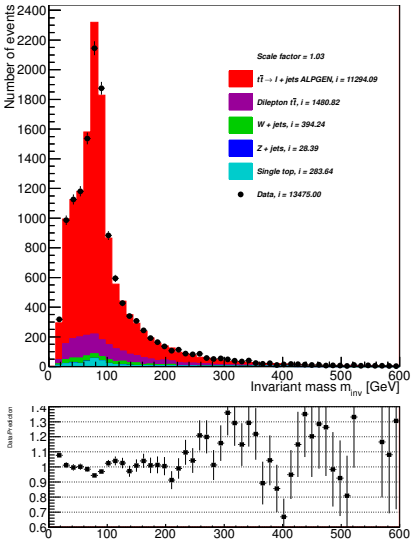

(b) ALPGEN generator and muon channel.

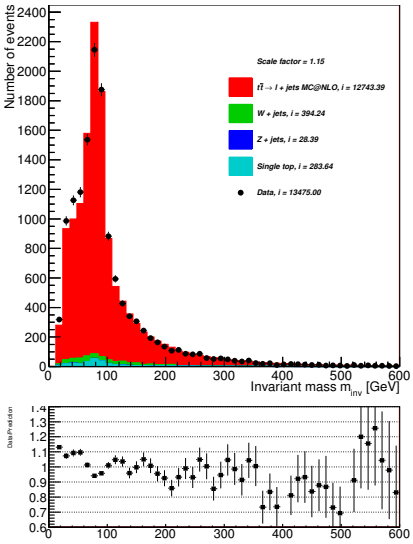

(d) MC@NLO generator and muon channel.

Figure 8.2: Invariant mass of hadronically decaying W boson reconstructed from two non b tagged (light) jets with minimal value of ΔR. Jets transverse momenta used $p_T > 25$ GeV.

The leptonically decaying W boson should have been reconstructed from lepton and neutrino. As we can't be able to detect the neutrino in the ATLAS detector so as the first approach we will use the missing transverse energy for x and y component of the neutrino instead of its transverse momentum. The initial value of the z component can be computed the condition of the expected m_T^W:

$$M_{\text{inv}}^2 \equiv (P_l + P_\nu)^2 = M_W^2 \equiv M^2(l, \nu)\,, \tag{8.3}$$

where P_x is the four momentum of particle x and M_W is mass of W boson. This leads to a quadratic equation, which has in general two solution $p_{z,\pm}^\nu$. If the discriminant in equation is smaller then zero, only the real part is taken. We neglected lepton and neutrino masses with respect to the mass of W boson.

The result for positive solution of $p^{\nu}_{z,+}$ component of Equation (8.3) and the result for negative solution of $p^{\nu}_{z,-}$ component is in Figure (8.3). It has been shown there is no difference in the position of W boson invariant mass peak for both solutions. The same results were obtained from the resting channel and generators. That is why we will use the negative $p^{\nu}_{z,-}$ solution of z component for the neutrino four vector which is smaller than for the positive $p^{\nu}_{z,+}$ solution in order to not have a large boost of the $t\bar{t}$ system along the z axis. Moreover for the negative solution $p^{\nu}_{z,-}$ data are in better agreement with MC then for the positive solution $p^{\nu}_{z,+}$. By choosing between two solutions we do a bias. The only difference between the positive and negative solution will show at the distribution of the pseudorapidity of the $t\bar{t}$ system which is anti symmetric, shown in Figure (9.7) in the Appendix.

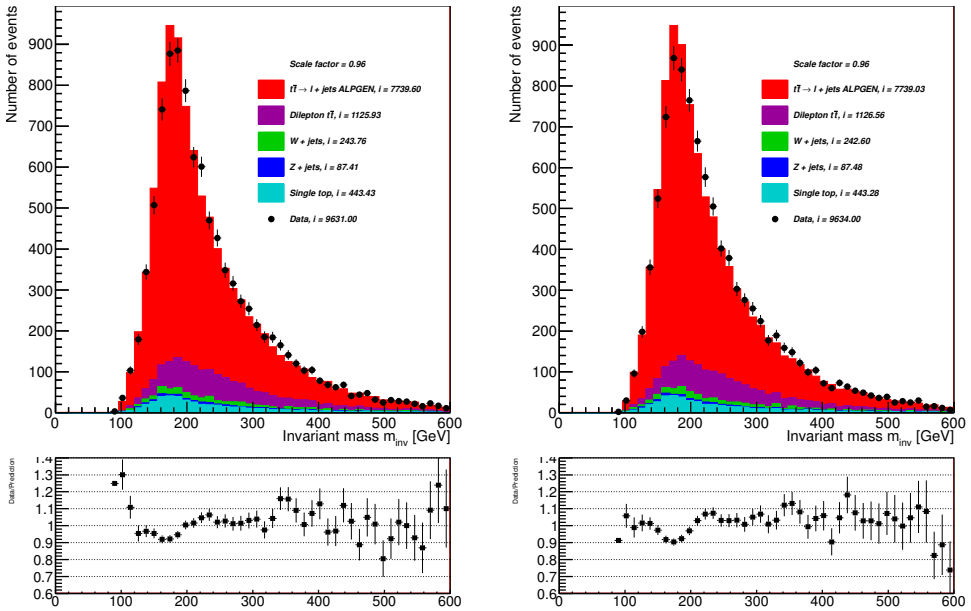

Figure 8.3: Invariant mass of the top quark reconstructed from leptonic W boson and b jets with the highest value of transverse momentum for ALPGEN generator and electron channel. On the left side is leptonic W boson consisting of lepton and neutrino where neutrino z component of four momentum is the negative solution $p^{\nu}_{z,-}$ and on the right side is with the positive solution $p^{\nu}_{z,+}$ of Equation (8.3).

In order to reconstruct the t quark invariant mass we need to know how to assign b jets to the W bosons. In the first approach we can assign first and second b jets to the W boson decaying leptonically and assign first and second b jets to the W boson decaying hadronically as well resulting in two permutations per event. Result are shown in Figures (8.4) and (8.5) respectively.

Now we will reconstruct the top quark invariant mass from condition on minimal value of $\Delta R\,(b\text{jet}, \text{lepton})$. This b jet we will assign to the leptonically decaying W boson because we except this b jet to be closer to the leptonically decaying W boson. The other b jet is then assigned to the hadronic W boson. Results are shown in Figures (8.6) and (8.7).

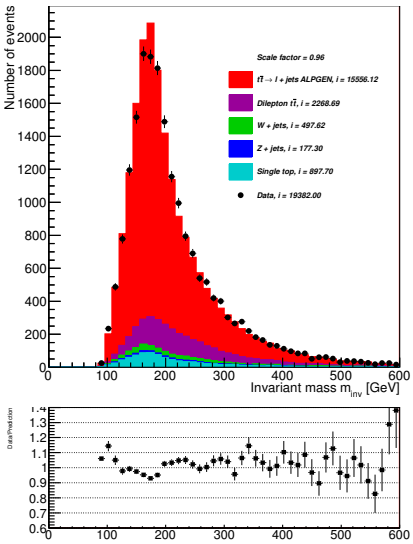

(a) ALPGEN generator and electron channel.

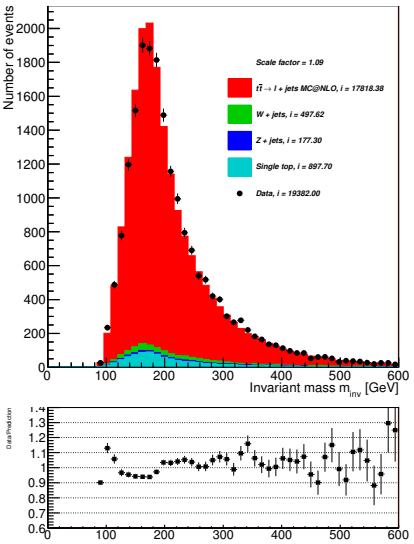

(c) MC@NLO generator and electron channel.

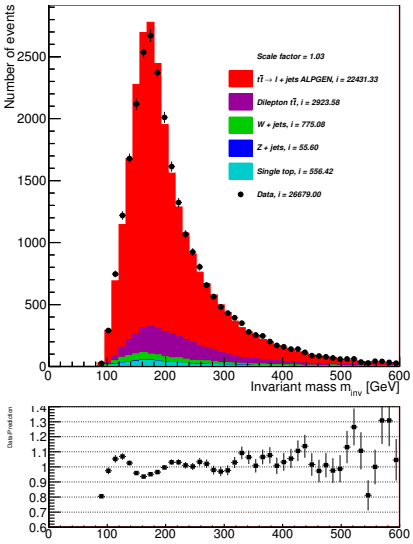

(b) ALPGEN generator and muon channel.

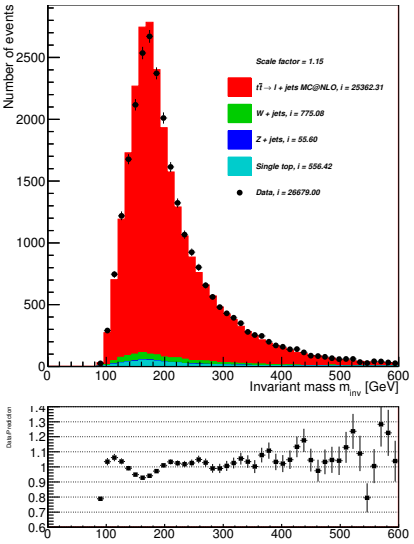

(d) MC@NLO generator and muon channel.

Figure 8.4: Invariant mass of the top quark reconstructed from the leptonic W boson b and a jet where both b jets were tried. In this case we have two entries per event.

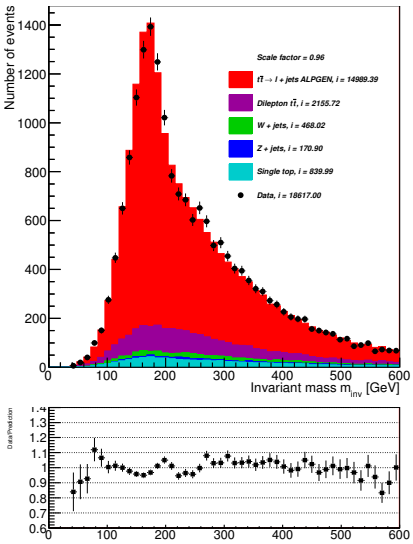

(a) ALPGEN generator and electron channel.

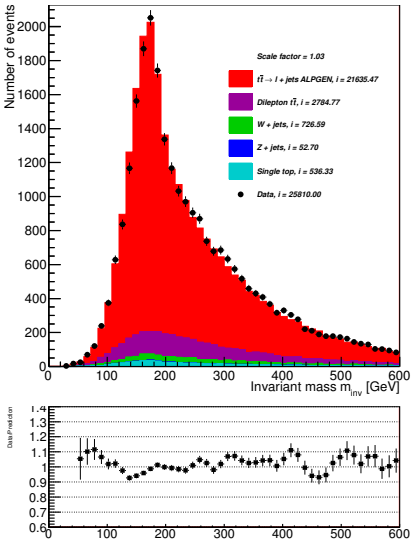

(b) ALPGEN generator and muon channel.

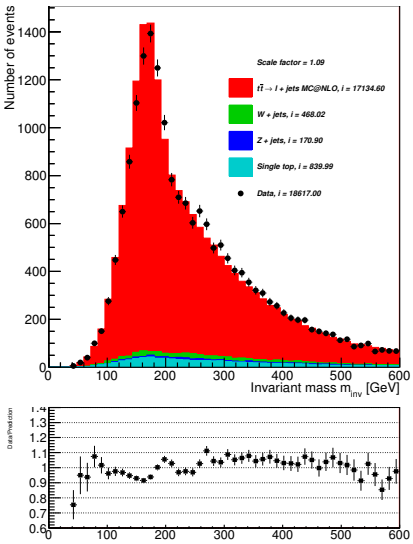

(c) MC@NLO generator and electron channel.

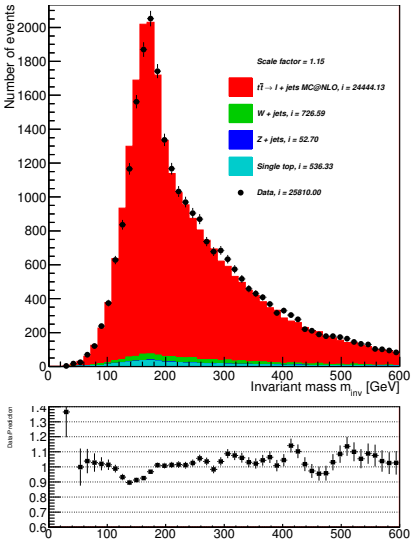

(d) MC@NLO generator and muon channel.

Figure 8.5: Invariant mass of the top quark reconstructed from the hadronic W boson and a b jet where both b jets were tried. In this case we have two entries per event from first and second b jet.

From now jet labels as $b1$ is the b jet with the largest value of transverse momentum and jet label as $b2$ is the b jet with the second largest value of transverse momentum.

The last two ways how to assign the b jets to the W boson is to introduce two pairs of new variables $\chi^2_{b1,b2,\text{fixed}}$, $\chi^2_{b2,b1,\text{fixed}}$ and $\chi^2_{b1,b2,\text{free}}$, $\chi^2_{b2,b1,\text{free}}$ described in Equations (8.4), (8.5) and (8.6), (8.6) respectively.

$$\chi^2_{b1,b2,\text{fixed}} = \frac{\left(m_{\ell\nu b1} - m^{\text{top}}\right)^2}{\sigma^2_{\ell\nu b1}} + \frac{\left(m_{jjb2} - m^{\text{top}}\right)^2}{\sigma^2_{jjb2}} \tag{8.4}$$

$$\chi^2_{b2,b1,\text{fixed}} = \frac{\left(m_{\ell\nu b2} - m^{\text{top}}\right)^2}{\sigma^2_{\ell\nu b2}} + \frac{\left(m_{jjb1} - m^{\text{top}}\right)^2}{\sigma^2_{jjb1}} \tag{8.5}$$

$$\chi^2_{b1,b2,\text{free}} = \left(m_{\ell\nu b1} - m_{jjb2}\right)^2 \tag{8.6}$$

$$\chi^2_{b2,b1,\text{free}} = \left(m_{\ell\nu b2} - m_{jjb1}\right)^2, \tag{8.7}$$

where $m_{\ell\nu b1}$ is the invariant mass of the leptonic W boson that consists of a b jet with the highest value of transverse momentum and with two non b tagged jets where first jet has the highest value of transverse momentum and the other jet has the second highest p_T, m_{jjb2} is invariant mass of the hadronic W that consists of a b jet with second highest value of transverse momentum and with two non b tagged jets where first jet has the highest value of transverse momentum and the other jet has the second highest value as well. Pole mass of the top quark is $m^{\text{top}} = 172.5$ GeV listed in Table (1.1). For $\sigma_{\ell\nu b}$ and σ_{jjb} were used RMS values from method where first and second b jet was assigned to the leptonic W boson and first and second b jet was assigned to the hadronic W boson as well resulting in two permutations per event, Figures (8.4) and (8.5). Typical values are $\sigma_{\ell\nu b} = 80$ GeV and $\sigma_{jjb} = 110$ GeV.

It is desired to find a smaller value of $\chi^2_{b1,b2,\text{fixed}}$ and $\chi^2_{b2,b1,\text{fixed}}$ indicating the consistency. When $\chi^2_{b1,b2,\text{fixed}}$ is smaller then $\chi^2_{b2,b1,\text{fixed}}$ then we assign $b1$ jet which has the biggest value of transverse momentum to the leptonic W boson and $b2$ jet which has the second highest value of transverse momentum to the hadronic W boson. If $\chi^2_{b2,b1,\text{fixed}}$ is smaller then $\chi^2_{b1,b2,\text{fixed}}$ then the assignment of the b jets is opposite. Results are shown in Figures (8.8), (8.9) for top quarks that consists of a leptonic and hadronic W boson plus b jets assign on the result of variables $\chi^2_{b1,b2,\text{fixed}}$, $\chi^2_{b2,b1,\text{fixed}}$ respectively and in Figures (8.10), (8.11) for top quarks consisting from leptonic and hadronic W boson plus b jets assign on the result of variables $\chi^2_{b1,b2,\text{free}}$, $\chi^2_{b2,b1,\text{free}}$ respectively.

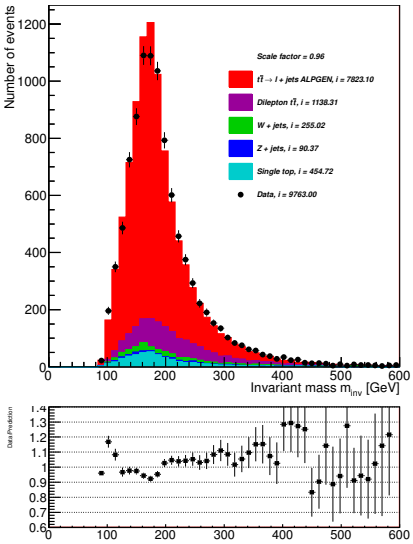

(a) ALPGEN generator and electron channel.

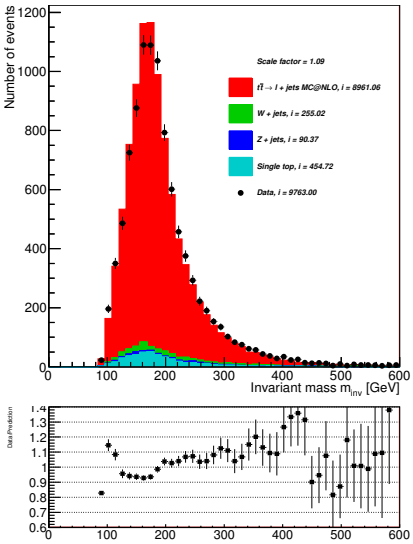

(c) MC@NLO generator and electron channel.

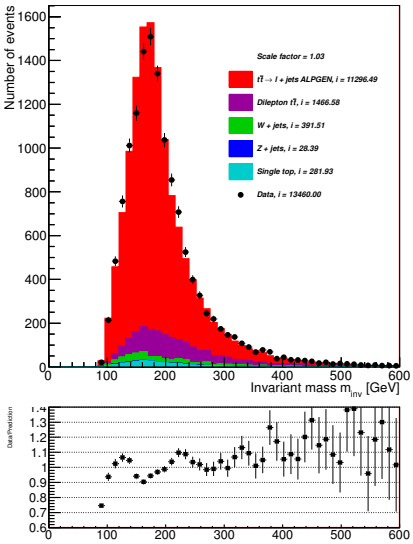

(b) ALPGEN generator and muon channel.

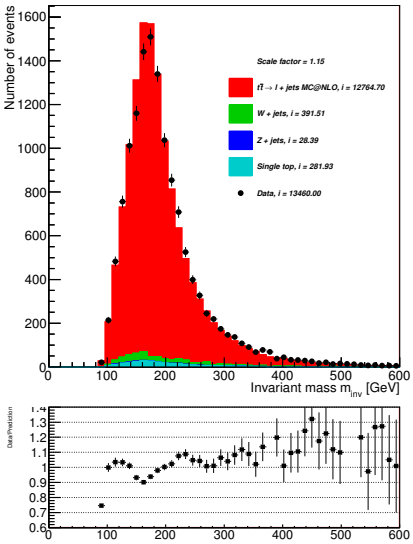

(d) MC@NLO generator and muon channel.

Figure 8.6: Invariant mass of the top quark reconstructed from the leptonic W boson and one b. The leptonic W boson is composed from lepton and neutrino. In our case we use missing transverse energy instead of the neutrino. We chose such a b jet closest to the lepton so we require the condition $\Delta R\,(b\text{jet}, \text{lepton}) = \text{min}$ to be met.

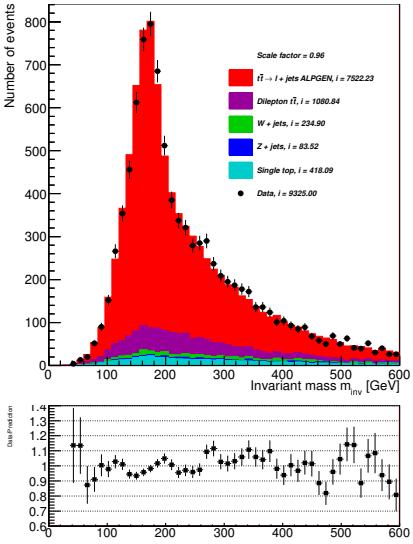

(a) ALPGEN generator and electron channel.

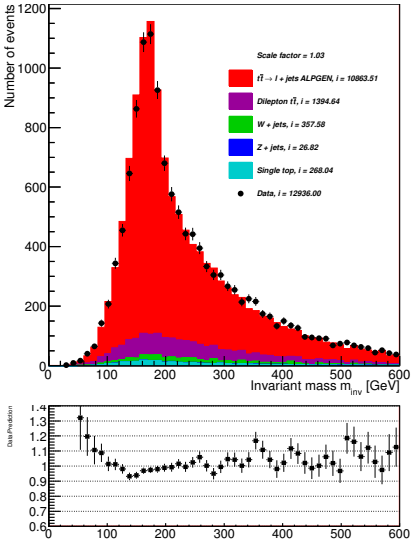

(b) ALPGEN generator and muon channel.

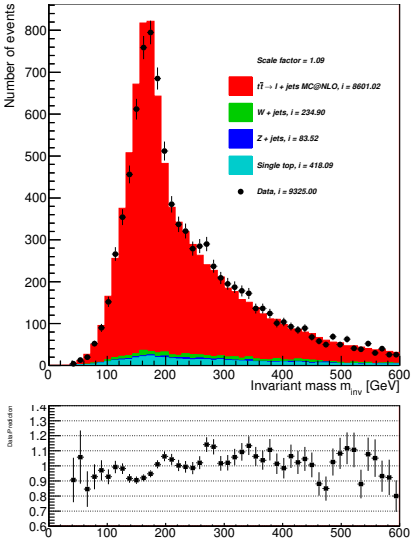

(c) MC@NLO generator and electron channel.

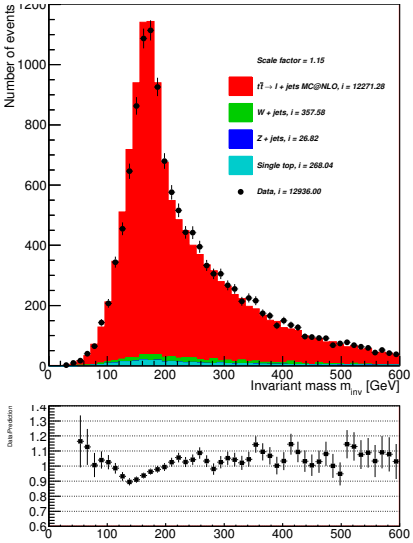

(d) MC@NLO generator and muon channel.

Figure 8.7: Invariant mass of the top quark reconstructed from the hadronic W boson and one b. The hadronic W boson is composed from two non b jets where first non b tagged jet has the highers value of transverse momentum and the other non b tagged jet has the second highest value. One b jet has been already assigned to the leptonic W boson by meeting the condition $\Delta R\,(b\text{jet}, \text{lepton}) = \text{min}$, see Figure (8.6). The remaining b jet is then assigned to the hadronic W boson.

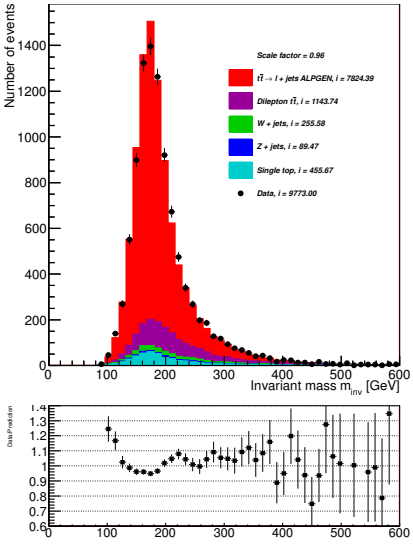

(a) ALPGEN generator and electron channel.

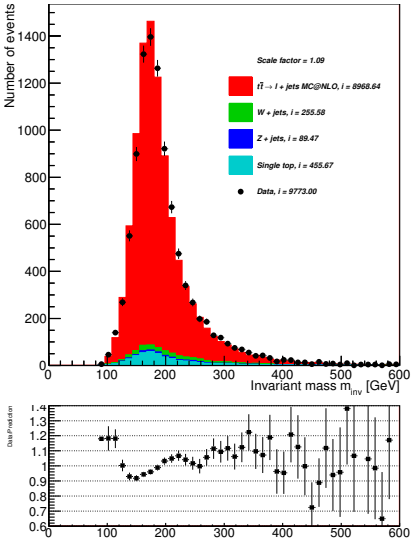

(c) MC@NLO generator and electron channel.

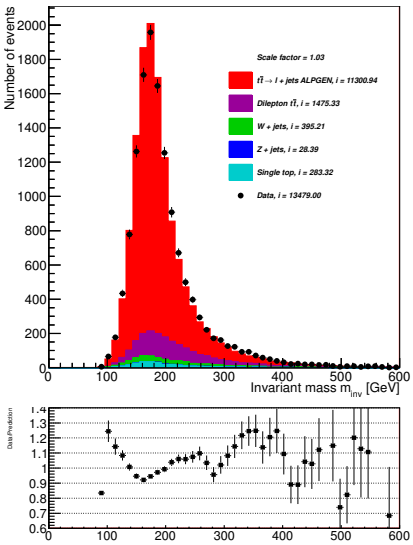

(b) ALPGEN generator and muon channel.

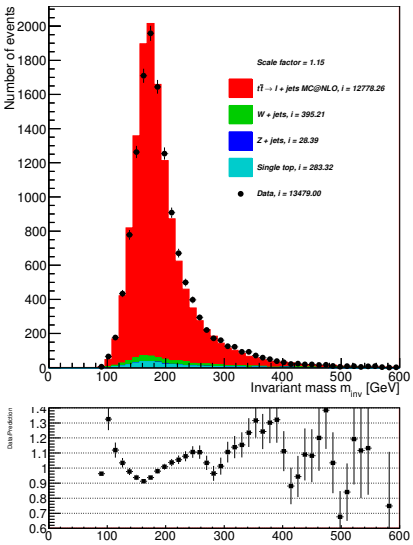

(d) MC@NLO generator and muon channel.

Figure 8.8: Invariant mass of the top quark reconstructed from the leptonic W boson and a b jet assigned based on the result of $\chi^2_{b1,b2,\text{fixed}}$ test described in Equations (8.4), (8.5). If $\chi^2_{b1,b2,\text{fixed}}$ is smaller then $\chi^2_{b2,b1,\text{fixed}}$, the b jet with highest value of p_T is assign to the leptonic W boson. The hadronic W boson is composed from two non b jets where first non b tagged jet has the highers value of transverse momentum and the other non b tagged jet has the second highest value.

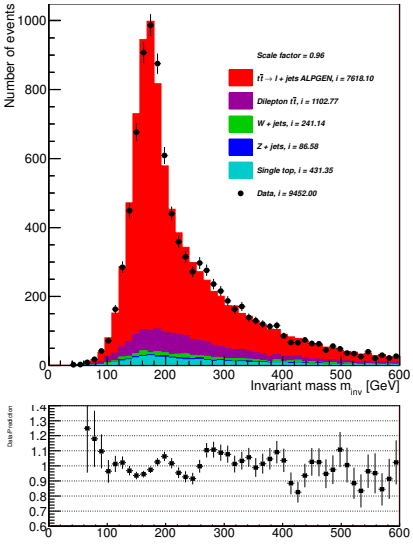

(a) ALPGEN generator and electron channel.

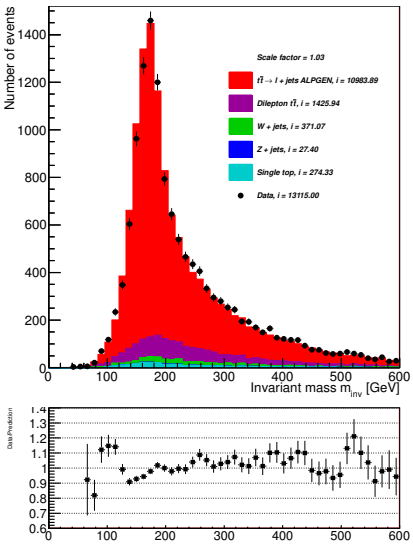

(b) ALPGEN generator and muon channel.

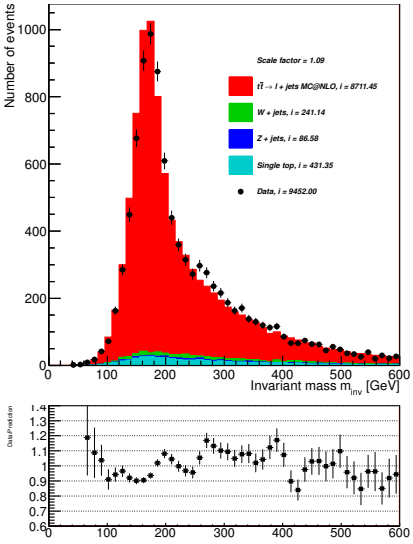

(c) MC@NLO generator and electron channel.

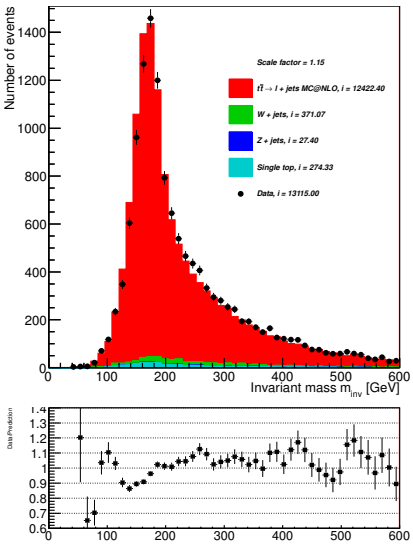

(d) MC@NLO generator and muon channel.

Figure 8.9: Invariant mass of the top quark reconstructed from the leptonic W boson and a b jet assigned based on the result of $\chi^2_{b1,b2,\text{fixed}}$ test described in Equations (8.4), (8.5). If $\chi^2_{b1,b2,\text{fixed}}$ is smaller then $\chi^2_{b2,b1,\text{fixed}}$, the b jet with highest value of p_T is assign to the hadronic W boson. The hadronic W boson is composed from two non b jets where first non b tagged jet has the highers value of transverse momentum and the other non b tagged jet has the second highest value.

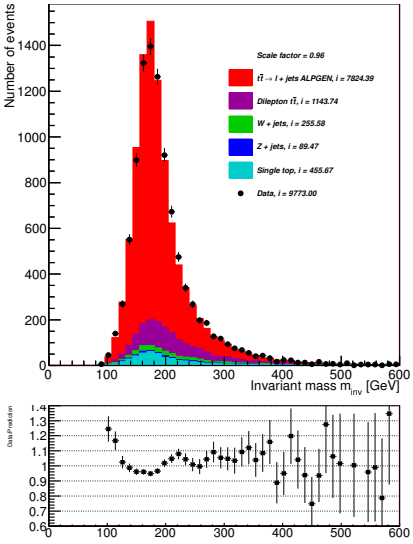

(a) ALPGEN generator and electron channel.

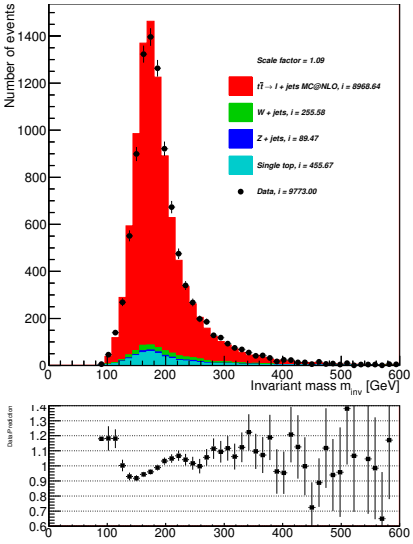

(c) MC@NLO generator and electron channel.

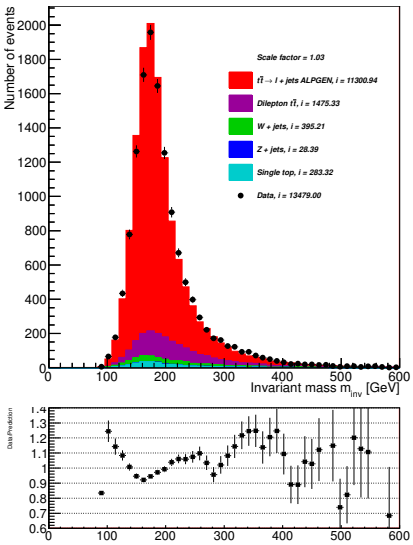

(b) ALPGEN generator and muon channel.

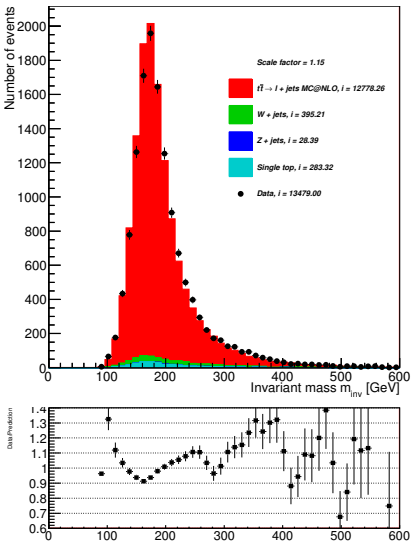

(d) MC@NLO generator and muon channel.

Figure 8.10: Invariant mass of the top quark reconstructed from the leptonic W boson and a b jet assigned based on the result of $\chi^2_{b1,b2,\text{free}}$ test described in Equations (8.6), (8.7). If $\chi^2_{b1,b2,\text{free}}$ is smaller then $\chi^2_{b2,b1,\text{free}}$, the b jet with highest value of p_T is assign to the leptonic W boson. The hadronic W boson is composed from two non b jets where first non b tagged jet has the highers value of transverse momentum and the other non b tagged jet has the second highest value.

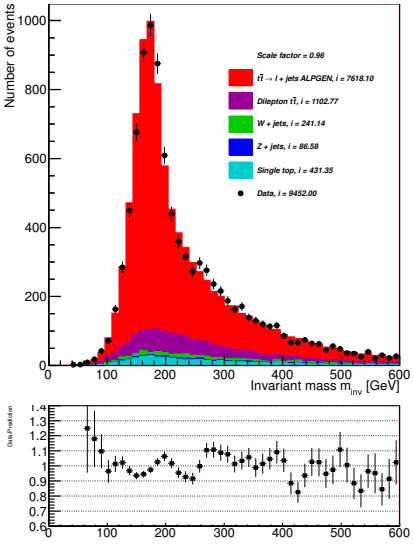

(a) ALPGEN generator and electron channel.

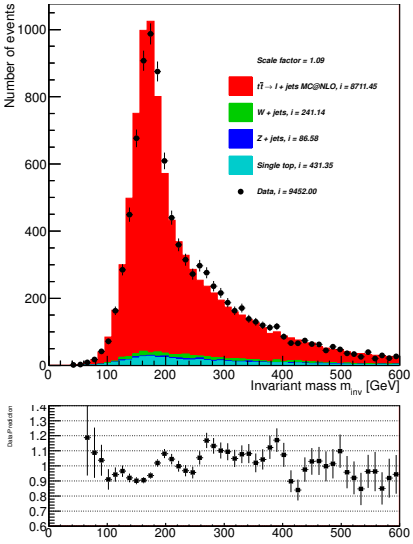

(c) MC@NLO generator and electron channel.

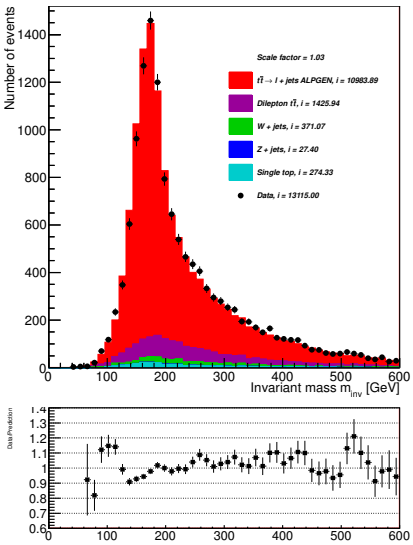

(b) ALPGEN generator and muon channel.

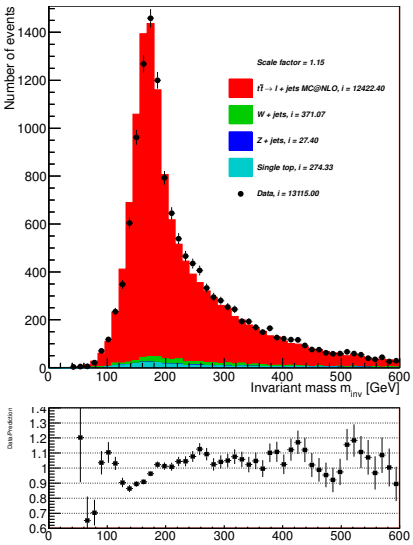

(d) MC@NLO generator and muon channel.

Figure 8.11: Invariant mass of top quark reconstructed from the hadronic W boson and b jet assigned based on the result of $\chi^2_{b1,b2,\text{free}}$ test described in Equations (8.6), (8.7). If $\chi^2_{b1,b2,\text{free}}$ is smaller then $\chi^2_{b2,b1,\text{free}}$, the b jet with highest value of p_T is assign to the hadronic W boson. The hadronic W boson is composed from two non b jets where first non b tagged jet has the highers value of transverse momentum and the other non b tagged jet has the second highest value.

In Table (8.1) of the reconstruction of the leptonic top quark mass m_t for MC@NLO and muon channel are listed the MEAN and its error SIGMA and the standard deviation RMS for different methods used for reconstruction of the leptonic W boson for the MC@NLO generator and muon channel. Based on this result the method that assigns first b jet to the leptonic and second b jet to the hadronic W boson using the $\chi^2_{b1,b2,\text{fixed}}$ test described in Equations (8.4), (8.5) was chosen to be the method from which $t\bar{t}$ pairs will be reconstructed. The results for the other generator and channel are consistent and therefore there aren't shown.

The comparison of different methods used to assign b jets to the leptonically and hadronically decaying W boson are shown in Figures (8.12) and (8.13) respectively. In the next step we want to apply a cut on the W mass which is restricted on interval $60<m^W<100$ GeV. In Figure (8.14) is comparison of different methods used to assign b jets to the hadronically decaying W boson after cut on W boson mass. The shape of top quark invariant mass is more lower and narrow so the invariant mass is more precise after cut. The invariant mass of $t\bar{t}$ pairs is shown in Figure (8.15). There invariant mass are also added three samples from the theoretical particle Z' with masses generated on values 500, 700 and 1600 GeV by PYTHIA [18]. In figures these samples are multiplied by factor 10, 20 and 400 respectively. The $t\bar{t}$ system can origin from the Z' particle as in Figure (3.1a) where Z' is in the propagator instead of gluon. After cut on W boson mass (8.16) is the reconstruction of the $t\bar{t}$ system more accurate. For Z' particle with masses generated on 500 and 700 GeV the cut on the W mass accurates the reconstruction of Z'. However cut on the W boson mass isn't suitable for the Z' particle with mass generated on 1600 GeV because we aren't able to reconstruct Z' particle peak. The efficiency for the cut on the W mass is approximately for ALPGEN 58% and for MC@NLO generator 60% for both channels.

When the Z' particle with mass simulated on 1600 GeV decays to $t\bar{t}$ system then the pair has a high value of transverse momentum. That is why in Figures for the leptonic and hadronic W boson and one b jet and for the leptonic and hadronic W boson and one b jet after cut on W mass for distribution of top quark transverse momentum (8.17), (8.18), (8.19), (8.20), we can't see a peak for the Z' particle. While for the Z' particles with masses simulated on 500 and 700 GeV the peak is visible.

In Figures (8.21) and (8.22) are transverse momenta for the $t\bar{t}$ system before and after the cut on the W boson mass. One can see the difference between transverse momentum of the Z' particle specially for Z' with mass generated on 1600 GeV after cut on W boson mass. When Z' decays the product $t\bar{t}$ pair have huge transverse momentum. Then the reconstruction of peak in not possible. If we want to reconstruct Z' we need to develop different approaches and selection criteria.

Scatter plots of invariant mass of top quark composed on x axis from leptonically and on y axis from hadronically decaying W boson and one b jet for different methods of b jets assignment for MC@NLO as signal model and muon channel before and after cut on W boson mass are shown in Figures (8.23) and (8.24) respectively. When cut on W boson mass is performed one can see that the distribution of invariant masses is more diagonal and the non-diagonal contributions are suppressed.

MC@NLO generator	μ+jets channel	1. method	2. method	3. method	4. method
Signal	MEAN [GeV]	210.54	191.22	195.32	207.29
	SIGMA [GeV]	0.12	0.14	0.13	0.16
	RMS [GeV]	80	62	59	71
Data	MEAN [GeV]	213.97	195.47	200.00	212.06
	SIGMA [GeV]	0.54	0.61	0.58	0.68
	RMS [GeV]	83	67	63	74

Table 8.1: MEAN and its error SIGMA, the standard deviation RMS of the top quark invariant mass for data and signal samples are listed for different methods used for reconstruction of the leptonic W boson for the MC@NLO generator and muon channel. The first method refers to assignment of first and second b jet to the W boson decaying hadronically and assignment of first and second b jet to the W boson decaying leptonically as well. The second method assigns such a b jet to the lepton where $\Delta R\,(b\text{jet}, \text{lepton}) = \text{min}$. This b jet is assign to the leptonic W boson and the other b jet to the hadronic W boson. The third method assigns first b jet to the leptonic and second b jet to the hadronic W boson on the result of $\chi^2_{b1,b2,\text{fixed}}$ test described in Equations (8.4), (8.5). Finally the fourth method assigns first b jet to the leptonic and second b jet to the hadronic W boson on the result of $\chi^2_{b1,b2,\text{free}}$ test described in Equations (8.6), (8.7).

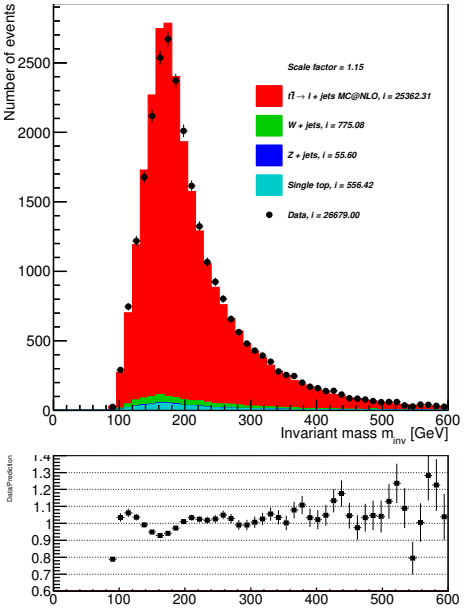

(a) Method where first and second b jet was assigned to the leptonic and hadronic W boson.

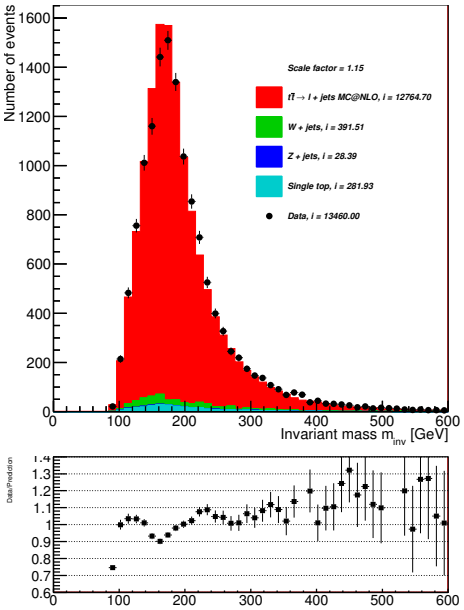

(b) Method with minimum of ΔR. To the leptonic W boson was assigned such a b jet with less value of ΔR.

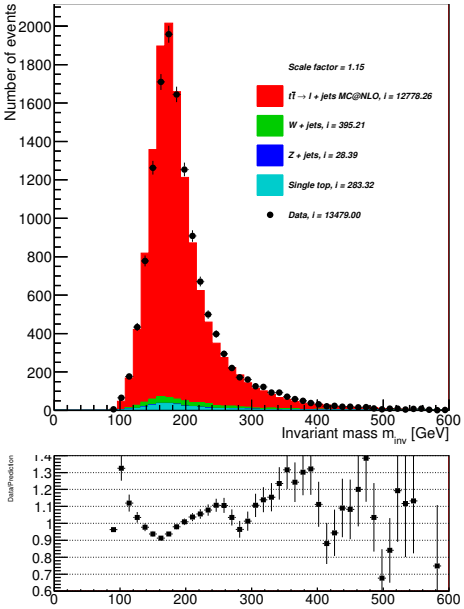

(c) $\chi^2_{b1,b2,\text{fixed}}$ test method where b jets were assigned at the basics of the result of the Equation (8.4) and (8.5).

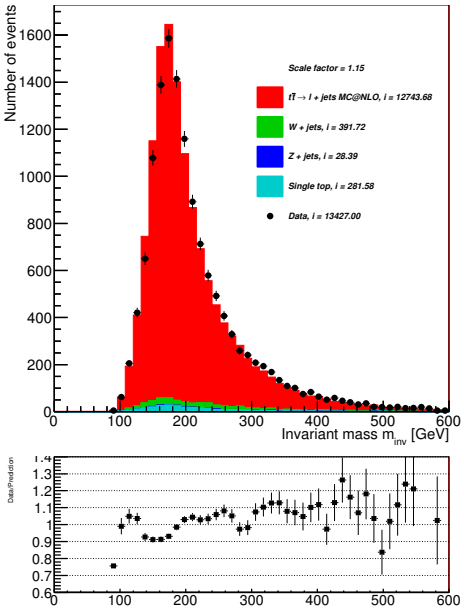

(d) $\chi^2_{b1,b2,\text{free}}$ test method where b jets were assigned at the basics of the result of Equation (8.6) and (8.7).

Figure 8.12: Comparison of invariant masses of the top quark composed from the leptonically decaying W boson and one b jet for different methods of b jets assignment for MC@NLO signal generator and muon channel.

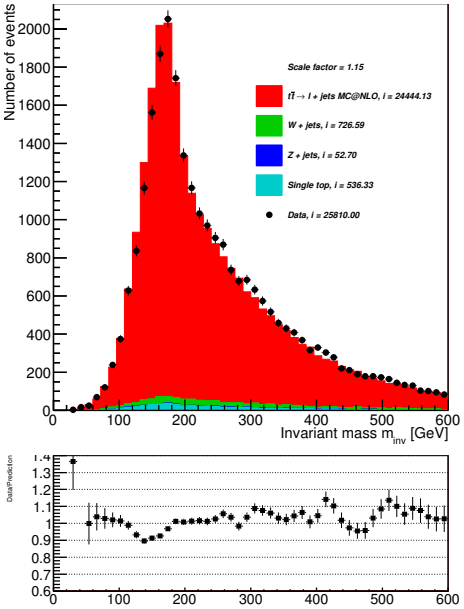

(a) Method where first and second b jet was assigned to the leptonic and hadronic W boson.

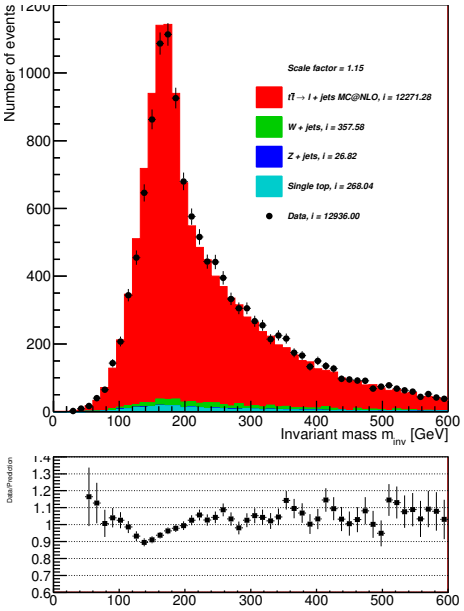

(b) Method with minimum of ΔR. To the leptonic W boson was assigned such a b jet with less value of ΔR.

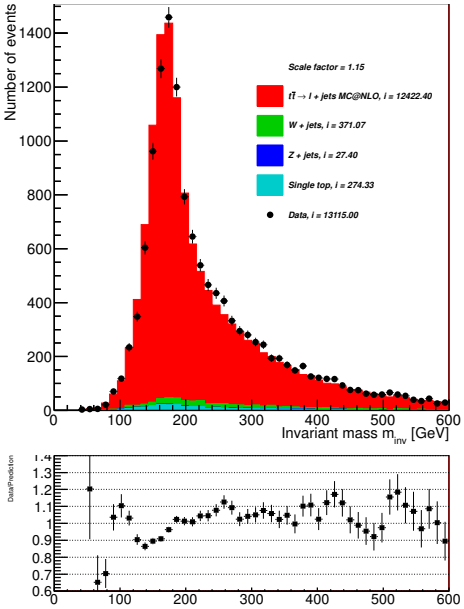

(c) $\chi^2_{b1,b2,\text{fixed}}$ test method where b jets were assigned at the basics of the result of the Equation (8.4) and (8.5).

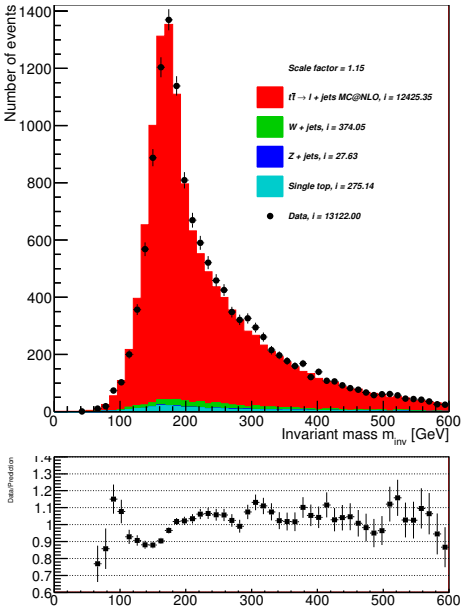

(d) $\chi^2_{b1,b2,\text{free}}$ test method where b jets were assigned at the basics of the result of Equation (8.6) and (8.7).

Figure 8.13: Comparison of invariant masses of the top quark composed from the hadronically decaying W boson and one b jet for different methods of b jets assignment for MC@NLO signal generator and muon channel.

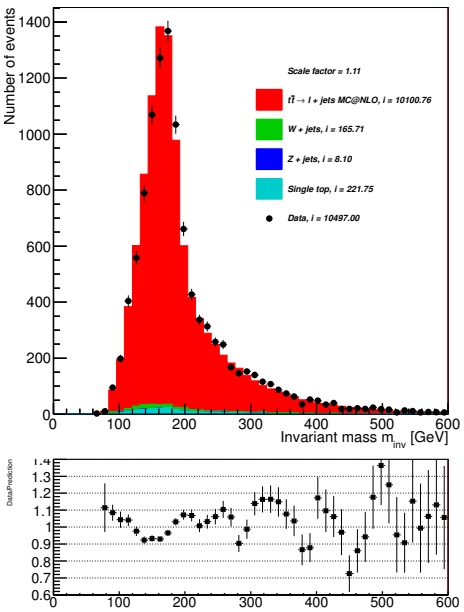

(a) Method where first and second b jet was assigned to the leptonic and hadronic W boson.

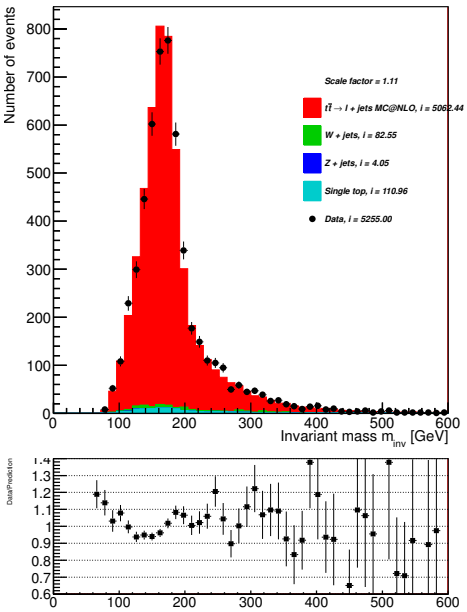

(b) Method with minimum of ΔR. To the leptonic W boson was assigned such a b jet with less value of ΔR.

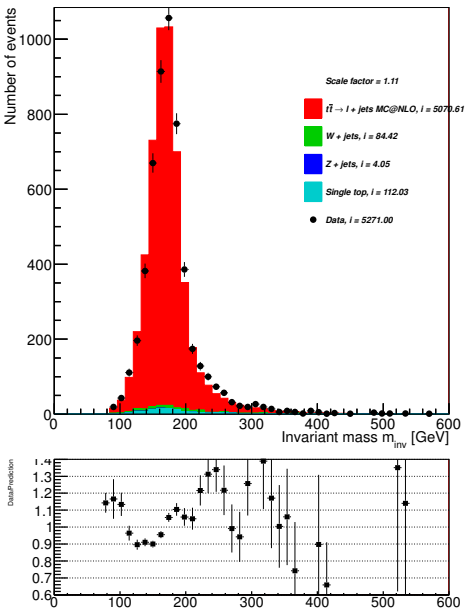

(c) $\chi^2_{b1,b2,\text{fixed}}$ test method where b jets were assigned at the basics of the result of the Equation (8.4) and (8.5).

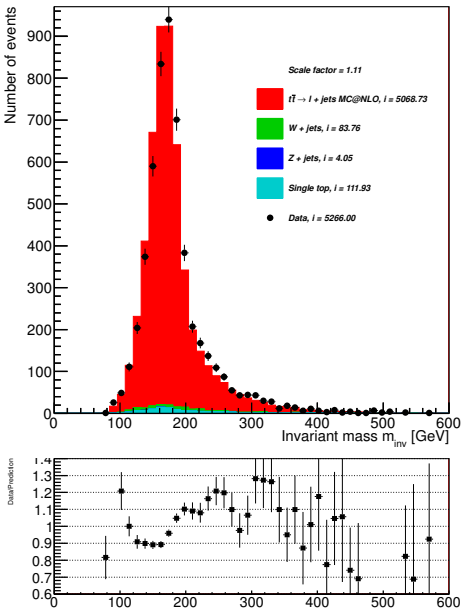

(d) $\chi^2_{b1,b2,\text{free}}$ test method where b jets were assigned at the basics of the result of Equation (8.6) and (8.7).

Figure 8.14: Comparison of invariant masses of the top quark composed from the hadronically decaying W boson and one b jet for different methods of b jets assignment after cut on W boson mass for MC@NLO signal generator and muon channel.

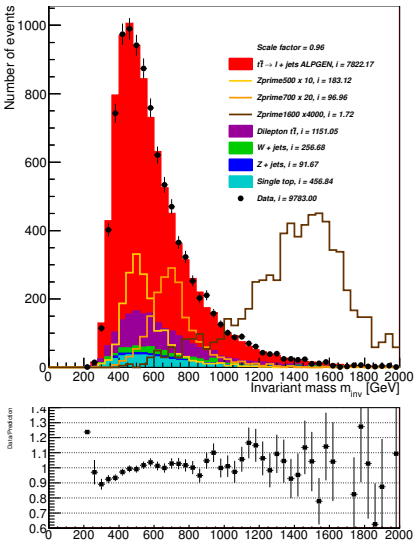

(a) ALPGEN generator and electron channel.

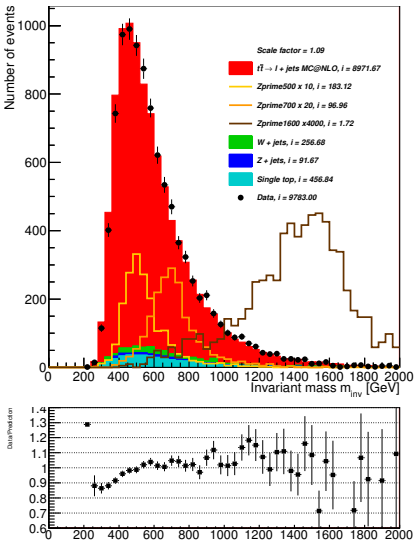

(c) MC@NLO generator and electron channel.

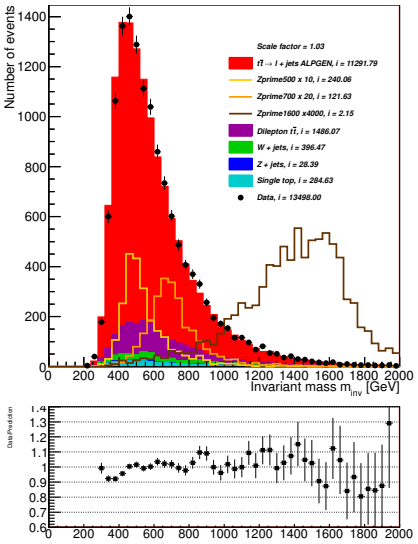

(b) ALPGEN generator and muon channel.

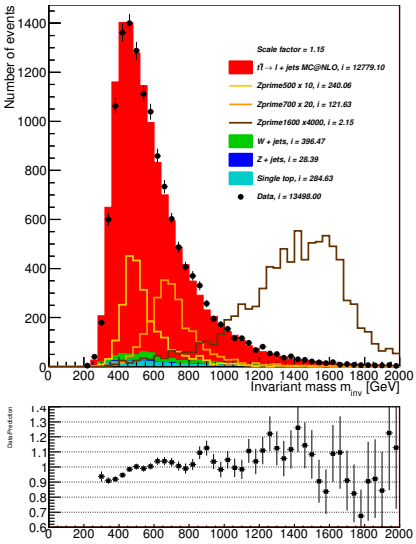

(d) MC@NLO generator and muon channel.

Figure 8.15: Invariant mass of the $t\bar{t}$ system before the cut on the W boson mass reconstructed by using $\chi^2_{b1,b2,\text{fixed}}$ test method where b jets were assigned at the basics of the result of the Equation (8.4) and (8.5). The hadronic W boson is composed from two non b jets where first non b tagged jet has the highers value of transverse momentum and the other non b tagged jet has the second highest value and the leptonic W boson consists of lepton and neutrino where instead of neutrino x and y component were used missing transverse energy as a first approach. There are also added contributions from the hypothetical particle Z' simulated with masses of 500, 700 and 1600 GeV. Samples were multiplied by different factors shown in the legend to be clearly visible.

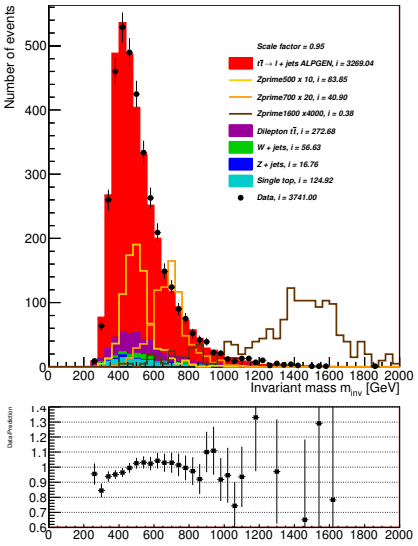

(a) ALPGEN generator and electron channel.

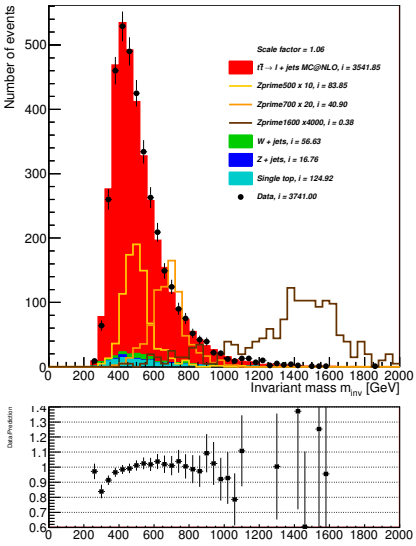

(c) MC@NLO generator and electron channel.

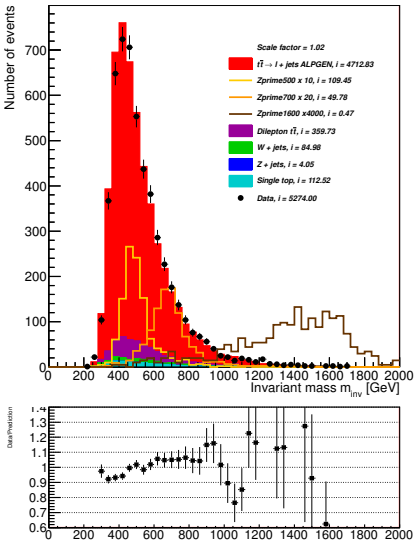

(b) ALPGEN generator and muon channel.

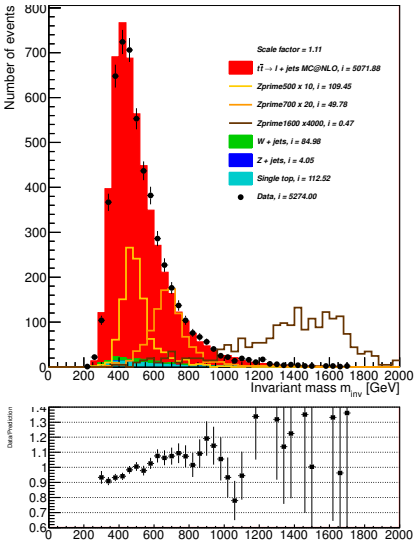

(d) MC@NLO generator and muon channel.

Figure 8.16: Invariant mass of the $t\bar{t}$ pair after the cut on the W boson mass which was limited in the interval 60 GeV $< m^W <$ 100 GeV. There are also added contributions from Z' particle simulated with masses of 500, 700 and 1600 GeV. Samples were multiplied by different factors shown in the legend to be clearly visible.

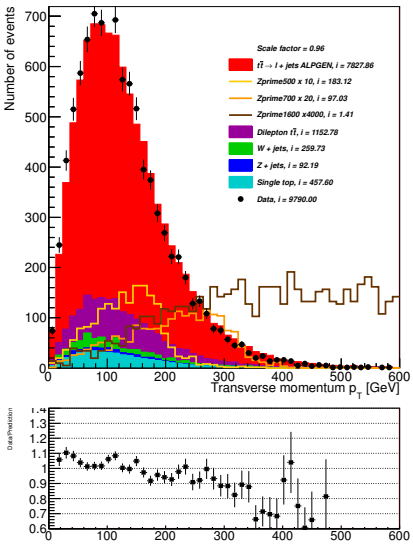

(a) ALPGEN generator and electron channel.

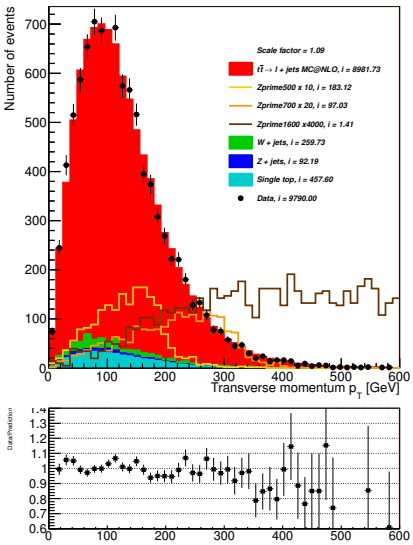

(c) MC@NLO generator and electron channel.

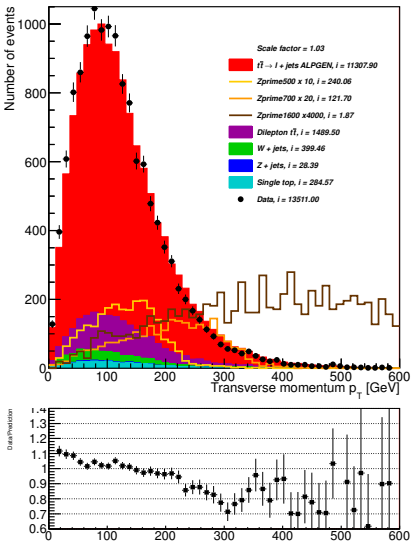

(b) ALPGEN generator and muon channel.

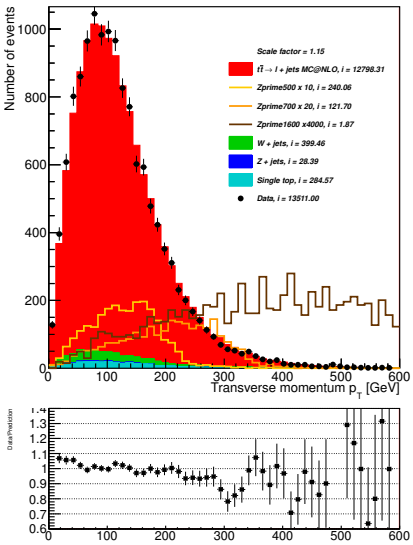

(d) MC@NLO generator and muon channel.

Figure 8.17: Transverse momentum of top quark reconstructed from the leptonic W boson and one b jet based on $\chi^2_{b1,b2,\text{fixed}}$ test. There are also added contributions from Z' particle simulated with masses of 500, 700 and 1600 GeV. Samples were multiplied by different factors shown in the legend to be clearly visible.

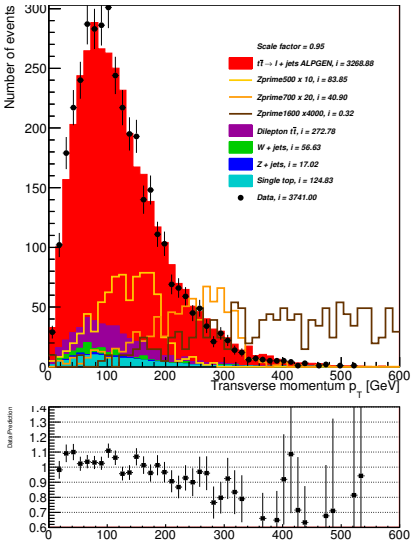

(a) ALPGEN generator and electron channel.

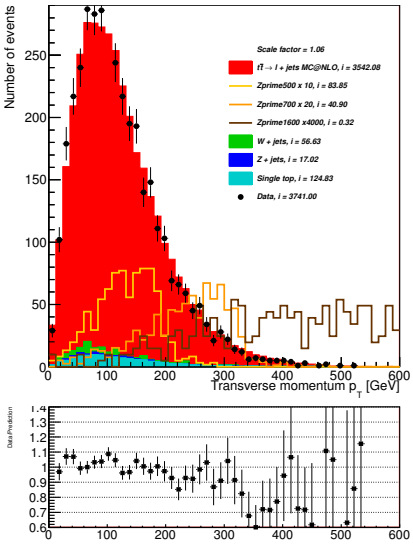

(c) MC@NLO generator and electron channel.

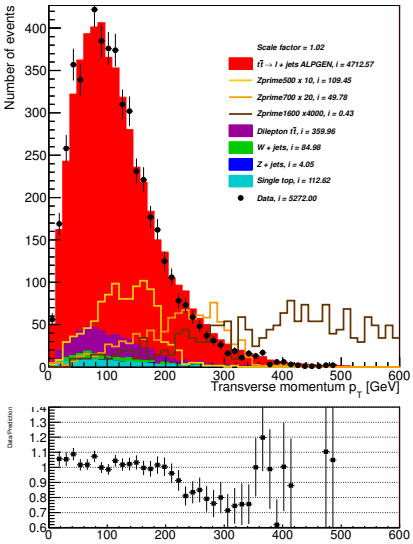

(b) ALPGEN generator and muon channel.

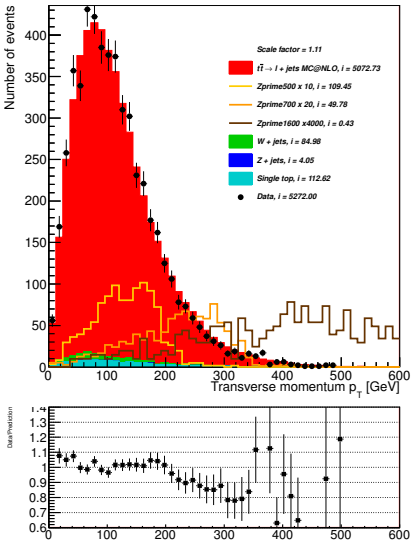

(d) MC@NLO generator and muon channel.

Figure 8.18: Transverse momentum of top quark reconstructed from the leptonic W boson and one b jet based on $\chi^2_{b1,b2,\text{fixed}}$ test after cut on W boson mass. There are also added contributions from the Z' particle simulated with masses of 500, 700 and 1600 GeV. Samples were multiplied by different factors shown in the legend to be clearly visible.

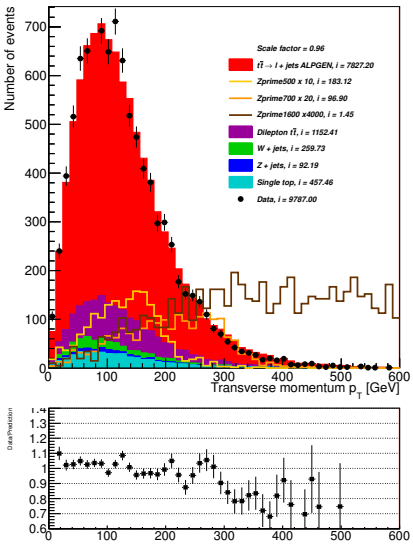

(a) ALPGEN generator and electron channel.

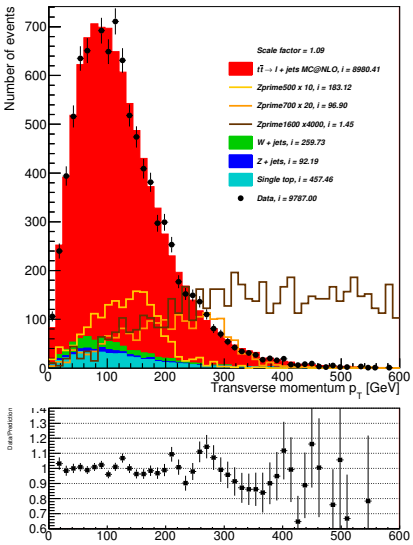

(c) MC@NLO generator and electron channel.

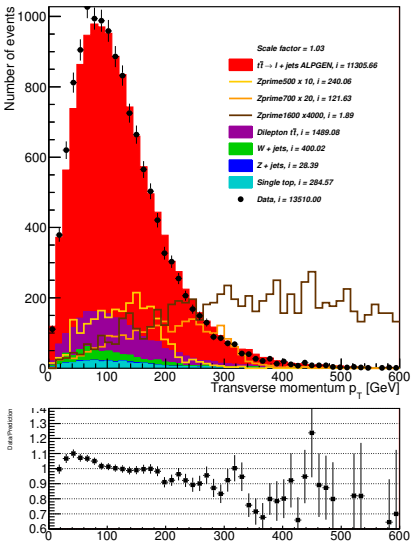

(b) ALPGEN generator and muon channel.

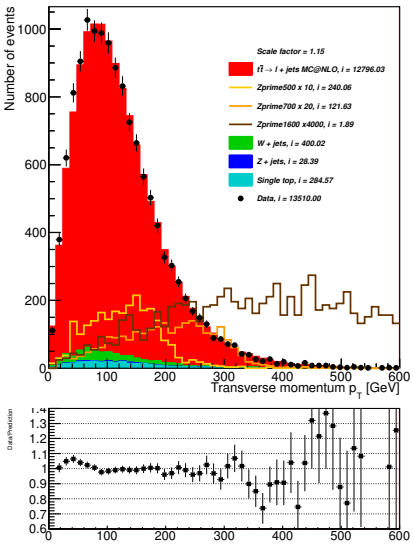

(d) MC@NLO generator and muon channel.

Figure 8.19: Transverse momentum of top quark reconstructed from the hadronic W boson and one b jet based on $\chi^2_{b1,b2,\text{fixed}}$ test. There are also added contributions from the Z' particle simulated with masses of 500, 700 and 1600 GeV. Samples were multiplied by different factors shown in the legend to be clearly visible.

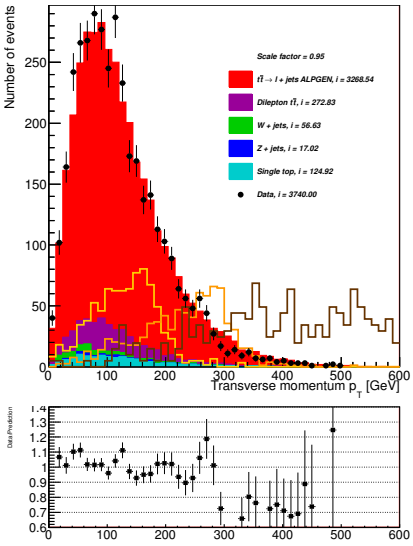

(a) ALPGEN generator and electron channel.

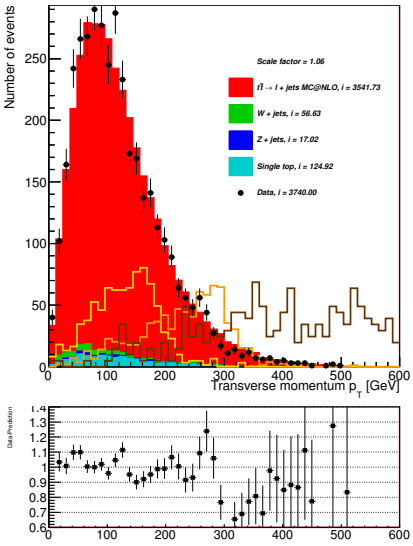

(c) MC@NLO generator and electron channel.

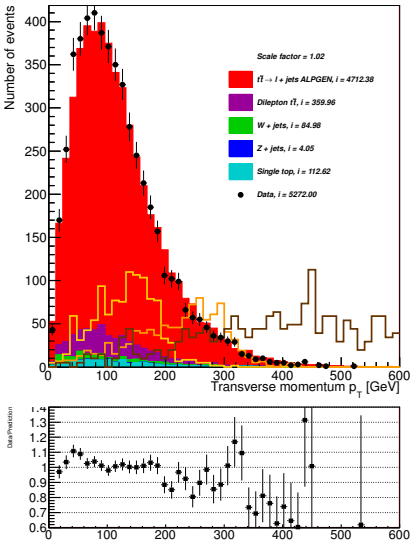

(b) ALPGEN generator and muon channel.

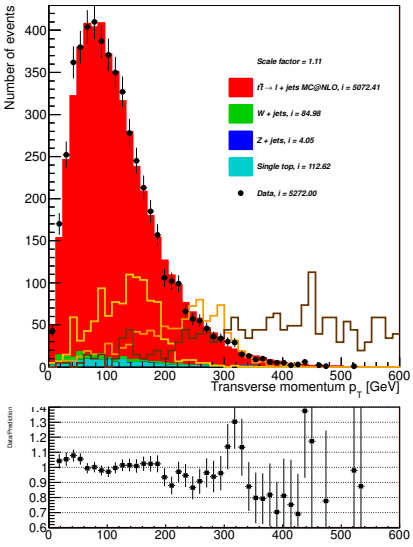

(d) MC@NLO generator and muon channel.

Figure 8.20: Transverse momentum of top quark reconstructed from the hadronic W boson and one b jet based on $\chi^2_{b1,b2,\text{fixed}}$ test after cut on W boson mass. There are also added contributions from Z' particle simulated with masses of 500, 700 and 1600 GeV. Samples were multiplied by different factors shown in the legend to be clearly visible.

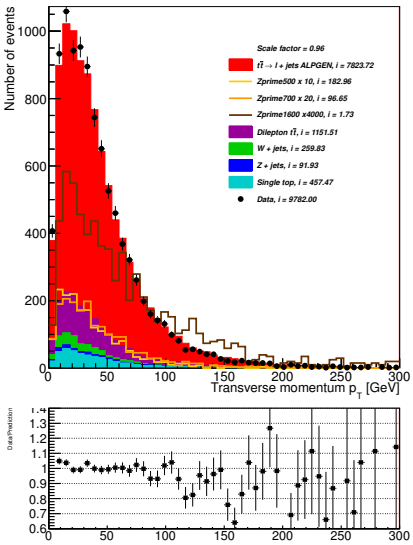

(a) ALPGEN generator and electron channel.

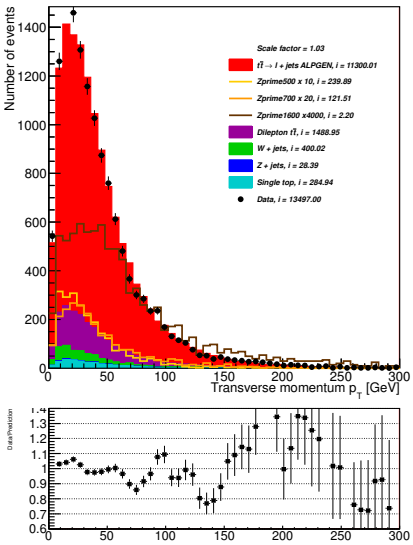

(b) ALPGEN generator and muon channel.

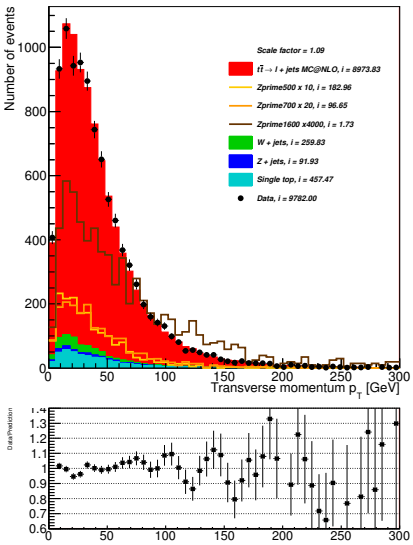

(c) MC@NLO generator and electron channel.

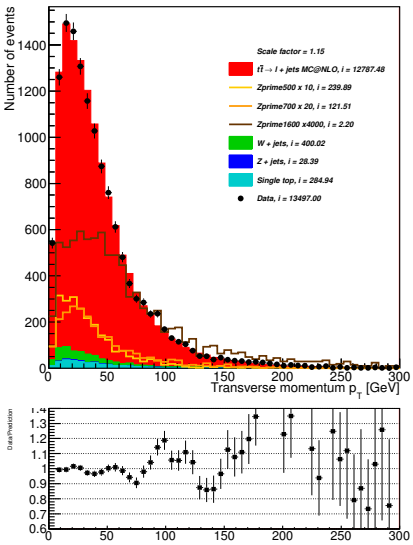

(d) MC@NLO generator and muon channel.

Figure 8.21: Distribution of the transverse momentum of the $t\bar{t}$ pair before the cut on the W boson mass. There are also added contributions from Z' particle simulated with masses of 500, 700 and 1600 GeV. Samples were multiplied by different factors shown in the legend to be clearly visible.

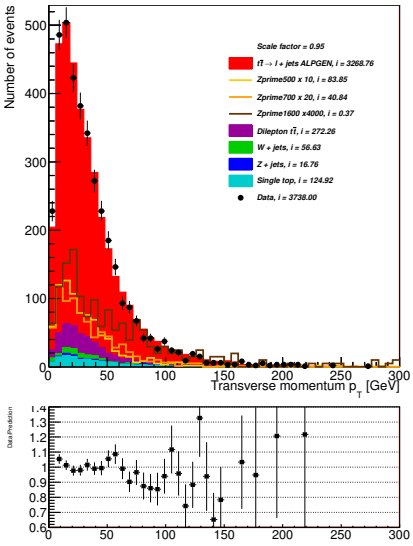

(a) ALPGEN generator and electron channel.

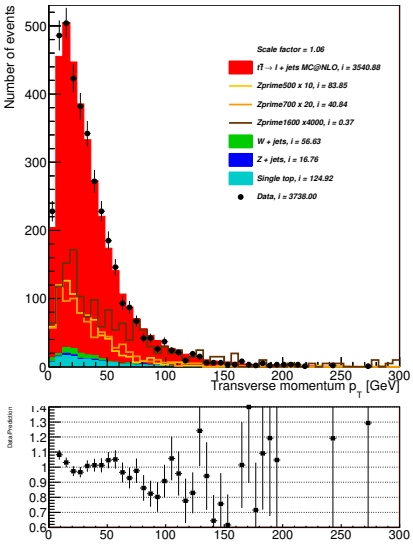

(c) MC@NLO generator and electron channel.

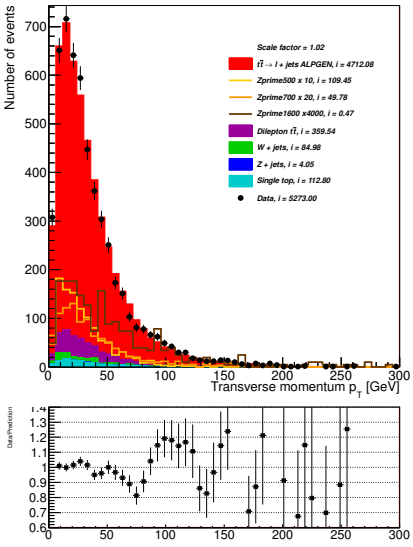

(b) ALPGEN generator and muon channel.

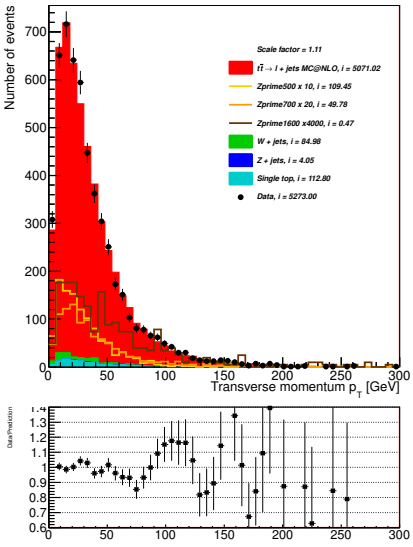

(d) MC@NLO generator and muon channel.

Figure 8.22: Distribution of the transverse momentum of the $t\bar{t}$ pair after the cut on the W boson mass which was limited in the interval 60 GeV $< m_T^W <$ 100 GeV. There are also added contributions from the Z' particle simulated with masses of 500, 700 and 1600 GeV. Samples were multiplied by different factors shown in the legend to be clearly visible.

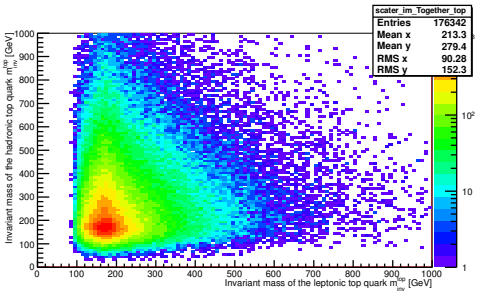

(a) Method where both b jets were assigned to the leptonic and hadronic W boson.

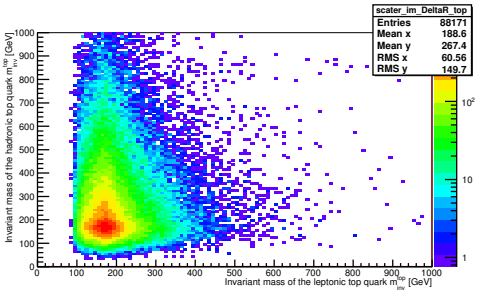

(b) Method with minimum of ΔR. To the leptonic W boson was assigned such a b jet with less value of ΔR.

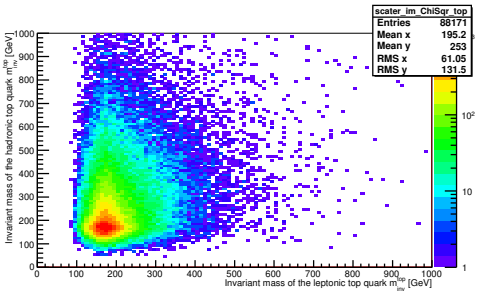

(c) $\chi^2_{b1,b2,\text{fixed}}$ test method where b jets were assigned at the basics of the result of the Equation (8.4) and (8.5).

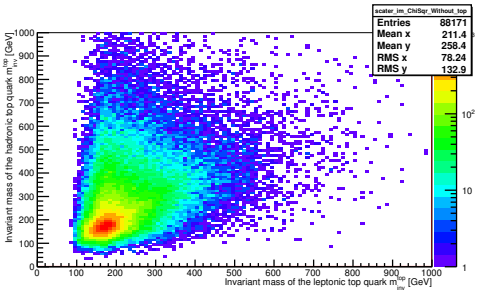

(d) $\chi^2_{b1,b2,\text{free}}$ test method where b jets were assigned at the basics of the result of Equation (8.6) and (8.7).

Figure 8.23: Scatter plots of invariant mass of top quark composed on x axis from leptonically and on y axis from hadronically decaying W boson and one b jet for different methods of b jets assignment for MC@NLO as signal model and muon channel before cut on W boson mass.

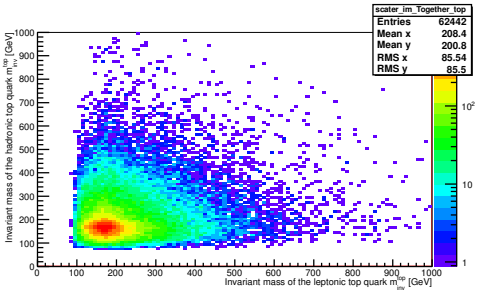

(a) Method where both b jets were assigned to the leptonic and hadronic W boson.

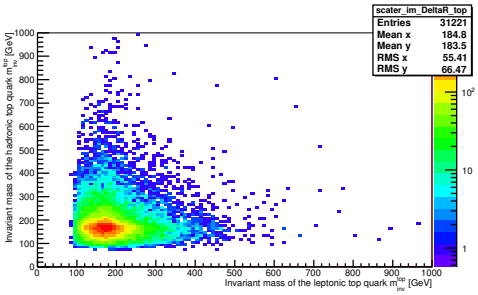

(b) Method with minimum of ΔR. To the leptonic W boson was assigned such a b jet with less value of ΔR.

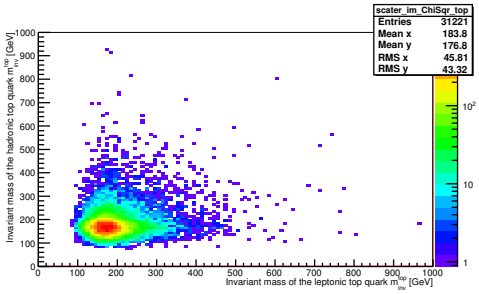

(c) $\chi^2_{b1,b2,\text{fixed}}$ test method where b jets were assigned at the basics of the result of the Equation (8.4) and (8.5).

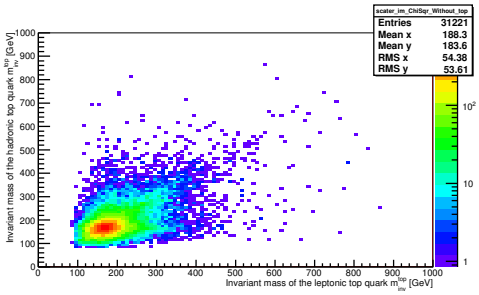

(d) $\chi^2_{b1,b2,\text{free}}$ test method where b jets were assigned at the basics of the result of Equation (8.6) and (8.7).

Figure 8.24: Scatter plots of invariant mass of top quark composed on x axis from leptonically and on y axis from hadronically decaying W boson and one b jet for different methods of b jets assignment for MC@NLO as signal model and muon channel after cut on W boson mass which was limited in the interval 60 GeV $< m^W <$ 100 GeV.

Conclusions

In the thesis we analyzed $t\bar{t}$ pairs reconstruction. Detailed studies of the kinematics of the $t\bar{t}$ pairs has the potential to help to model spectra where the top quark production is a background to processes beyond the standard model (SM). Individual spectra themselves are also an important tests of perturbative quantum chromodynamics, and a model-independent window on physics beyond the SM and non-standard top-pairs production mechanisms. We studied data from the ATLAS experiment and appropriate pseudo-data from detector simulations.

We shortly described the ATLAS detector including its subdetectors as one of the main experiments at the LHC. Then we summarized basics facts about event generators ALPGEN and MC@NLO. These two generator simulated physics in the ATLAS detector during pp collisions for signal while also PYTHIA generator was used for the Z' particle. We were given samples generated by ALPGEN and MC@NLO to analyze. We described background and performed cuts to diminished it to a reasonable level. Because ALPGEN and MC@NLO generators differ in efficiency to pass cuts, we obtain different scaling factors which were used to scale generator to data. The ALPGEN generator describes the number of jets for bigger values that 6 while the MC@NLO is better in description for smaller number. The MC@NLO generator better explains the transverse momentum of the top quark than the ALPGEN generator.

We developed methods how to reconstruct hadronically and leptonically decaying W bosons and top and antitop quarks. For the top and antitop quarks reconstructions several methods were also developed. The best of them was then used to reconstructed the $t\bar{t}$ system. Various variables related to the top quark and top antitop system were shown and discussed in the thesis. In the end we also added samples from the hypothetical particle Z' with masses generated on 500, 700 and 1600 GeV by the PYTHIA generator. Specially the invariant mass and the transverse momentum of Z' particle were studied. The cut on the W boson mass accurates the reconstruction of Z' with masses generated on 500 and 700 GeV. We aren't able to reconstruct the Z' particle with mass generated on 1600 GeV. Moreover the peak for the Z' transverse momentum can't be also reconstructed because of high value of the transverse momentum for the $t\bar{t}$ system. To do so, we would need to develop a new approach and selection criteria. For the Z' particle with masses generated on 500 and 700 GeV the reconstruction of the invariant mass and transverse momentum was successful.

The control plots of $t, \bar{t}$ and $t\bar{t}$ for chosen variables are shown in the Appendix.

9 Appendix

The control plots of distribution of transverse momentum, pseudorapidity, rapidity and azimuthal angle for top quark reconstructed from leptonically decaying W boson and one b jet, for top quark reconstructed form hadronically decaying W boson and one b jet and for $t\bar{t}$ pair are shown here. The assignment of b jets to the W boson was according method where first b jet was assigned to the leptonic and second b jet to the hadronic W boson on the result of $\chi^2_{b1,b2,\text{fixed}}$ test described in Equations (8.4) and (8.5).

Rapidity y is an alternative to speed as a measure of motion, in the experimental particle physics is often used a modified definition of rapidity relative to a beam axis defined as:

$$y = \frac{1}{2} \ln \frac{E + p_z}{E - p_z}, \tag{9.1}$$

where E is a particles energy and p_z is the component of momentum along the beam axis.

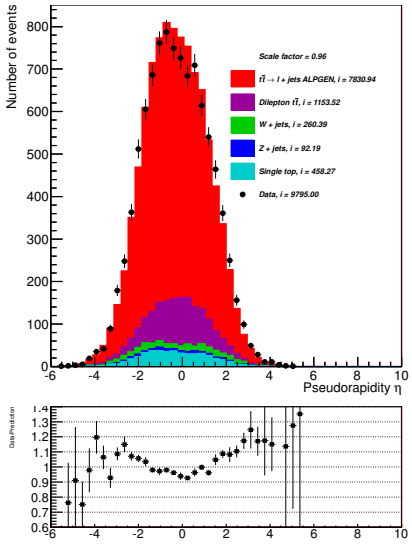

(a) ALPGEN generator and electron channel.

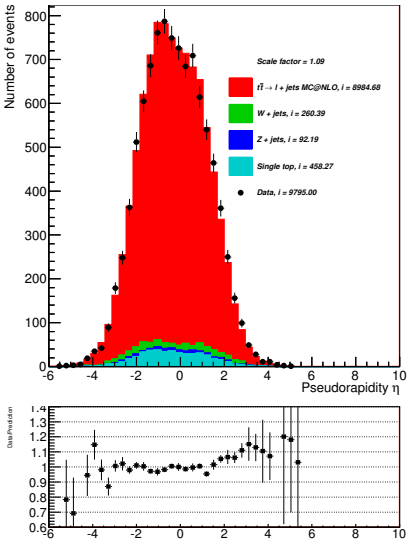

(c) MC@NLO generator and electron channel.

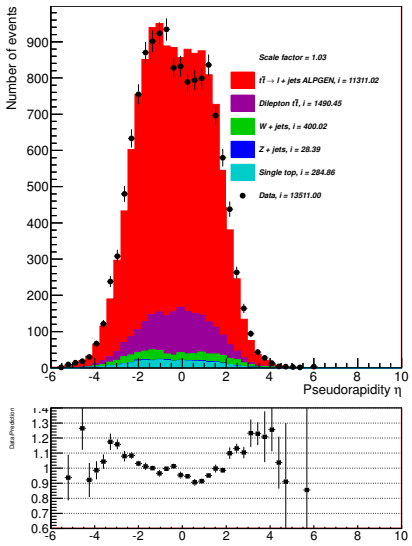

(b) ALPGEN generator and muon channel.

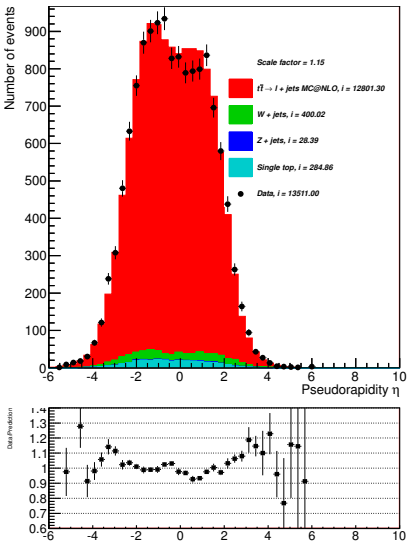

(d) MC@NLO generator and muon channel.

Figure 9.1: Distribution of the pseudorapidity of the leptonically decaying W boson and one b jet before the cut on the W boson mass.

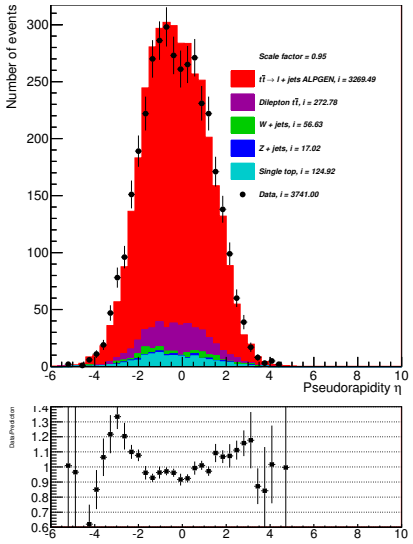

(a) ALPGEN generator and electron channel.

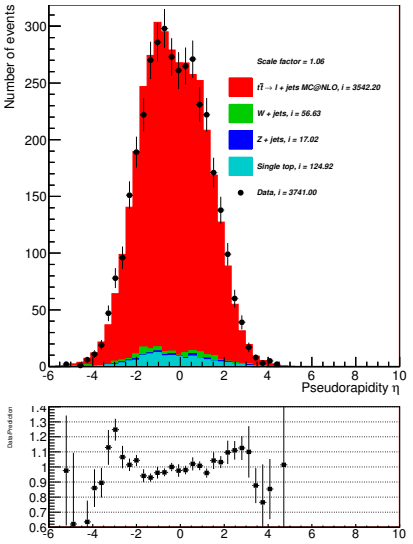

(c) MC@NLO generator and electron channel.

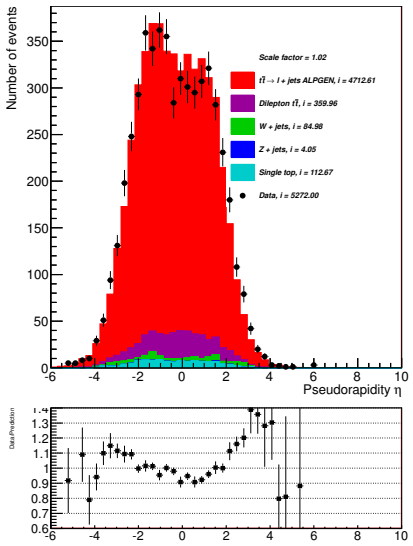

(b) ALPGEN generator and muon channel.

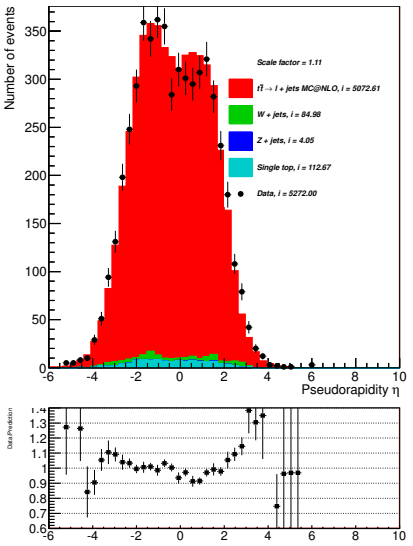

(d) MC@NLO generator and muon channel.

Figure 9.2: Distribution of the pseudorapidity of the leptonically decaying W boson and one b jet after the cut on the W boson mass.

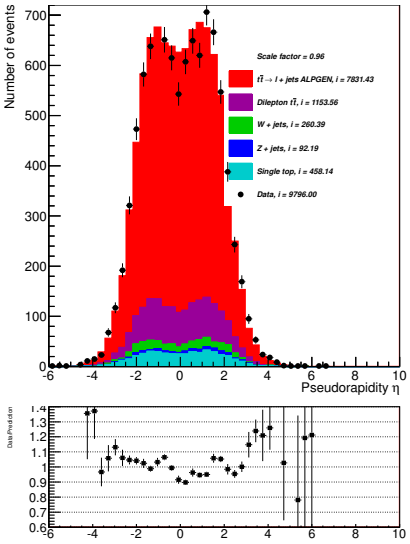

(a) ALPGEN generator and electron channel.

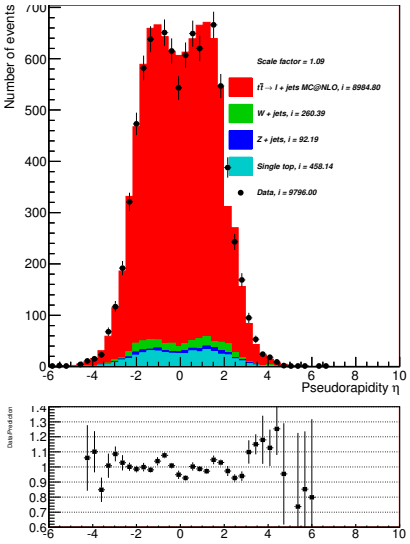

(c) MC@NLO generator and electron channel.

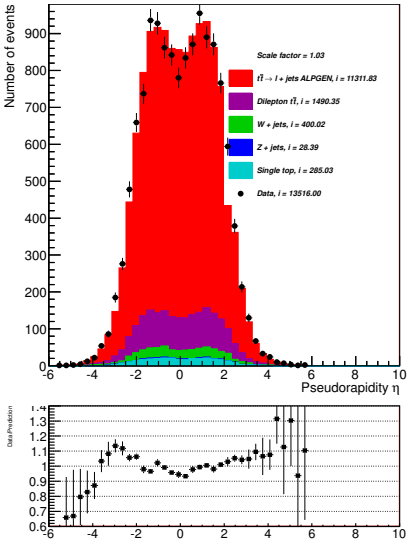

(b) ALPGEN generator and muon channel.

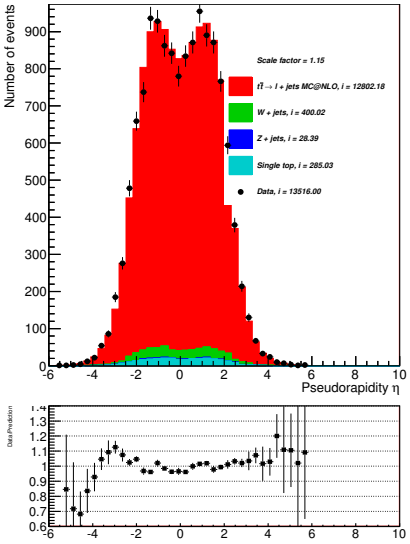

(d) MC@NLO generator and muon channel.

Figure 9.3: Distribution of the pseudorapidity of the hadronically decaying W boson and one b jet before the cut on the W boson mass.

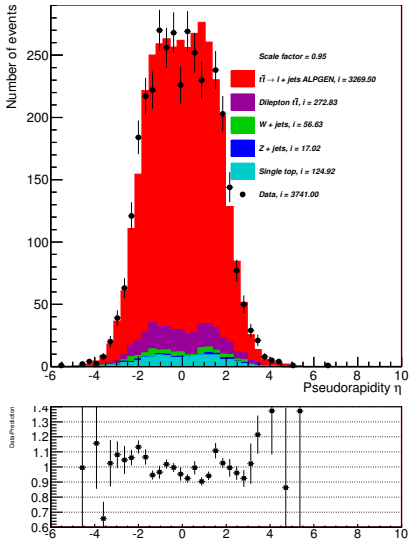

(a) ALPGEN generator and electron channel.

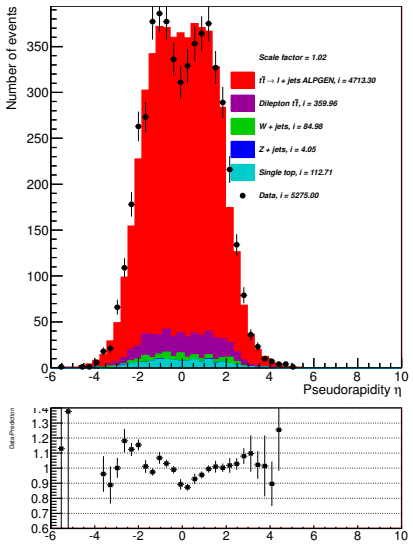

(b) ALPGEN generator and muon channel.

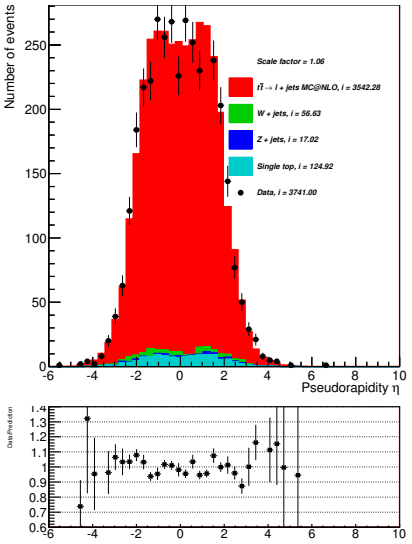

(c) MC@NLO generator and electron channel.

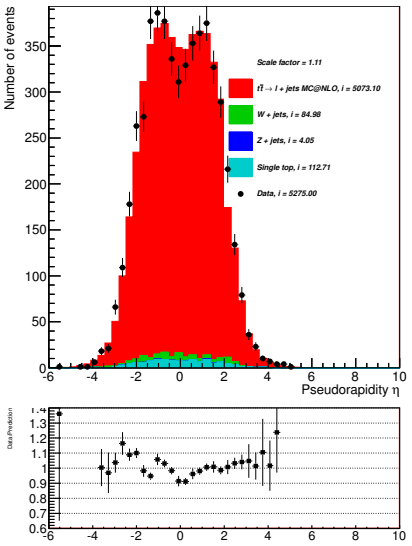

(d) MC@NLO generator and muon channel.

Figure 9.4: Distribution of the pseudorapidity of the hadronically decaying W boson and one b jet after the cut on the W boson mass.

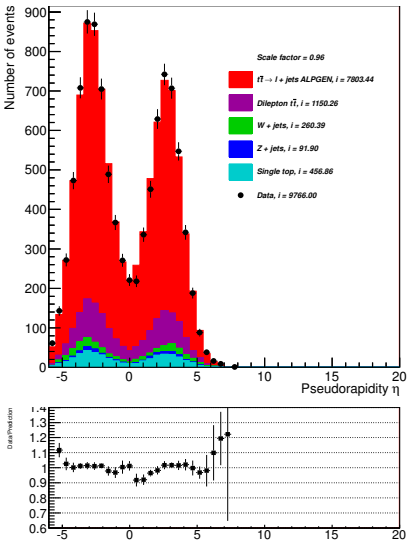

(a) ALPGEN generator and electron channel.

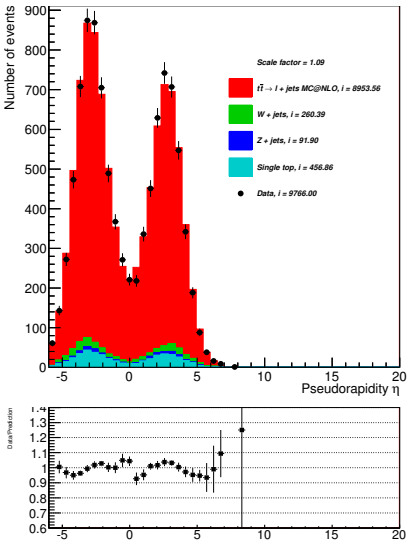

(c) MC@NLO generator and electron channel.

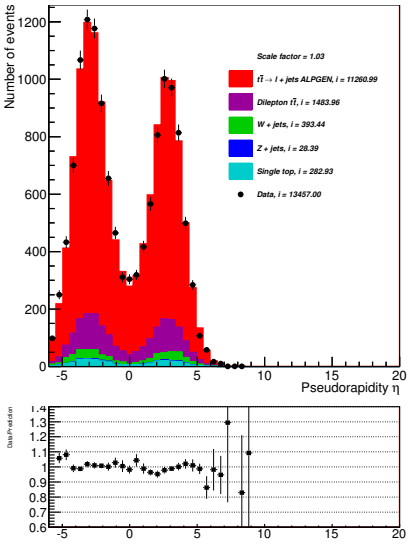

(b) ALPGEN generator and muon channel.

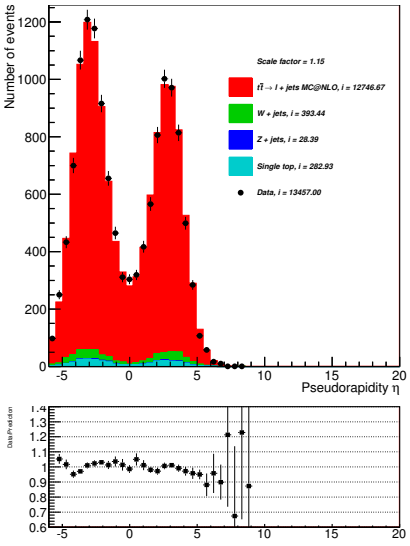

(d) MC@NLO generator and muon channel.

Figure 9.5: Distribution of the pseudorapidity of the $t\bar{t}$ pair before the cut on the W boson transverse mass.

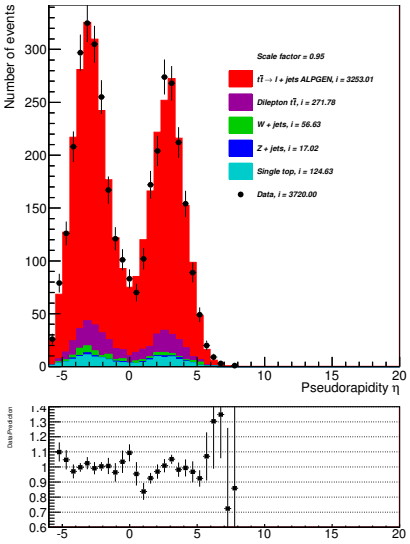

(a) ALPGEN generator and electron channel.

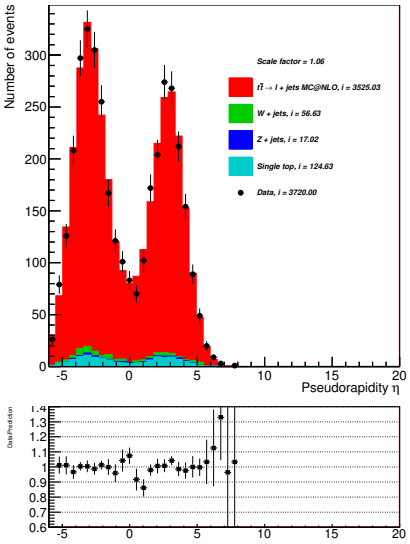

(c) MC@NLO generator and electron channel.

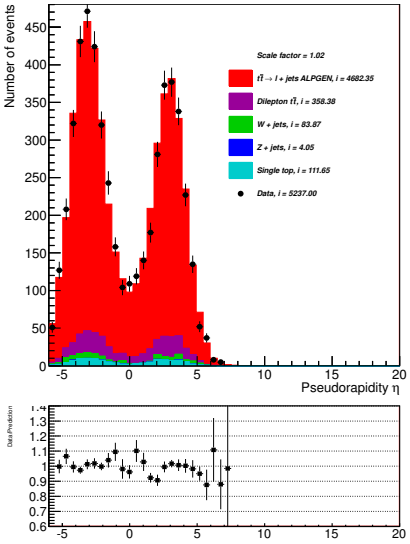

(b) ALPGEN generator and muon channel.

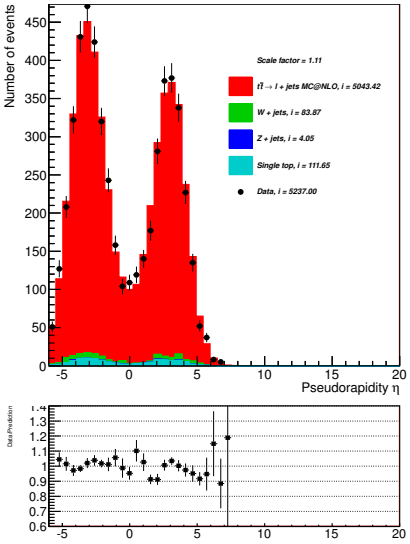

(d) MC@NLO generator and muon channel.

Figure 9.6: Distribution of the pseudorapidity of the $t\bar{t}$ pair after the cut on the W boson mass.

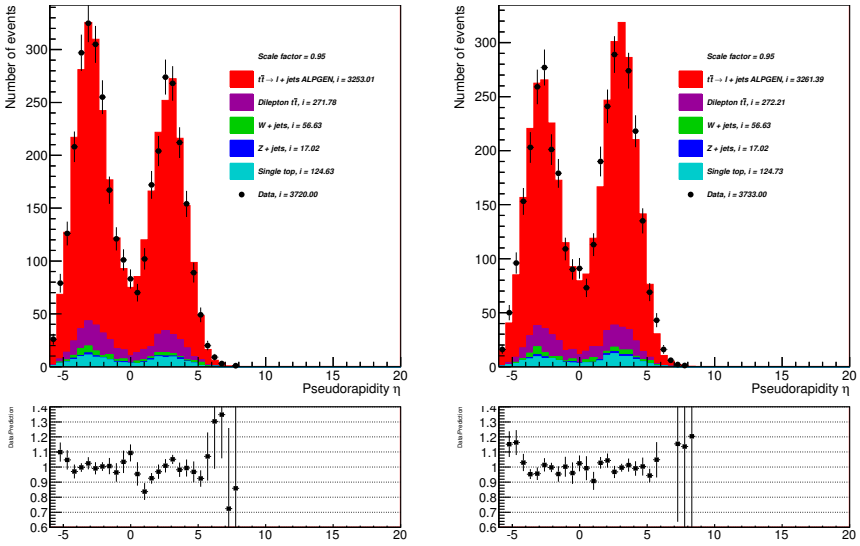

Figure 9.7: Comparison of distribution of the pseudorapidity of the $t\bar{t}$ pair after the cut on the W boson mass where the leptonic W boson was reconstructed from lepton with different solutions of Equation (8.3) of the z component of neutrino four vector for ALPGEN generator and electron channel. On the left side is negative solution $p_{z,-}$ and on the right side is positive solution $p_{z,+}$. The different composition of the leptonic W boson explains the antisymmety of the pseudorapidity of $t\bar{t}$ pair. The hadronic W boson was reconstructed from two non b tagged jets where first jet has the highest value of transverse momentum and the second jet has the second highest value of transverse momentum. The assignment of b jets to the W boson was according method where first b jet was assigned to the leptonic and second b jet to the hadronic W boson on the result of $\chi^2_{b1,b2,\text{fixed}}$ test described in Equations (8.4) and (8.5).

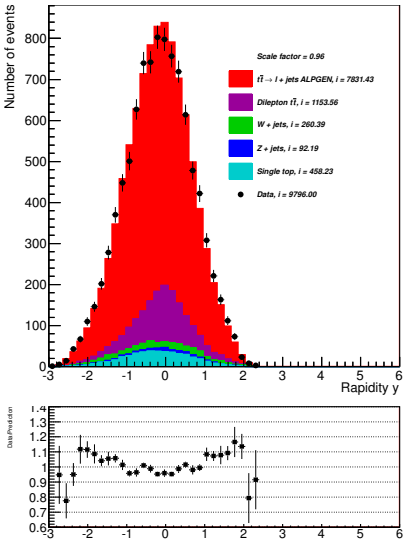

(a) ALPGEN generator and electron channel.

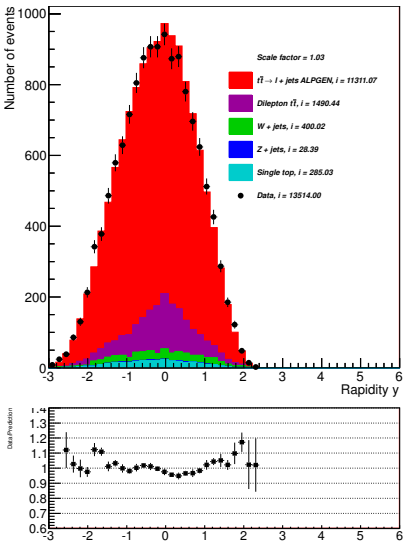

(b) ALPGEN generator and muon channel.

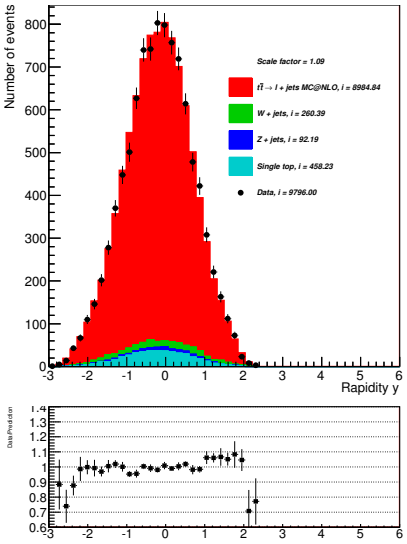

(c) MC@NLO generator and electron channel.

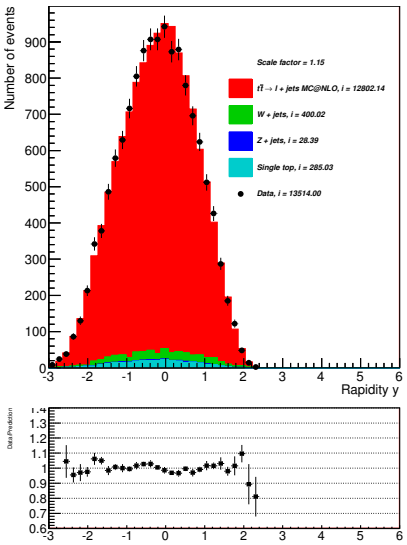

(d) MC@NLO generator and muon channel.

Figure 9.8: Distribution of the rapidity of the leptonically decaying W boson and one b jet before cut on W boson mass.

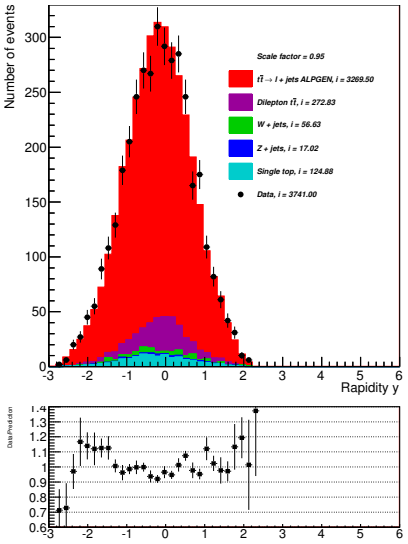

(a) ALPGEN generator and electron channel.

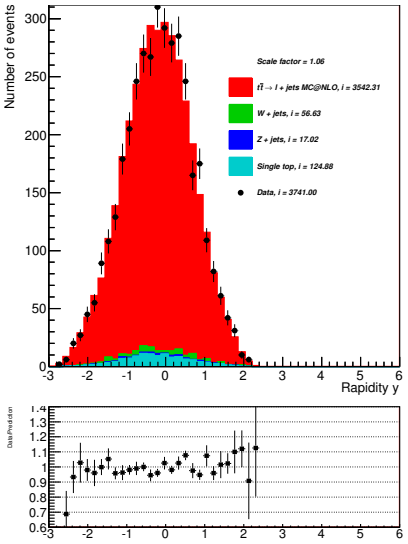

(c) MC@NLO generator and electron channel.

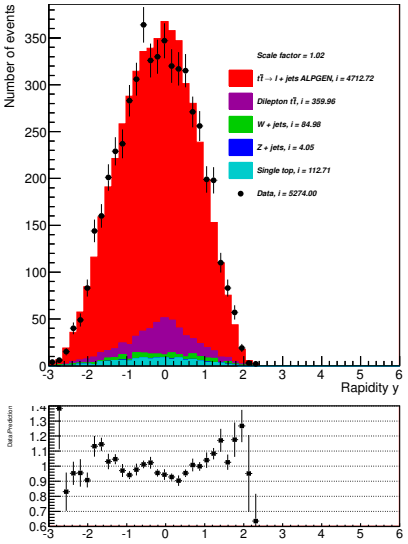

(b) ALPGEN generator and muon channel.

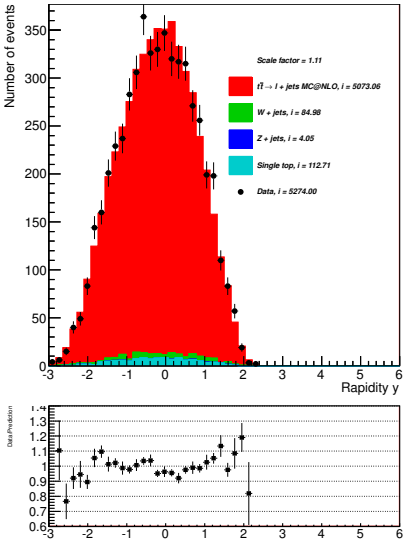

(d) MC@NLO generator and muon channel.

Figure 9.9: Distribution of the rapidity of the leptonically decaying W boson and one b jet after the cut on the W boson mass.

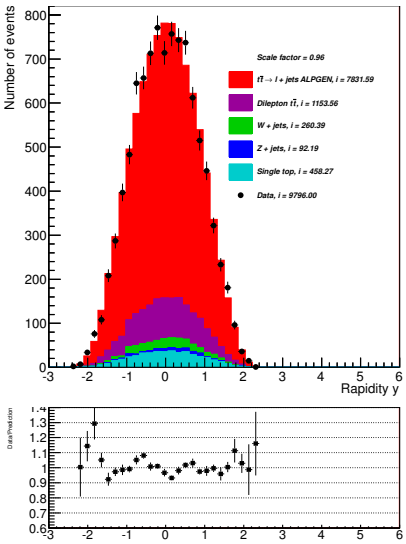

(a) ALPGEN generator and electron channel.

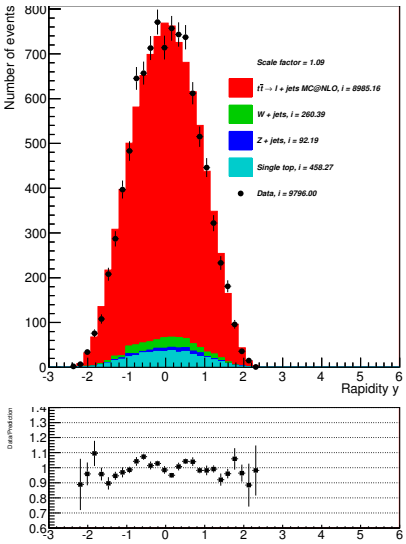

(c) MC@NLO generator and electron channel.

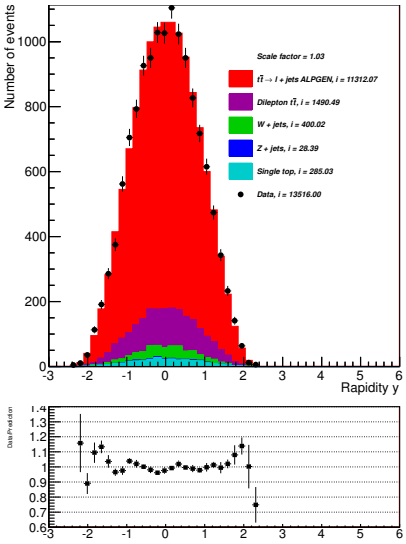

(b) ALPGEN generator and muon channel.

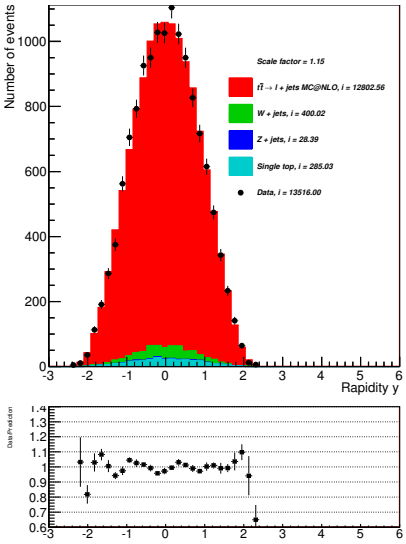

(d) MC@NLO generator and muon channel.

Figure 9.10: Distribution of the rapidity of the hadronically decaying W boson and one b jet before the cut on the W boson mass.

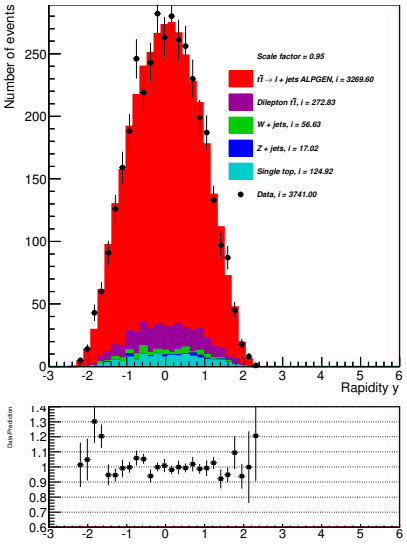

(a) ALPGEN generator and electron channel.

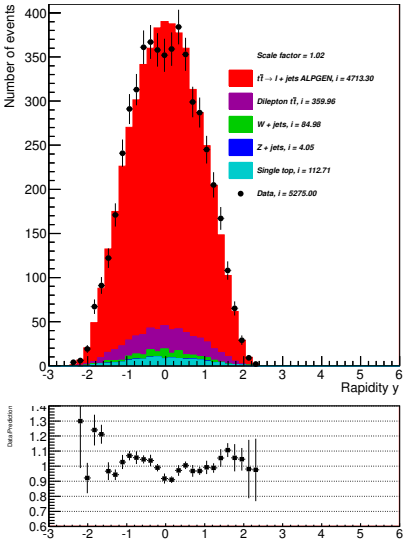

(b) ALPGEN generator and muon channel.

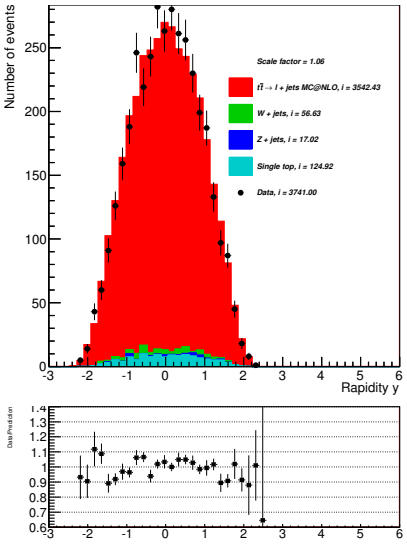

(c) MC@NLO generator and electron channel.

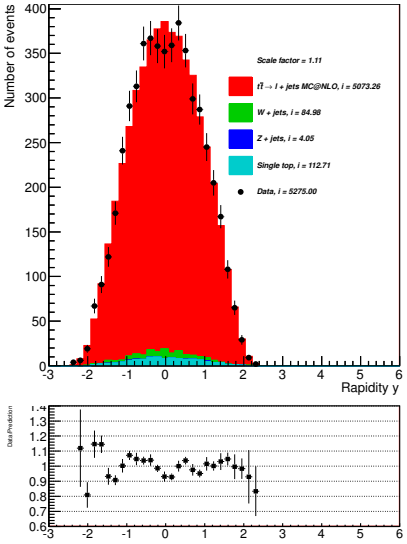

(d) MC@NLO generator and muon channel.

Figure 9.11: Distribution of the rapidity of the hadronically decaying W boson and one b jet after the cut on the W boson mass.

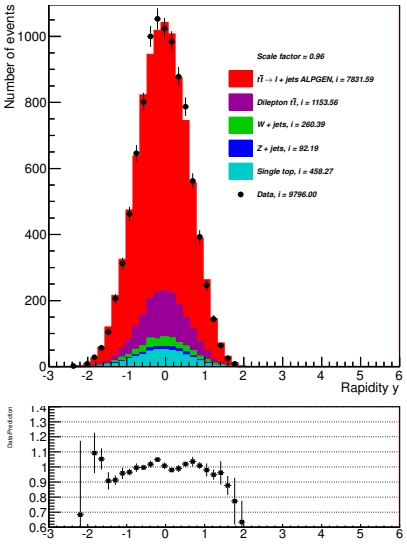

(a) ALPGEN generator and electron channel.

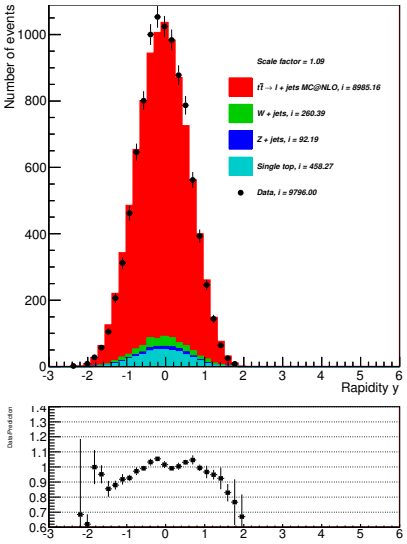

(c) MC@NLO generator and electron channel.

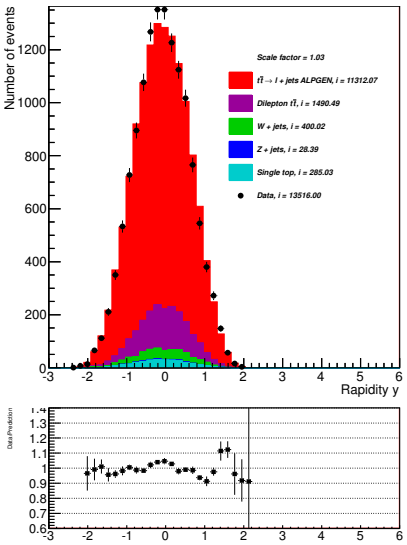

(b) ALPGEN generator and muon channel.

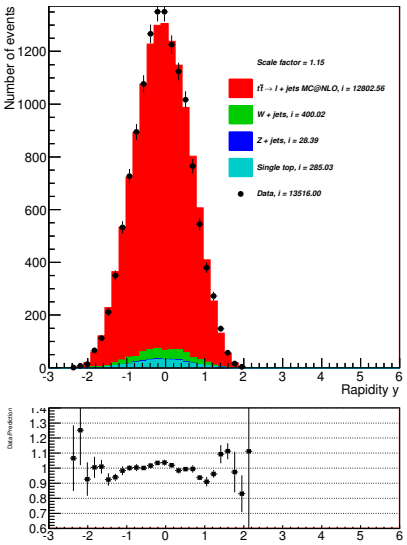

(d) MC@NLO generator and muon channel.

Figure 9.12: Distribution of the rapidity of the $t\bar{t}$ pair before the cut on the W boson transverse mass.

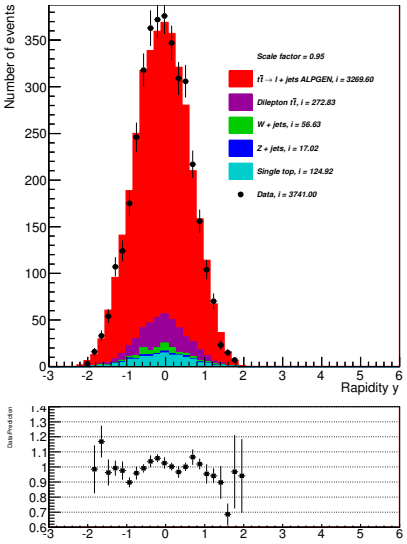

(a) ALPGEN generator and electron channel.

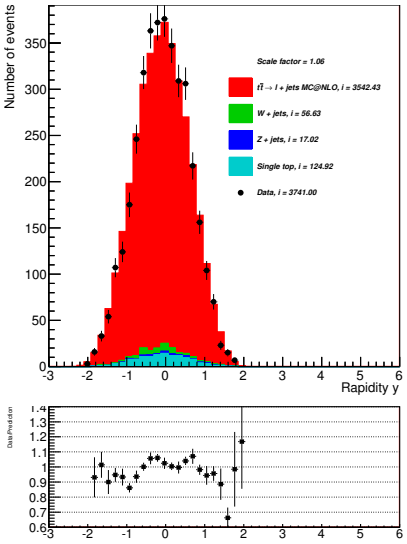

(c) MC@NLO generator and electron channel.

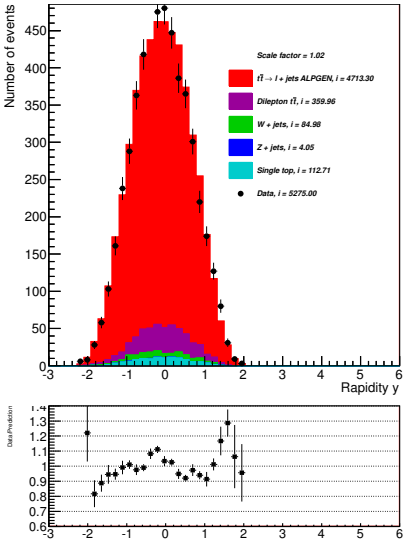

(b) ALPGEN generator and muon channel.

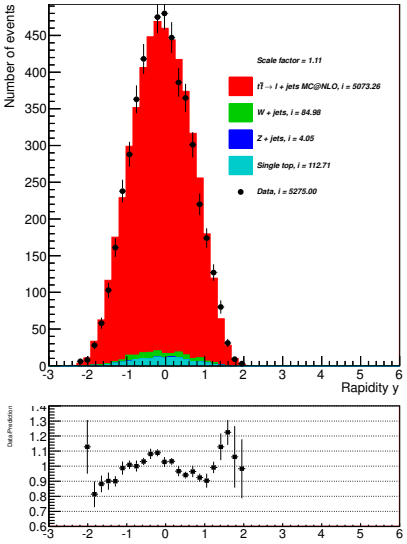

(d) MC@NLO generator and muon channel.

Figure 9.13: Distribution of the rapidity of the $t\bar{t}$ pair after the cut on the W boson mass.

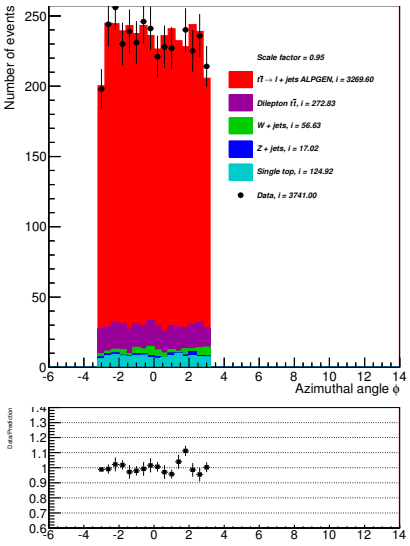

(a) ALPGEN generator and electron channel.

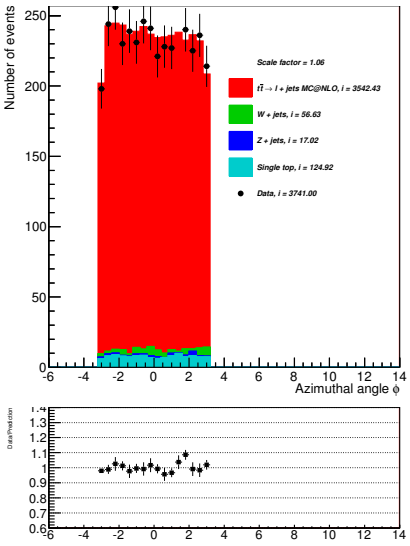

(c) MC@NLO generator and electron channel.

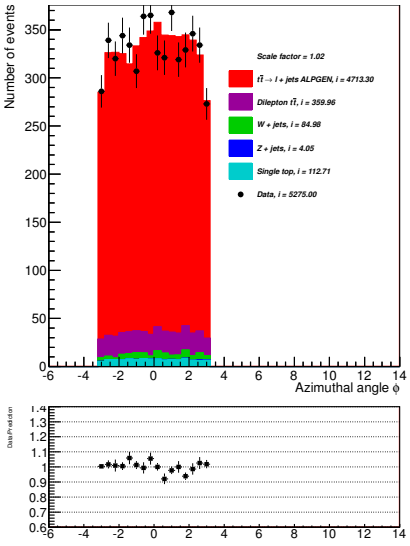

(b) ALPGEN generator and muon channel.

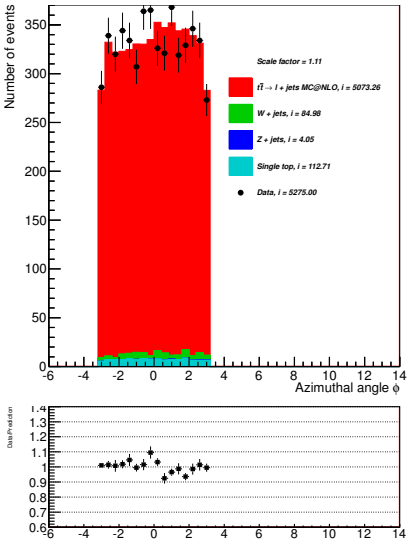

(d) MC@NLO generator and muon channel.

Figure 9.14: Azimuthal angle distribution of the leptonically decaying W boson and one b jet after the cut on the W boson mass.

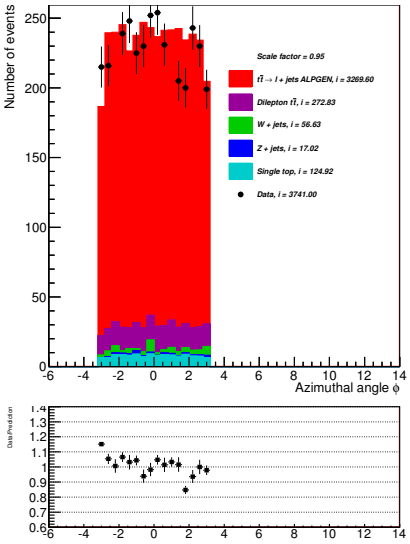

(a) ALPGEN generator and electron channel.

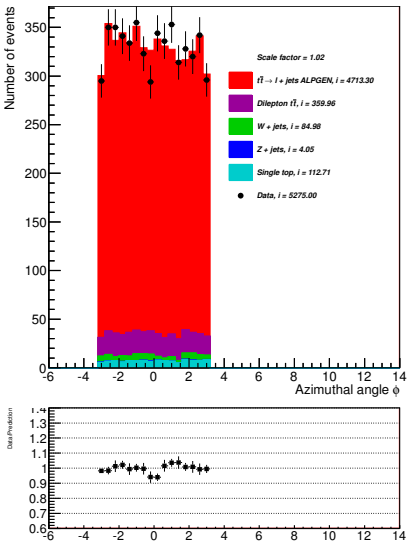

(b) ALPGEN generator and muon channel.

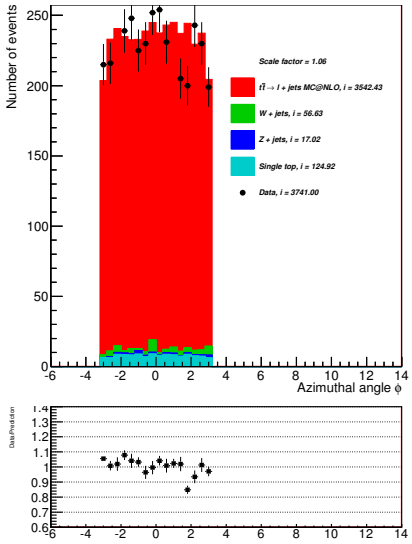

(c) MC@NLO generator and electron channel.

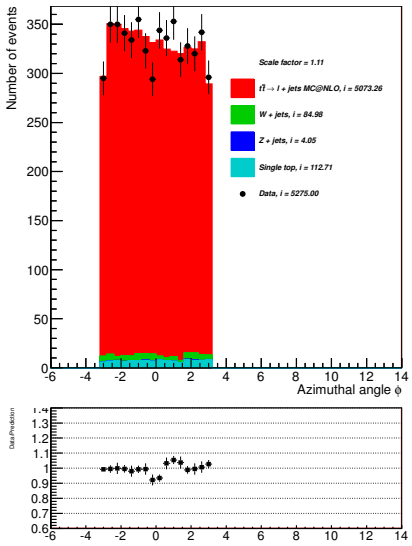

(d) MC@NLO generator and muon channel.

Figure 9.15: Azimuthal angle distribution of the hadronically decaying W boson and one b jet after the cut on the W boson mass.

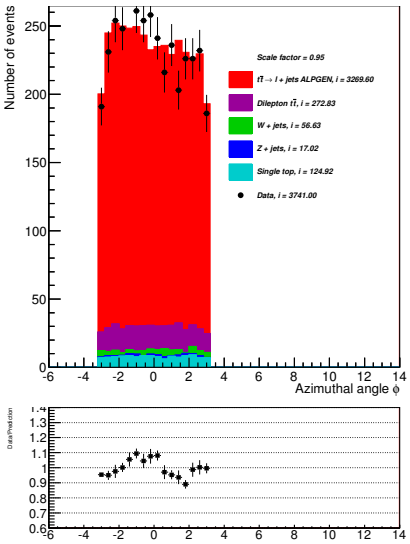

(a) ALPGEN generator and electron channel.

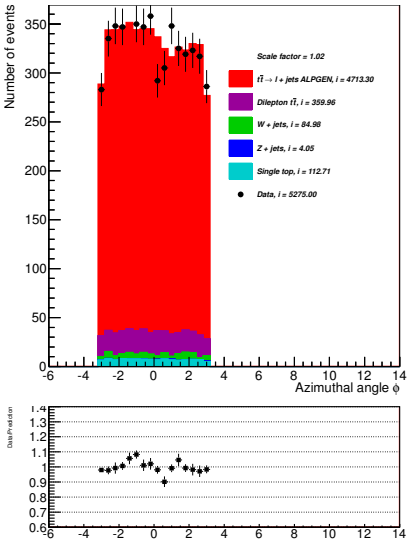

(b) ALPGEN generator and muon channel.

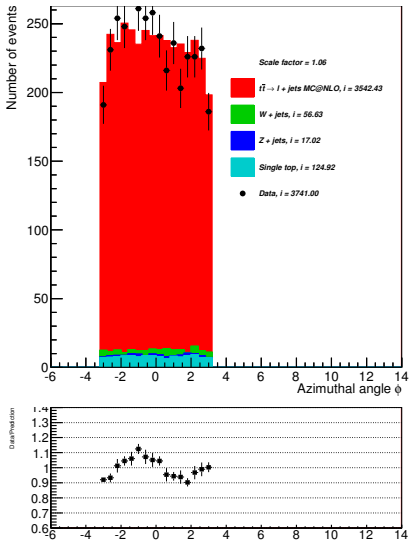

(c) MC@NLO generator and electron channel.

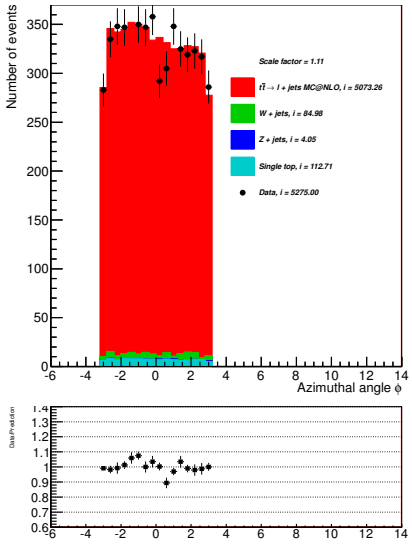

(d) MC@NLO generator and muon channel.

Figure 9.16: Distribution of the azimuthal angle of the $t\bar{t}$ pair after the cut on the W boson transverse mass.

References

[1] Peskin M and Schroeder D., *An Introduction to Quantum Field Theory*, ISBN 0-201-50397-2

[2] Halzen and Martin, *Quarks and leptons*, ISBN 0-471-88741-2

[3] Griffiths, *Introduction to elementary particles*, ISBN 0-471-60386-4

[4] Beringer J. ET AL., *Particle Data Group* (web page)
URL - `http://http://pdg.lbl.gov/`

[5] The ATLAS Collaboration, *The ATLAS experiment at the CERN Large Hadron Collider*
URL - `http://iopscience.iop.org/1748-0221/3/08/S08003`

[6] The ATLAS Collaboration, *The ATLAS Inner Detector commissioning and calibration*, arXiv:1004.5293
URL - `http://arxiv.org/abs/1004.5293`

[7] The ATLAS Collaboration, *Readiness of the ATLAS Tile Calorimeter for LHC collisions*, arXiv:1007.5423
URL - `http://arxiv.org/abs/1007.5423`

[8] The ATLAS Collaboration, *Calibration and Performance of the ATLAS Muon Spectrometer*, arXiv:1109.6933
URL - `http://arxiv.org/abs/1109.6933`

[9] Schilling Frank-Peter, *Top quark physics at the LHC: A review of the first two years*, arXiv:1206.4484
URL - `http://arxiv.org/pdf/1206.4484v2.pdf`

[10] Eidelman S. ET AL., *The review of particle physics*, Journal of Physics G

[11] Bruning O.S. ET AL., *LHC Design Report*, ISBN 9789290832249

[12] Mangano M. L. ET AL., *ALPGEN generator V2.14* (web page)
URL - `http://alpgen.web.cern.ch/alpgen`

[13] Frixone S. ET AL., *The MC@NLO 4.0 Event Generator*, arXiv:1010.0819v1 (October 2010)
URL - `http://arxiv.org/pdf/1010.0819v1.pdf`

[14] Corcella G. ET AL., *HERWIG 6.5: an event generator for Hadron Emission Reactions With Interfering Gluons*
URL - `http://arxiv.org/abs/hep-ph/0011363`

[15] Butterworth J. ET AL., *Jimmy Generator*
URL - `http://jimmy.hepforge.org/news`

[16] Aliev M., Lacker H., Langenfeld U., Moch S., Uwer P., Wiedermann M., *HATHOR – HAdronic Top and Heavy quarks crOss section calculatoR*
URL - `http://www.sciencedirect.com/science/article/pii/S0010465510005333`

[17] The ROOT Team, *ROOT - A Data Analysis Framework* (web page)
URL - http://root.cern.ch/drupal/

[18] Sjotrand T. ET AL., *PYTHIA*
URL - http://home.thep.lu.se/~torbjorn/Pythia.html